To the Graduate Council:

I am submitting herewith a dissertation written by Tony Alan Hancock entitled "An Experimental and Theoretical Study of the Wet Spinning Process." I recommend that it be accepted in partial fulfillment of the requirements for the degree of Doctor of Philosophy, with a major in Chemical Engineering.

James L. White, Major Professor

We have read this dissertation
and recommend its acceptance:

Accepted for the Council:

Vice Chancellor
Graduate Studies and Research

AN EXPERIMENTAL AND THEORETICAL STUDY OF THE WET SPINNING PROCESS

A Dissertation

Presented for the

Doctor of Philosophy

Degree

The University of Tennessee, Knoxville

Tony Alan Hancock

March 1981

3049550

DEDICATION

This dissertation is dedicated to my wife, Rhonda M. Hancock, and to my mother, Mrs. Ressie Hancock; both have continually encouraged me and kept me oriented toward God.

ACKNOWLEDGMENTS

The author wishes to express his appreciation to his advisor, Professor James L. White, for his guidance during the research. Many helpful discussions with Professor Joseph E. Spruiell and Professor Donald C. Bogue are also much appreciated. Services rendered by H. B. Thompson and the machine shop personnel, Ted Long and the electronic shop personnel, Al Carter, Ted Dehart, and the facilities group, and the entire Chemical, Metallurgical, and Polymer Engineering Department faculty and staff were greatly appreciated.

The help of many industrial researchers was also much appreciated: Dr. J. Preston, Dr. Fred Kanel, Dr. Arnold McPeters, and Dr. P. H. Hobson of Monsanto, Dr. John M. Davis and Dr. Earl B. Adams of DuPont, Dr. James Parker of American Enka, and Dr. Les LaNieve of Celanese. The encouragement of Dr. Sam Blair of IBM was greatly appreciated.

Financial support for this work was provided by the Plastics Institute of America and the Polymer Consortium and was appreciated.

ABSTRACT

Wet spinning apparatus was designed and built which is capable of producing commercial quality fibers. The materials studied were nylon-6, nylon-66, redissolved DuPont Nomex® and Kevlar®, polyacrylonitrile/7.5% vinyl acetate copolymer, and Bisacid A-2. Several solvents and coagulants were examined and their effects on the fiber superstructures were studied.

The superstructure of wet spun fibers may be classified as either (1) hollow core, (2) fluted core, or (3) sponge-like. All wet spun fibers may be considered to represent one or more of these classifications. Examples of each type were spun and examined by scanning electron microscope. The fibers were also studied with small angle x-ray diffraction.

A microscopic static coagulation technique was used to observe coagulation and the void forming process. By this technique and a hydrodynamic stability analysis, the fluted fibers were associated with a dimensionless group, $F = \frac{\mathcal{D}QC}{\kappa \bar{T}}$, i.e., the product of the diffusivity, heat of mixing, and the concentration divided by the product of the thermal conductivity and the temperature. The characteristic value for this group is $\frac{\mathcal{D}Q}{\kappa}(\frac{dC}{d\bar{T}})_{equil}$. Assuming that $(\frac{dC}{d\bar{T}})_{equil}$ is 0.1, fluted fibers are formed for values of F greater than 0.018.

The draw down of the fiber during the coagulation process was mathematically modeled. Plots of dimensionless fiber diameter vs.

dimensionless distance from the spinneret are presented and compared to experimental data. Hollow fibers were formed when a chemical reaction occurred at the fiber surface between the bath and solvent. This increased the mass transfer rate and it was shown that hollow fibers were prevalent at initial external Sherwood numbers greater than 20.

TABLE OF CONTENTS

CHAPTER		PAGE
I.	INTRODUCTION	1
II.	LITERATURE SURVEY	5
	System Dynamics	5
	Spinnability	5
	Force balance	8
	Emergence into the bath	10
	Analyses of wet spinning	12
	Solutions of Polymers	14
	General	14
	Aliphatic polyamides	15
	Aromatic polyamides	16
	Acrylics	18
	Diffusion and Coagulation	18
	Superstructure of Wet Spun Fibers	20
	Wet Spinning of Polyamides	22
	Wet Spinning of PAN	23
III.	EXPERIMENTAL DETAILS	24
	Materials	24
	Polymers	24
	Solvents	25
	Wet Spinning Equipment	25
	Scanning Electron Microscope (SEM)	29
	Small Angle X-ray Scattering (SAXS) Studies	30
	Optical Microscopy	30
	Interfacial Tension Measurements	31
	Drag Measurements	34
IV.	MODELING AND EXPERIMENTAL OBSERVATIONS OF THE WET SPINNING PROCESS	35
	Theoretical	35
	System dynamics	35
	Elongational viscosity	39
	Mass balances	43
	Mass transfer rate	44
	One dimensional model of wet spinning	46
	Initial conditions and extrudate swell	48
	Illustrative numerical solutions to one dimensional model	49
	Higher order analysis	53
	Solutions of special cases of higher order model	55

CHAPTER PAGE

Experimental 66
Systems studied 66
Types of fiber superstructures observed 68

V. MECHANISMS CAUSING HOLLOW CORE FIBERS 76
Introduction 76
Microscopic Observations 80
Proposed Mechanism for the Formation of Hollow Fibers . . 85
Radius Predictions 88
General 88
Illustrative calculations 92
Detailed calculations and comparison with experiments . 96

VI. MECHANISMS CAUSING FLUTED FIBERS 103
Characterization of Fibers Exhibiting Fluting 103
Observations of Mechanism of Fluting 108
Microscopic studies 108
Movement of the interface 116
Discussion 116
Comparison to observations on films 116
Statement of mechanism 118
Hydrodynamic stability interpretation 119
Stability Analysis for Coagulating Filament 121
Interpretation for Fiber Structure 127
Conclusions 130

VII. MECHANISMS CAUSING SPONGE-LIKE FIBERS 134
Systems Which Exhibit Sponge-Like Fibers 134
Microscopic Observations 138
Proposed Mechanism 141

VIII. CONCLUSIONS AND RECOMMENDATIONS 143

BIBLIOGRAPHY 145

VITA 156

LIST OF TABLES

TABLE		PAGE
III-1.	Solvents and Coagulants Used in This Study	26
IV-1.	Drag Forces at Various Velocities	37
IV-2.	Mass Transfer Coefficients by Analogy	47
IV-3.	Mass Transfer Coefficients by Analogy for Our Experimental Conditions	62
IV-4.	Experimental Conditions	62
IV-5.	Wet Spinning Systems Studied	67
IV-6.	Fiber Superstructures Resulting from Wet Spinning	73
V-1.	Stable Interfaces Studied under Microscope	83
V-2.	Final Fiber Diameters of Nylon-6 in Formic Acid	102
VI-1.	Systems Exhibiting Fluting	103
VI-2.	Characterization of Fluted Fibers	107
VI-3.	Systems Examined by Static Coagulation Technique	110
VI-4.	Studies of the Onset of Fingering	114
VI-5.	Physical Parameters of Solvent and Coagulants	128
VI-6.	Physical Parameters of Polymer Solutions and Coagulants .	129

LIST OF FIGURES

FIGURE		PAGE
I-1.	The wet spinning operation; (a) wet jet, (b) dry jet . . .	2
III-1.	Dope delivery system for wet spinning	27
III-2.	Wet spinning spinneret assembly	28
III-3.	Static observation of coagulation apparatus	32
III-4.	Addison and Elliot contracting jet apparatus	33
IV-1.	Drag force vs. fiber velocity from various correlations .	38
IV-2.	Shear viscosity vs. polymer concentration for several systems	42
IV-3.	Log dimensionless filament diameter vs. dimension distance from the spinneret as calculated the one dimensional model of wet spinning	51
IV-4.	Log dimensionless filament diameter vs. dimensionless distance from the spinneret at (a), (b), (c)	58
IV-5.	Solvent concentration profiles across the filament cross-section for water coagulant	63
IV-6.	Effective elongational viscosity vs. distance	64
IV-7.	Dimensionless filament diameter vs. dimensionless distance from the spinneret at various Trouton ratios	65
IV-8.	SEM photomicrograph of nylon-6 fiber spun from formic acid into 5% NaOH in water (100X).	69
IV-9.	SEM photomicrograph of Nomex fiber spun from sulfuric acid into water (200X).	70
IV-10.	SEM photomicrograph of nylon-6 fiber spun from formic acid into 4% methanol in water (200X)	72
IV-11.	Dimensionless filament diameter vs. dimensionless distance from the spinneret—theoretical predictions compared to experimentally measured final fiber diameters	75

FIGURE PAGE

V-1. SEM photomicrograph of nylon-6 fiber spun from formic acid into 5% NaOH in water; (a) 100X, (b) 200X 77

V-2. SEM photomicrograph of Nomex fiber spun from sulfuric acid into 5% NaOH in water (50X) 79

V-3. Optical micrographs of static coagulation of nylon-6 in formic acid with (a) water coagulant (b) 5% NaOH in water coagulant 81

V-4. Skin growth vs. time for static coagulation of nylon-6 in formic acid with various coagulants 82

V-5. Schematic of skin growth in coagulating filament 87

V-6. Log dimensionless filament diameter vs. dimensionless distance from the spinneret at (a), (b), (c) 93

V-7. Dimensionless filament diameter vs. dimensionless distance from the spinneret for various coagulants and die swells . 98

VI-1. Schematic of fluted fiber 104

VI-2. SEM photomicrographs of wet spun fibers; (a) 25% PAN/VA copolymer in DMAc water coagulation (200X), (b) 25% PAN/VA copolymer in DMAc water coagulation (2000X), (c) 20% Nomex in DMAc water coagulation (200X), (d) 16% Nomex in sulfuric acid water coagulation (200X) 105

VI-3. Static coagulation studies of PAN/VA in DMAc and water coagulant 111

VI-4. Static coagulation studies of polystyrene in DMAc and water coagulant 112

VI-5. Static interfacial studies between DMAc and water 113

VI-6. Coagulated distance vs. time 117

VII-1. SEM photomicrographs of (a) nylon-6 spun from formic acid into 10% formic acid; (b) nylon-66 spun from formic acid into 25% formic acid; (c) nylon-6 spun from formic acid into 4% methanol in water; (d) nylon-6 spun from formic acid into 4% methanol in water 135

VII-2. SAXS pattern of (a) wet spun nylon-6 from formic acid into 15% formic acid/water coagulant; (b) melt spun nylon-6 137

FIGURE PAGE

VII-3. Static coagulation studies of nylon-6 in formic acid with water coagulant 139

VII-4. Static coagulation or interfacial movement for formic acid 140

CHAPTER I

INTRODUCTION

There are three major methods for making synthetic fibers: (1) melt spinning, (2) dry spinning, and (3) wet spinning. Melt spinning involves melting a polymer and extruding the melt through a spinneret. The molten filament cools and solidifies to form the fiber. The other two spinning techniques involve dissolving the polymer with some solvent. The solvents must be carefully chosen; for dry spinning the solvent must be volatile to allow coagulation of the fiber. Dry spinning involves the extrusion of the polymer solution through a spinneret into a moving gas stream. The solvent evaporates into the gas stream leaving the solid fiber. Wet spinning involves the extrusion of a polymer solution through a spinneret into a liquid coagulation bath. This bath contains a polymer nonsolvent and allows the solvent to diffuse away from the polymer leaving a solid fiber.

A schematic representation of wet spinning is given in Figure I-1. This includes both wet jet and dry jet techniques. For a short distance into the coagulation bath, the threadline is a viscous liquid. As the filament coagulates a gel is formed of solid polymer and solvent. This gel becomes progressively more solid as it moves toward the rotating cylinder wind-up.

The first man made fibers were cellulosic and were produced by solution spinning because the cellulosic materials do not melt. In

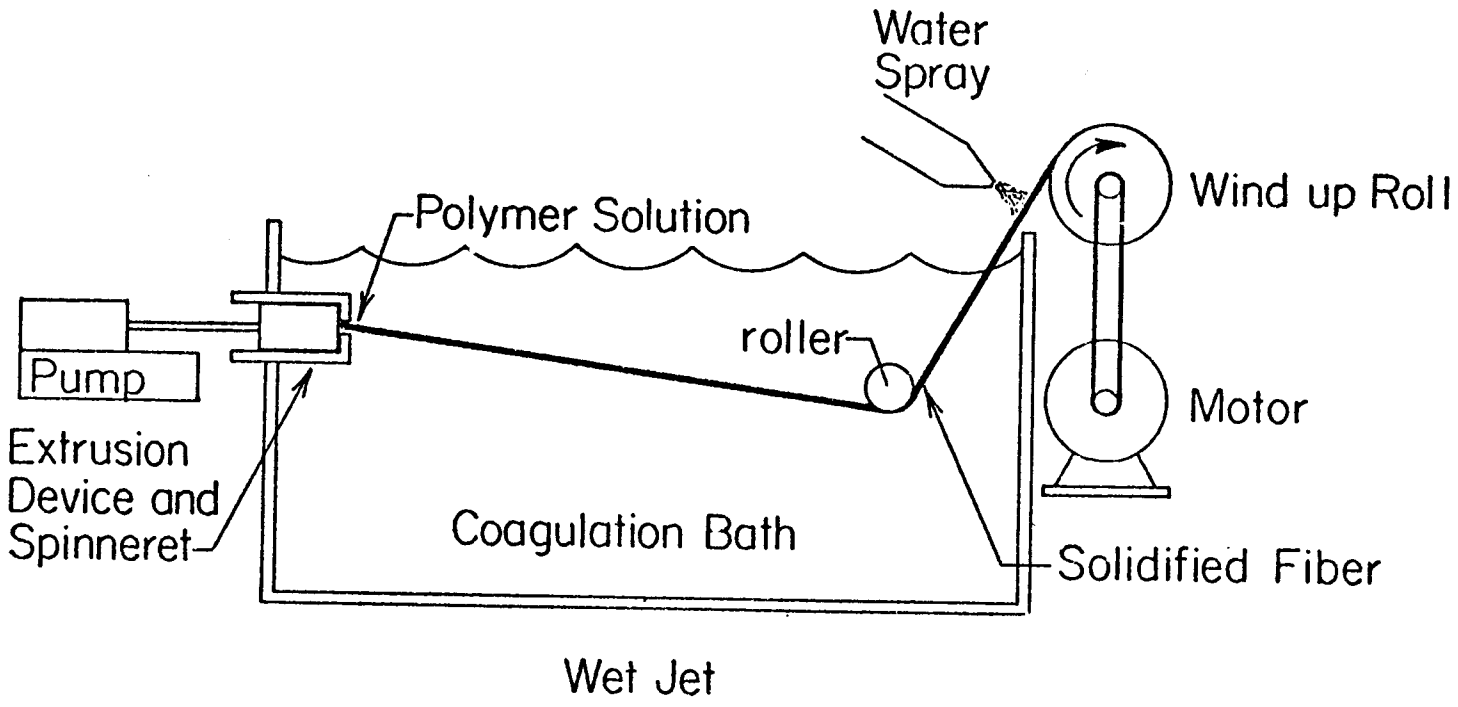

(a)

Figure I-1. The wet spinning operation; (a) wet jet, (b) dry jet.

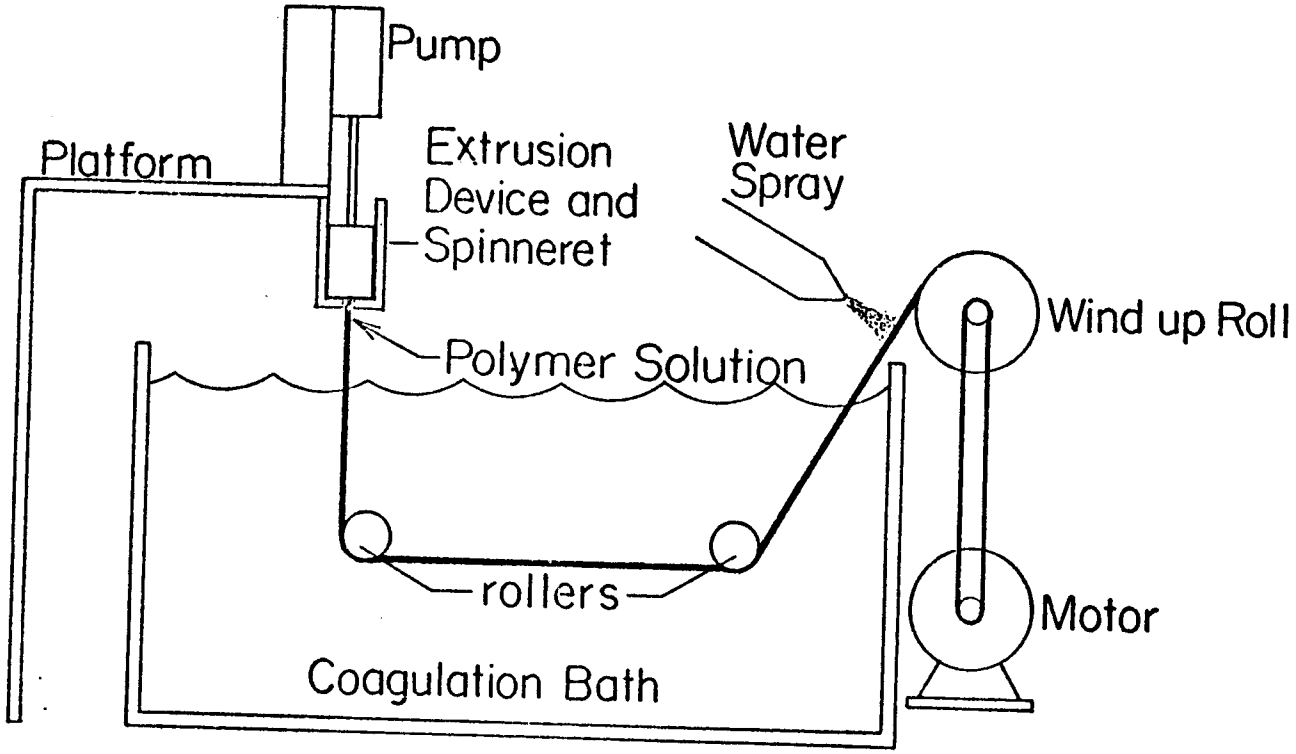

Dry Jet

(b)

Figure I-1. (Continued)

the 1400's the Chinese examined a process for grinding up dead silk worms in water and pulling out fibers. In 1884, Chardonnet documented and perfected a cellulose nitrate fiber by wet spinning. Two English chemists, C. F. Cross and E. J. Bevan, concentrated their efforts on pure cellulosic materials and fibers. In 1892, they began to commercially produce a regenerated fiber by wet spinning which is now known as viscose Rayon. More recently, polyacrylonitrile fibers produced by both wet and dry spinning have been commercialized. Nomex® and Kevlar® are two recently developed fibers which, due to their very high melting point, must be solution spun. Wet spinning has traditionally been over shadowed by melt spinning, but with the advent notably of the Kevlar super strength aromatic polyamide, wet spinning techniques have gained greater attention.

This dissertation deals with analyzing the wet spinning process. Several polymers were studied with several solvents and coagulants. The coagulation process was studied in depth using a microscopic technique. The structures developed in the fibers were studied via the scanning electron microscope as well as the optical microscope.

Various classes of void structures were detected and the mechanisms leading to their development were investigated. Theoretical models of the development of these void structures are considered.

CHAPTER II

LITERATURE SURVEY

I. SYSTEM DYNAMICS

Spinnability

Spinnability is an important consideration in any fiber forming operation. For successful wet spinning the polymer solution must be able to support the spin line force until a solid skin of polymer is formed due to coagulation. Rayleigh (148) first discussed the capillarity instabilities of a long cylindrical column of incompressible, inviscid liquid. He followed Plateau's observations and gave a mathematical analysis of the tendency of a cylindrical jet to break up into drops. He observed (149) this break up into droplets and correlated the wavelength of the instability with the pressure on the jet. Later on Rayleigh (150) included the viscosity of the jet as well as inertial forces in his analysis. Without viscous forces the filament tends to be unstable if the wavelength of the instability is greater than the circumference of the cylinder, but with viscous forces included the critical wavelength is much longer. This means that a viscous jet will break up into sections, but the sections will be longer. The growth rate of the instability is also damped by the viscous forces. Weber (186) obtained an assymptotic, one-dimensional linear solution for a viscous jet under surface tension. He included the effects of an inviscous surrounding. Tomotika (180) has further

extended this analysis to include effects of the viscosity of a surrounding liquid on the filament. He found that the wavelength of the instability was a function of the ratio of viscosities of the filament and its surroundings. He verified this experimentally. He also studied the effects of moving the surroundings at a uniform rate (181). This stabilized the filament and allowed it to remain cylindrical much longer. He predicted that the resulting droplets would be much smaller when the surroundings were caused to flow than when the surroundings were stationary.

Spinnability requires that the filament not break up into droplets. Nitschmann and Schrade (126) have argued that spinnability requires an increase in the stretching viscosity with deformation rate. This marked the first attempt to explain spinnability with changing fluid properties. More recently Kroesser and Middleman (102) have extended Weber's theory for a Newtonian jet to a linear viscoelastic fluid. The theory predicts that the maximum length of viscoelastic jets before break up is shorter than that for Newtonian jets. They introduce an elasticity number (the ratio of the Weissenberg number to the Reynolds number) which they call a key parameter and correlate break up lengths with it. They neglect the effects of normal stresses generated in the die. Goldin et al. (68,69) came to similar conclusions using a linearized stability analysis to show that a liquid jet of viscoelastic fluid exhibits a more rapid growth of axisymmetric wave disturbances than a Newtonian fluid of the same shear viscosity. They support this with experiments on weakly elastic fluids, but concede that highly elastic fluids show nonlinear

phenomena. This elasticity accounts for the unusual stability of such fluids. Tomotika (181) and later Ide and White (84, 86, 87) have studied capillarity instabilities in filaments under extension. Tomotika caused the surroundings of the jet to move and thus extended the jet. He found that the jet was stable to longer lengths and had lower growth rates of the instability. This resulted in smaller drops when the jet was being extended. Ide and White carried out a linear stability analysis using a White-Metzner convected Maxwell model with a deformation rate dependent relaxation time. They found that viscosity tended to stabilize and viscoelasticity tended to stabilize or destabilize depending on the deformation rate dependence of the relaxation time. Under stable conditions cohesive failure was presumed to occur at some critical stress level. Filament stability and elongation to break was shown to depend upon the product of the relaxation time and the elongation rate (Weissenberg number) and material parameters which represent the deformation rate dependence. This was experimentally verified using a constant elongation rate apparatus and polymer filaments above their melting point or glass transition temperature. Relationships between failure of the filament and polymer molecular weight were also developed.

A great many experiments relating to the wet spinnability of PAN/VA copolymer have been performed by Paul (133). He defined the general area but does not state a single, fundamental mechanism. In general, he discusses two possible mechanisms of failure: (1) a telescopic type notion separating the solid-liquid boundary in a partially coagulated

section of fiber and (2) a rupture of the skin due to excessive tensile stress. Ferguson and Ibrahim (55) have studied the rheological properties of cellulose acetate spinning solutions using a Weissenberg rheogoniometer. They found that the rheological properties which they measured (e.g., viscosity at various shear rates, relaxation time, elastic modulus, normal stress) of the solutions had little effect on spinnability. The properties of the partially coagulated filaments were found to determine the spinnability criterion. This finding is in agreement with other studies (133, 188) which conclude that spinnability is a function of almost every variable in the wet spinning process.

Force Balance

Ziabicki (192) has presented a force balance for fiber spinning processes. This analysis was demonstrated for the melt spinning of polycaproamide, but can be generalized to include wet spinning. The implications of this were discussed qualitatively. Brinegar and Epstein (30) have developed a similar analysis from a phenomenalogical approach. They write the integrated force balance:

$$F_T = F_{SF} + F_{KE} + F_H + F_D + F_{SB} + F_{RH} \qquad (2\text{-}1)$$

where,

F_T = the total force required to draw the filament from the spin bath.

F_{SH} = the filament surface tension force acting near the spinneret tending to shrink the filament into droplets.

F_{KE} = the kinetic energy momentum force required to accelerate the fiber from extrusion velocity to take-up velocity.

F_H = the hydraulic drag force required to overcome the hydraulic resistance in moving the filament through the bath.

F_D = the frictional drag force required to overcome the friction at the guides and rollers.

F_{RH} = the rheological force acting near the spinneret.

They evaluated the hydraulic drage force from the empirical Fanning friction factor as follows:

(inside spinning tube)

$$F_{HI} = \frac{\pi}{2} DL\rho V^2 f \text{ where } f = 0.00140 + .35N_{R_e}^{-.32} \quad (2\text{-}2)$$

(outside spinning tube)

$$F_{HO} = 0.664\ \pi D\ (\rho\mu\beta V^3)^{\frac{1}{2}} \quad (2\text{-}3)$$

The kinetic energy force was determined from:

$$F_{KE} = \left(\frac{\pi}{8}\right) \Delta\ (\rho D^2 V^2) \quad (2\text{-}4)$$

They experimentally determine F_T using a tension measurement, and by measuring the other terms of the force balance they evaluate the rheological force.

Ziabicki and Kedzierska (193) first examined the mechanical aspects of the melt spinning process. Their efforts included studies of the drag on the filaments which they estimated with coefficients developed by Prandtl for a flat plate. Drag on cylinders and the boundary layer near the surface has been extensively studied by Sakiadis (156, 157). Sakiadis used the von Karman momentum integral method and

assumed velocity profiles (that satisfy the boundary conditions) to derive the relationship between the drag coefficient and the Reynolds number. Sano and Orii (158) have carried out experimental measurements of the melt spinning of polypropylene filaments. Empirical drag correlations were developed by analyzing the change in tension at various distances along the spinline. These correlations are somewhat lower than the values derived by Sakiadis. Vasudevan and Middleman (184) have also used boundary layer (similarity transformation)techniques to solve the transport equations for the region around a cylindrical jet issuing continuously from an orifice. They allow for the effects of mass transfer normal to the jet and show that the local skin friction is reduced by the mass transfer. Several other groups (2, 3, 71) have developed experimental correlations. These are compared in Chapter IV.

More recently Ziabicki (194) has surveyed the literature on wet spinning force balances. He describes a drag force on the filament due to the viscosity of the bath (i.e., the force necessary to move the bath along with the filament). Ziabicki argues that under spinning conditions of interest, this force comprises 75-95% of the total spinning tension.

Emergence into the Bath

A phenomena known as extrudate swell has long been observed in extrusion processes such as fiber spinning operations. Harmon (76) used a mass and momentum balance between the exit of the jet and the point downstream where the velocity profile is flat to analyze the behavior of Newtonian liquid jets. His work accounted only for the contraction of the jet and predicted a value of 0.866 for the ratio of the jet diameter

to the capillary diameter. Middleman and Gavis (117, 118) examined the expansion and contraction of capillary jets of Newtonian fluids. They used hydrodynamic and dimensional analysis arguments to predict the ratio of the jet diameter to the capillary diameter. This ratio was shown to be a function of the Reynolds number and the Weber number. At Reynolds numbers less than six, the ratio was independent of Reynolds number and limited to 1.06. The ratio was observed to approach 0.866 for high Reynolds numbers.

Metzner et al. (115) proposed using capillary jet diameter measurements as a method of obtaining normal stresses. They made a momentum-force shell balance between the fluid leaving the capillary and a point downstream where the velocity distribution is flat. They assumed steady, simple shear flow, incompressible fluid and neglected interfacial and gravitational effects. Their equations reduce to Harmon's analysis for such low viscosity fluids as water and alcohol. They showed that for polymer solutions at high Reynolds numbers, the existence of normal stresses greatly increased extrudate swell. The normal stresses computed were consistent with rheogoniometer normal stresses. More recently, Tanner (173) has approached the low Reynolds number problem using the concept of unconstrained elastic recovery. He made two simplifying assumptions: (1) negligible inertial effects, and (2) Maxwellian behavior with no delayed recovery. With these assumptions and the more classical assumptions of isothermal and incompressible flow and a very long die, his theoretical analysis fits the experimental data for polystyrene nicely. White and Roman (155) have examined extrudate

swell for several kinds of polyethylene, polypropylene, and polystyrene. They analyze the problem in terms of dimensional analysis, force-momentum balances, and partially constrained elastic recovery and show the relation between the extrudate swell and applied take-up force. Their experimental data agree reasonably well with Tanner's prediction, if only instantaneous elastic recovery is considered. Paul (133) has confirmed that extrudate swell occurs in wet spinning and that the fiber diameter may be larger or smaller than the spinneret hole diameter depending upon the take-up velocity.

A largely experimental study by Fitzgerald and Craig (57) has defined three major wet spinning variables as: flow rate, spinneret hole size, and spinning speed. These may be lumped into one term, the jet stretch (i.e., the ratio of the velocity of the fiber out of the spin bath to the average velocity in the spinneret). They determined that their solutions were viscoelastic and shear thinning and further noted that under normal spinning conditions the major contribution to flow retardation was the elastic properties and not the viscosity. Paul and Armstrong (140) have also examined the effects of the elastic forces during wet spinning. They found that the spinning pressure was a function of the jet stretch. The shape of the jet was examined under a microscope at various jet stretches.

Analyses of Wet Spinning

Han and Segal (72, 73) have carried out an analysis of the wet spinning of polyacrylonitrile in a bath of sodium thiocyanate. They obtained elongational viscosity of the filament as a function of

distance from the spinneret by measuring the total force (tension) on the filament bundle and the filament diameter. They did this for several bath concentrations and extrapolated their results to a point of no coagulation. Further studies use this information to model the process using variables such as free velocity, throughput rate, maximum take-up velocity, jet stretch, and filament tension. Yerushalmi and Shinnar (189, 68, 69) have also modeled the wet spinning of viscous fluids. They presume a Newtonian fluid with no coagulation and derive a prediction for the maximum filament length (i.e., the length beyond which the take-up and drag forces break the filament). It is shown that the maximum filament length is directly proportional to the initial radius of the filament and the square root of the ratio of the viscosities of the fluid and its environment. They also calculate a drag force on the filament based on the take-up velocity, bath viscosity, and filament radius.

Terada (175-179) has analyzed the diffusion process in wet spinning. His experimental work points out a new method for calculating an apparent diffusion coefficient. This will be discussed in the section on coagulation in this chapter. Griffith (70) used an optical microscope to experimentally measure the velocity distribution. He then theoretically calculated the temperature and concentration profiles around a single filament during wet spinning. The theoretical calculations were based on solving the laminar axisymmetric boundary layer equations for a solid cylinder moving with uniform velocity through a semiinfinite, homogeneous

bath. He also found that the elastic forces within the spinneret were responsible for most of the tension needed in the spinning of PAN.

Throughout all of this work no mathematical analysis has been found which includes concentration changes across the radius. Kase and Matsuo (91, 92) have derived such a set of equations for melt spinning. Their analysis involves the simultaneous solution of a heat, force, and material balance and provides a good prediction for melt spinning, but it does not account for radial temperature variations.

Modeling of the dry spinning process has been carried out by Ohzawa and Nagana (127, 128) and Brazinsky, Williams, and LaNieve (28). These authors have dealt with the accompanying mass transfer, but they have neglected any radial variation of concentration.

II. SOLUTIONS OF POLYMERS

General

The behavior of concentrated polymer solutions is not completely understood, but many experimental and theoretical studies have been carried out in the area. Low molecular weight solutions are more easily understood because kinetic terms are not as important as equilibrium thermodynamics. At equilibrium, it is evident that for maximum solubility ΔG must be minimized (i.e., $\Delta G < 0$). This in turn means that ΔH should increase or remain small. Flory (58) and Huggins (83) formulated a quantitative theory of the change in conformational entropy produced by the mixing of flexible chain polymers with a low

molecular weight solvent. They evaluated the number of possible ways in which a given number of solvent molecules of a specific molar volume and a given number of polymer chains with a specific molar volume could be placed on a lattice so that each lattice site was occupied by a solvent molecule or polymer chain segment. Clearly, it is not possible for two molecules to occupy the same position in space. This fact was used to approximate the probability of occupancy of each lattice site based on the overall fraction of occupied sites. The theory should be most applicable to hydrocarbon polymers in nonpolar solvents. Hydrocarbon crystalline polymers such as polyolefins are generally insoluble below their melting point. This is not the case for polar polymers. The thermodynamics of solution are enhanced by large heats of solution (i.e., negative ΔH).

Aliphatic Polyamides

Nylon-6 is known to dissolve in several solvents including formic acid, sulfuric acid, chloral hydrate, and hexafluoroisopropanol. It is also known that high molecular weight nylon-6 has limited solubility in all solvents. The Flory-Huggins theory predicts such a decrease in solubility with an increase in molecular weight. This is due to the polymer-solvent interactions (hydrogen bonding) and the crystallinity of the polymer. Huglin and Richards (84) have examined the nature of chloral hydrate as a solvent for nylon-6 and 66. It is reported that due to the high temperature necessary to melt chloral hydrate and the time required for dissolving nylon-6 that much degradation occurs. Sbrolli (161) has studied the behavior of nylon-6 and sulfuric acid

solutions. Viscosity versus concentration and viscosity versus molecular weight curves are given. Kiyotsukuri et al. (96) examined five spinning solvents for nylon-6: (1) phenol, (2) o-chlorophenol, (3) sulfuric acid, (4) formic acid, and (5) dichloroacetic. They determined that the formic acid solutions produced the most uniform fibers. Aoki, White and Fellers (5) report extensive normal stress measurements.

Aromatic Polyamides

Dimethylacetamide, dimethylformamide, and sulfuric acid are among the solvents for poly (m-phenylene isophthalamide) which is commercially called Nomex®. Klenin, Prozorov, Prozorova, and Zhizdyuk (100) studied the structure of solutions of poly (m-phenylene isophthalamide) in dimethylacetamide using turbidity measurements. These values were then related to end product properties. Harwood (77) has studied the dilute solution behavior of Nomex in DMAc with lithium chloride present. The polymer was found to exhibit a polyelectrolyte effect as a result of complexes formed between the polymer, DMAc, and LiCl. Aoki, et al. (4, 5, 6,) has further examined Nomex solutions in several solvents at concentrations up to 25 weight percent. Viscosity versus shear rate and normal stress data were taken and compared with similar measurements on a para-linked analog. It was found, in general, to behave as a flexible molecule with rheological properties strongly dependent on concentration. Baird (13) has further discussed and characterized these solutions and their stabilization. The physical properties of these

solutions in products are discussed in U.S. patents by Foldi (60), Kwolek (104), and Bair (2).

The para-linked aromatic polyamide, poly (p-phenylene terephthalamide), is very insoluble in many solvents. Two possible solvents are hexamethylphosphoramide and fuming sulfuric acid. Sulfuric acid must contain no more than 2% water if it is an acceptable solvent. The dopes form liquid crystalline suspensions at high polymer concentrations.

Most liquid crystals are low molecular weight organic compounds. Generally liquid crystals are classified as smectic, nematic, and cholesteric depending upon the detailed type of order developed. High molecular weight liquid crystals behave in a similar manner. Elliot and Ambrose (47) first noted spherulites in an evaporating solution of poly-γ-benzyl-L-glutamate in chloroform. Robinson et al. (152,153) interpreted these observations as due to the formation of cholesteric liquid crystals in the concentrated solution. They also established the critical concentration for forming anisotropic phases and showed that this concentration is a function of molecular weight. They viewed the liquid crystalline phases as having the chains arranged in layers which twist relative to each other. This has been used to explain the flow properties of liquid crystalline solutions.

Flory (59) has developed a statistical thermodynamic theory of solutions of rigid rod-like macromolecules. He used a simplified model and derived an expression for the free energy of mixing. It was found that the assymetry of rigid macromolecules caused the phase separation and was not aided by a change in heat of solution.

Acrylics

Polyacrylonitrile homopolymer is not easily soluble in any common solvent, but a copolymer of PAN/2.5% vinyl acetate is soluble in dimethyl acetamide, dimethyl formamide, and propylene carbonate among other solvents. The solutions formed are easily coagulated with water or water-solvent mixtures. When similar solvents are used, PAN and poly (m-phenylene isophthalamide) solutions behave similarly and are typical of polymer solutions. They are isotropic, viscous solutions.

III. DIFFUSION AND COAGULATION

As the filament of polymer solution is drawn through the coagulation bath, the solvent diffuses out of the filament and on some occasions the coagulant diffuses into the filament. Coagulation is the precipitation mechanism by which the polymer solution forms a solid fiber. When the concentration of the polymer solution reaches an equilibrium limit (as a result of the diffusion process), the polymer precipitates out of solution forming the fiber.

Epstein and Rosenthal (54) have wet spun poly hexamethylene terephthalamide and studied the coagulation process. After defining optimum coagulation conditions, they examined the coagulation phenomena under an optical microscope. Motion pictures were made of the microscopic studies and these photographs show finger-like intrusions which grow into the polymer solution. These intrusions are not explained but are described very well and discussed in terms of a diffusion model. It was found that the linear relationship between square root of time

and penetration distance holds only for very short times at the beginning of the coagulation.

The wet spinning of rayon is omitted from discussion since the process involves a chemical reaction at the interface which chemically modifies the polymer rather than a typical coagulation process which does not. Hermans (80) used an analysis which allowed for diffusion with moving and discontinuous boundary to model the coagulation process in wet spinning. Paul (132) has done a considerable amount of work on the wet spinning of acrylic fibers. His work has involved both experimental studies and equimolar diffusion theory. Much of this work was done on rods of gelled PAN/DMAc many times larger than fibers. The large samples lengthened the time scale of coagulation so that the diffusion process could be observed at varying intervals. This work was used later in conjunction with a spinnability study (133).

Paul (135, 137, 139, 140) also used swollen rubbery membranes to study diffusion and measure diffusivities of several organic liquids. Diffusivities of several solvents in concentrated polystyrene solutions (136,141) have also been measured by the wedge interferometer technique. Diffusivity was found to vary with polymer molecular weights up to a limiting molecular weight value. Booth (25) also examined filaments at varying degrees of coagulation. He postulated a two-stage coagulation technique to achieve this and analyzed the results in a similar way to Herman's diffusion reaction model of Xanthate ripening. Booth studied the coagulation of PAN fibers in aqueous zinc chloride and found the apparent diffusion coefficient to be of order $10^{-6} cm^2/sec$. Many classical diffusion studies have been reviewed by Crank (39). These

classical methods are intimately intertwined in most of the coagulation models.

IV. SUPERSTRUCTURE OF WET SPUN FIBERS

Wet spun fibers are generally observed to be much more porous than their melt spun counterparts. This porosity was noted in 1945 by Morehead and Sisson (124) in Rayon fibers. The porosity was explained in terms of a skin and core structure. They show that one can obtain either an unoriented skin and unoriented core or an equal axial orientation throughout the cross section by varying the stage of stretch during wet spinning. This is true because drawing in the region where a liquid core exists simple produces an oriented skin, whereas drawing after complete coagulation produces a totally oriented fiber. In 1956, Scott and Ferguson (56) further studied the superstructure of several kinds of fibers with the electron microscope. They verified the existence of voids in wet spun fibers. In the same year Statton (167) used small angle x-ray scattering to study the void content in cellulosic fibers. He gives experimental scattering results and interprets the data qualitatively. Crystallites also scatter x-rays. This causes difficulties in distinguishing between diffraction from crystallites and voids. Statton (168) further studied this problem in 1962. He examined melt, wet, dry, and dispersion spun fibers and found that the diffuse scattering (i.e., void content) increased from melt spun fibers (least), dry spun, wet spun, dispersion spun fibers (most). The change of these voids with drawing was also examined.

Singleton, Sieminski, and Sprague (165) have also studied the skin and core structure. They used cellulose triacetate and showed that the skin and core effect was more drastic on rapidly coagulated fibers. Craig, Knudsen, and Holland (40) have examined the structure of acrylic fibers. These wet spun fibers are reported to have a fine structure as examined through gas adsorption, density, electron microscopy, and light microscopy. This structure was further characterized as fibril-void with fibrils and voids of the order 200A diameter. The size and shape of the voids were examined using the BET surface area method. As-spun fibers were found to be very permeable to gases and liquids, whereas oriented fibers collapsed and uncollapsed were less permeable. Rebenfeld (151) has also examined a number of fibers with the optical microscope and reported similar findings.

Knudsen (101) examined the effects of the coagulation process on the resulting fiber properties and structure. He used an acrylic system, but in general, the results indicate that as bath temperature is lowered the fiber properties improve. This may be due to a decrease in porosity with temperature. Zwick and von Bochone (195) studied the wet spinning of polyvinyl alcohol fibers and defined the values of parameters necessary to produce low elongation, high strength fibers. They found that slowing down the coagulation produced optimum values of strength and stiffness. Van Veld, Morris, and Billica (183) used the scanning electron microscope along with peeling techniques to study the internal fiber superstructure. They compare both melt spun and wet spun fiber superstructure.

V. WET SPINNING OF POLYAMIDES

Kiyotsokuri and his coworkers (95-99) have studied the wet spinning of nylon-6. They have characterized the wet spun fibers using x-ray scattering and optical microscopy. It was reported that wet spun fibers were obtained of the α-form for all acidic coagulation baths, but the γ-form was obtained when alkaline coagulation baths were used. The effects of spinning solvents on fiber properties were also studied (96). Five spinning solvents—phenal, o-chlorophenol, sulfuric acid, formic acid, and dichloroacetic acid—were used. The fibers produced were reportedly very porous and exhibited a skin-core structure especially when formic acid was used as a solvent. Formic acid was defined as the optimum spinning solvent.

Considerable effort was expended in the Monsanto laboratories to study the wet spinning of nylon-66 (182). This work showed that nylon-66 spun from formic acid into sodium hydroxide yielded reasonable fiber. This was not pursued further due to the economics of the process. More recent work by Hancock, Spruiell, and White (74, 75) has dealt with wet spinning of both aliphatic and aromatic polyamides. Nylon-6 and nylon-66 were wet spun from formic acid and the resulting fibers were examined using physical properties, x-ray analysis, and electron microscopy. These same characterization techniques were applied to redissolved Nomex fibers wet spun from dimethylacetamide and to redissolved Kevlar fibers spun from sulfuric acid.

Several patents have been issued concerning the wet spinning of the aromatic polyamides. The patents (21, 26, 94) speak of polymer

dissolution and of spinning techniques. Specifically the dry jet wet spinning method is claimed for spinning the para-linked aromatic polyamides. This technique is characterized by an air gap between the spinneret and the coagulation bath. The spinning dopes used are generally anisotropic liquid crystals. Laszkiewicz and Lewandowski (105), Ciferri (36), and Jaffe (89) have reviewed the patent literature and conducted further experimental investigations of the spinning process. Jaffe (89) further analyzes the air gap and postulates a molecular mechanism for why strengths are higher with the air gap.

VI. WET SPINNING OF PAN

Polyacrylonitrile is wet spun commercially. Because of this commercial importance, much experimental work has been published concerning the PAN and DMAc system. Knudsen (101) has examined coagulation as a factor affecting fiber structure. His findings showed a strong dependence of porosity in the fibers on the coagulation bath temperature. He attributed this dependence to coagulation rate. Further examination of wet spun PAN fibers was carried out by Craig, Knudsen, and Holland (40). Their studies made use of electron microscopy to study the fiber microstructure. Much of the previously discussed wet spinning modeling work was done with PAN. Griffith (70), Paul (132, 133, 134) and Han and Segal (72, 73) all used PAN solutions for their work.

CHAPTER III

EXPERIMENTAL DETAILS

I. MATERIALS

Polymers

Five polymers were used for the majority of the wet spinning research. Four of these were polyamides, two each of the aliphatic and aromatic varieties. The fifth polymer was an acrylic.

Nylon-6 and nylon-66, the two aliphatic polyamides, were chosen because of their industrial importance and because of their unique wet spun fiber superstructure discussed in the literature survey and the author's M.S. thesis (41,42). The nylon-6 polymer was a high molecular weight (M_n~34,000) grade supplied by Allied Chemical. The nylon-66 polymer was also a high molecular weight grade (M_n~28,000) supplied by DuPont. It is a commercial polymer sold as Zytel® molding resin.

The two aromatic polymers chosen are also the two most industrially significant aromatic polyamides: Nomex® (poly m-phenylene isophthalamide) and Kevlar® (poly p-phenylene terephthalamide). The DuPont company supplied both polymers in the fiber form. The fiber was then chopped into short lengths and redissolved. The Nomex® was characterized by intrinsic viscosity and found to have a weight average molecular weight of 89,000. The Kevlar® was also characterized by intrinsic

viscosity and was found to have a number molecular weight of 50,000.

The acrylic polymer which was studied was a Polyacrylonitrile/vinyl acetate copolymer supplied by Monsanto. Its composition was 97.5% PAN/2.5% VA and it was supplied as a powder. This copolymer is commercially wet spun by Monsanto and was chosen for this reason. The PAN homopolymer was not easily available nor did it lend itself to the easy formation of solutions.

Polystyrene was also used for some of the microscopic coagulation studies. Dow Styron 678U was chosen because of availability. Polystyrene is readily soluble in a number of solvents and was used to check polymer-solvent-coagulant interactions.

Solvents

The main solvents used were formic acid, sulfuric acid, and dimethyl acetamide. The formic acid used was obtained from Fisher as 90% formic acid purified A119. The sulfuric acid used was 100% acid made by mixing appropriate amounts of Fisher concentrated reagent grade (95-98%) sulfuric acid and Fisher fuming sulfuric acid (30% excess SO_3). The n,n-dimethyl acetamide used was obtained from the Aldrich Chemical Company. Other solvents used in microscope coagulation studies were also obtained from Fisher. See Table III-1 for a summary of solvents and coagulants used in this study.

II. WET SPINNING EQUIPMENT

Three essential pieces of equipment are needed for wet spinning: (1) a method for extrusion of the solution through an orifice at a

TABLE III-1

SOLVENTS AND COAGULANTS USED IN THIS STUDY

Solvents	Coagulants
Formic acid	Water
Sulfuric acid	Methanol
Dimethyl acetamide	n-heptane
p-xylene	Acetone
Benzene	(Combinations of solvents & coagulants)
Methyl ethyl ketone	
Ethyl acetate	

constant and steady rate, (2) a bath for coagulation of the solution into a fiber, and (3) a take-up device.

A positive displacement pump, which supplies a constant rate regardless of pressure, was used for the delivery system. The first pump used was the Harvard Apparatus Infusion-Withdrawal Pump. This pump consisted of a constant drive for a piston in a cylinder full of spinning solution. This worked quite well up to a certain limit pressure beyond which it was not powerful enough to deliver at a constant rate. An extrusion device was fabricated from 316 stainless steel to fit this pump and several spinnerets were also made. The next generation delivery system was a much more flexible gear pump arrangement (see schematic Figure III-1). The gear pump used was obtained from Zenith (1/2 size 0.297 cc/rev., BPB-4391-.297). The motor drive was obtained from B & B Motors (D13-43C-1D, 324 in-lb, 1.3-52 RPM, 1/3 HP with motor controller MR-50). A 0.0048 inch square mesh filter was used to remove any gel particles, etc. from the solution. The spinnerets were supplied by the Monsanto Company (6 hole × .015 inch and 6 hole × .006 inch)(Figure III-2)

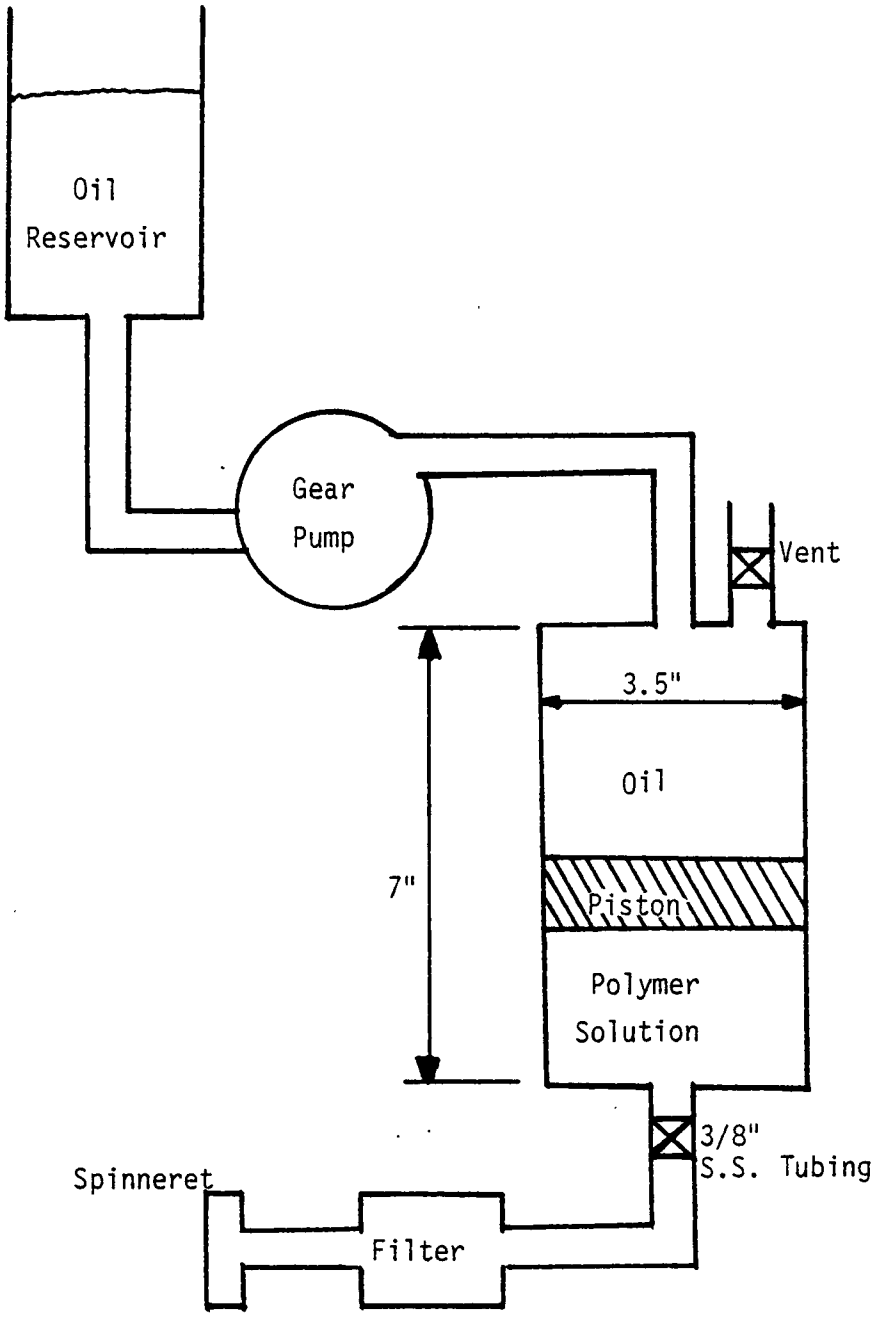

Figure III-1. Dope delivery system for wet spinning.

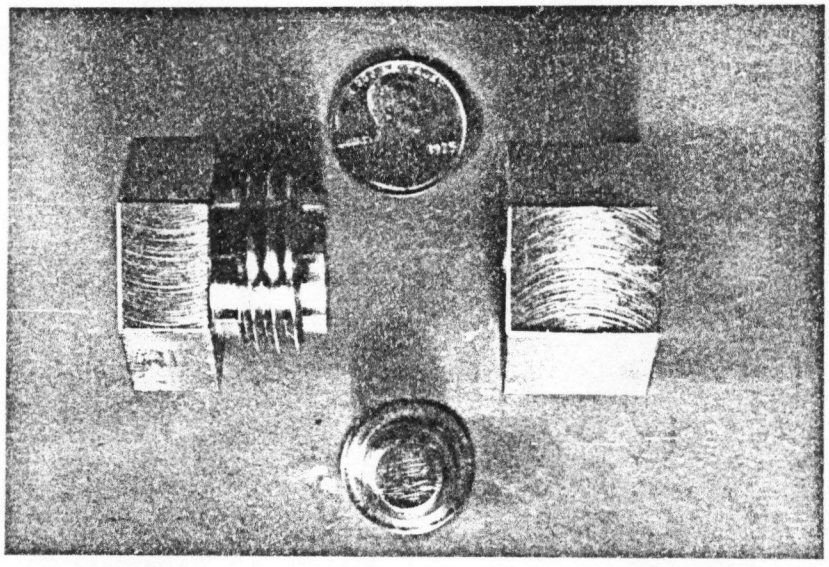

Figure III-2. Wet spinning spinneret assembly.

Adaptors were made so that the single hole spinnerets of the previous system also fit. For spinning dopes containing sulfuric acid,a secondary pumping fluid (motor oil) was used as shown in Figure III-1.

The primary coagulation bath was constructed of aluminum 6 feet × 8 inches × 4 inches. Other coagulation baths were used occasionally with glass sides so that the coagulation could be observed.

The wind-up device consisted of three variable speed motors with idler rolls and a textile winder. The first motor is a Bodine Electric Company, 1/20 HP motor with a wide spool, idler roll, and water spray. The second motor is a Heller GT21-18, 1/40 HP motor with a wide spool, idler roll, and heat lamp to dry the fiber. The third motor is a Heller GT60-40 & C-25 controller with an idler roll and is used to provide the Leesona 955 winder a constant feed. The winder speed is controlled by a constant tensioning arm.

III. SCANNING ELECTRON MICROSCOPE (SEM)

An AMR Model 900 High Resolution Scanning Electron Microscope (Advanced Metals Recearch Corporation, Burlington, Massachusetts) was used in this study. The surface and cross section of the as-spun fibers and films were observed. A primary advantage of the SEM is its great depth of field; thus both the surface and the center of the fiber may be observed in focus at relatively high magnifications. The fiber specimens were mounted using holders built for the fibers. A hole of approximately the same size as the fiber was drilled in the standard stools used for SEM work. The fiber was then pulled through the hole and glued in place with silver paint leaving several inches at either

end. The lower end was then clipped with scissors and the upper end was frozen in liquid nitrogen and fractured at about one-eighth inch above the stool. This process avoided the creation of artifacts by smearing as happens when cut. After the sample was mounted, it was then coated with a gold-palladium alloy or with silver. The coating was applied with a Technics Hummer I sputter coater.

IV. SMALL ANGLE X-RAY SCATTERING (SAXS) STUDIES

Small angle x-ray patterns were obtained using a Rigaku-General Electric Rotating Anode x-ray generator operated at 55 KV and 80 ma. The radiation used was nickel filtered copper K-α of wavelength 1.542 angstroms. The sample to film distance is 400 mm and the camera was evacuated with a mechanical pump. The diffraction patterns were taken on Kodak blue brand x-ray film BB54.

V. OPTICAL MICROSCOPY

Two optical microscopes were used for different portions of this work. A Leitz Wetzler ortholux microscope was used to obtain still photographs of coagulation. A Leitz Wetzler 4 inch × 5 inch automatic camera is mounted on the microscope for taking the still photographs. A Leitz Orthoplan microscope equipped with a Motorola S1140B-VSP17 closed circuit television camera was used for dynamic observations of the coagulating interfaces. The camera was attached to a Sony Videocorder EV-310 to record the time dependent nature of the interface.

The previously described microscopes were used primarily to observe coagulation by way of a static coagulation arrangement. This involved

placing a drop of polymer solution on a glass microscope slide, covering it with a cover slip, and surrounding it with coagulant (Figure III-3). The coagulant was drawn under the cover slip by capillary action and an interface between coagulant and polymer solution was formed. This interface was observed through the microscope at low magnifications (20-40X).

A metallurgical microscope (Leitz Orthoplan-Reflected Light) and stereo zoom Bausch & Lomb microscope were also used to examine frozen cross sections of partially coagulated fibers. This was used in conjunction with a cold stage and a liquid nitrogen reservoir. This process involved very rapid sampling and photography and was used only qualitatively for these reasons.

VI. INTERFACIAL TENSION MEASUREMENTS

A contracting jet apparatus similar to that described by Addison and Elliott (1) was constructed (Figure III-4). This device allowed the measurement of interfacial tension as a function of time for immiscible or partially miscible liquids. No calibration of the apparatus was performed because the data was only qualitatively useful. The liquids significant to this study are fully miscible at equilibrium and only exhibit a dynamic interfacial tension. This dynamic interfacial tension changes very rapidly and could not be measured. It was observed qualitatively for several different liquids that the interfacial tension does exist for some time period during mixing.

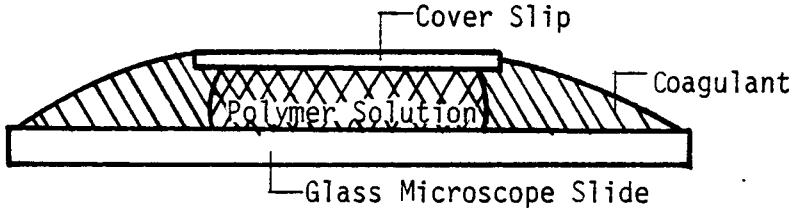

Figure III-3. Static observation of coagulation apparatus.

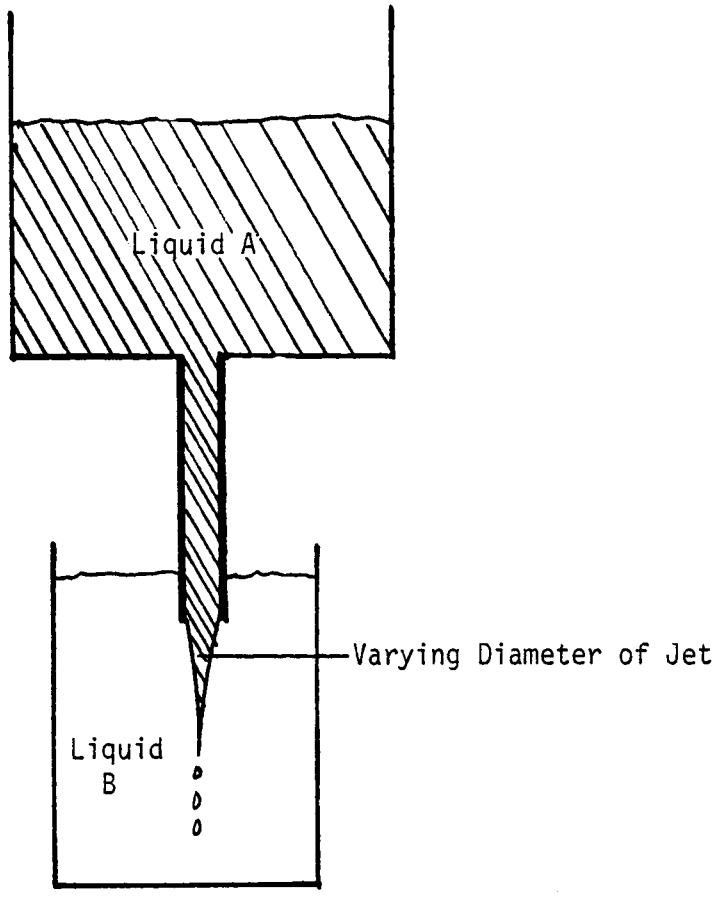

Figure III-4. Addison and Elliot contracting jet apparatus.

VII. DRAG MEASUREMENTS

A Rothchild tensiometer with a 0-10 gm head was used to make tension measurements on the spinline. The specifics of the measurement are discussed in Chapter IV.

CHAPTER IV

MODELING AND EXPERIMENTAL OBSERVATIONS OF THE WET SPINNING PROCESS

I. THEORETICAL

System Dynamics

We start with a general force balance and then examine the significance of and obtain an estimate of each term. We begin with

$$F_{rheo} = F_L - F_{drag} \qquad \text{(IV-1)}$$

The essential terms are the applied tension, F_L, the drag force, F_{drag}, and the forces inducing filament deformation (rheological force), F_{rheo}. The gravity force is negligible since most wet spinning is carried out horizontally. The surface tension and inertial forces are neglected because they are clearly small in comparison to other forces.

It is necessary to examine the drag force in more detail for our particular system. Many correlations exist in the literature which may be used for calculating drag on a moving filament. The work of Sakiadis (156, 157), Sano and Orii (158), Aoki et al. (3), and Hamana et al. (71) were used for these calculations. Most, if not all, of these correlations were developed for melt spinning. They appear to be valid over a fairly wide range of fiber Reynolds numbers, $\frac{V_{fiber}\, D_{fiber}\, \rho_{bath}}{\mu_{bath}}$ (~10-500). The theoretical calculations of Sakiadis are intended for

laminar flow. Typical Reynolds numbers for melt spinning are 20 to 60. The correlations have been verified in this range.

The drag force during wet spinning was calculated according to Equation IV-2.

$$F_{drag} = \int_{\sigma}^{L} 2\pi R \cdot C_f \rho V^2 dz \simeq 2\pi R C_f \rho V^2 L \qquad \text{(IV-2)}$$

where ρ = bath density (gm/cm^3)

R = fiber radius (cm)

V = fiber speed (cm/sec)

L = length of fiber in bath (cm)

C_f = drag coefficient from correlations, dimensionless

In our experiments, monofilaments were spun from a round spinneret of diameter 0.0381 cm. The extrusion rate was 2.0 gm/min and the initial velocity was 17.5 m/min. The take-up velocity was 7.5 m/min and the jet stretch was 0.43. Using the initial fiber diameter and the velocity of the solid fiber (i.e., the take-up velocity) the fiber Reynolds number is 47. It should be noted that our diameters are much larger than commercial fibers and our velocities are much lower and that these offset one another in the Reynolds number calculation.

Table IV-1 shows values of the predicted drag coefficient at several velocities. Figure IV-1 shows drag values in grams force plotted against take-up velocity. For our experimental conditions most of the correlations predict a drag force of less than 0.1 gm. It is noted that this increases very quickly with velocity.

The total force in an actual wet spinning situation with a spinline length of 1.5 meters running through a water bath, at 5-15

TABLE IV-1

DRAG FORCES AT VARIOUS VELOCITIES

Fiber Velocity (m/min)	Reynolds Number	Diameter of Wet Spun Fiber (cm)	Researchers and Findings: Sakiadis (156,157) Theoretical Drag L/R	Sakiadis (156,157) Theoretical Drag (gms force)	Hamana et al. (71) Air Drag (gms force)	Sano & Orii (158) Air Drag (gms force)	Aoki et al. (3) Air Drag (gms force)	Andrews (2) Air Drag (gms force)
1	6.4	.0381	10^4	.0032	.0037	.014	.0025	.013
5	32	.0381	10^4	.025	.035	.033	.030	.12
10	64	.0381	10^4	.057	.091	.076	.090	.32
50	318	.0381	10^4	.36	.86	.53	1.1	3.0
100	635	.0381	10^4	.81	2.2	1.2	2.2	7.9
500	3200	.0381	10^4	8.0	20.1	8.3	40.2	74.0
1000	6400	.0381	10^4	18.0	55.0	19.1	118.0	193.0

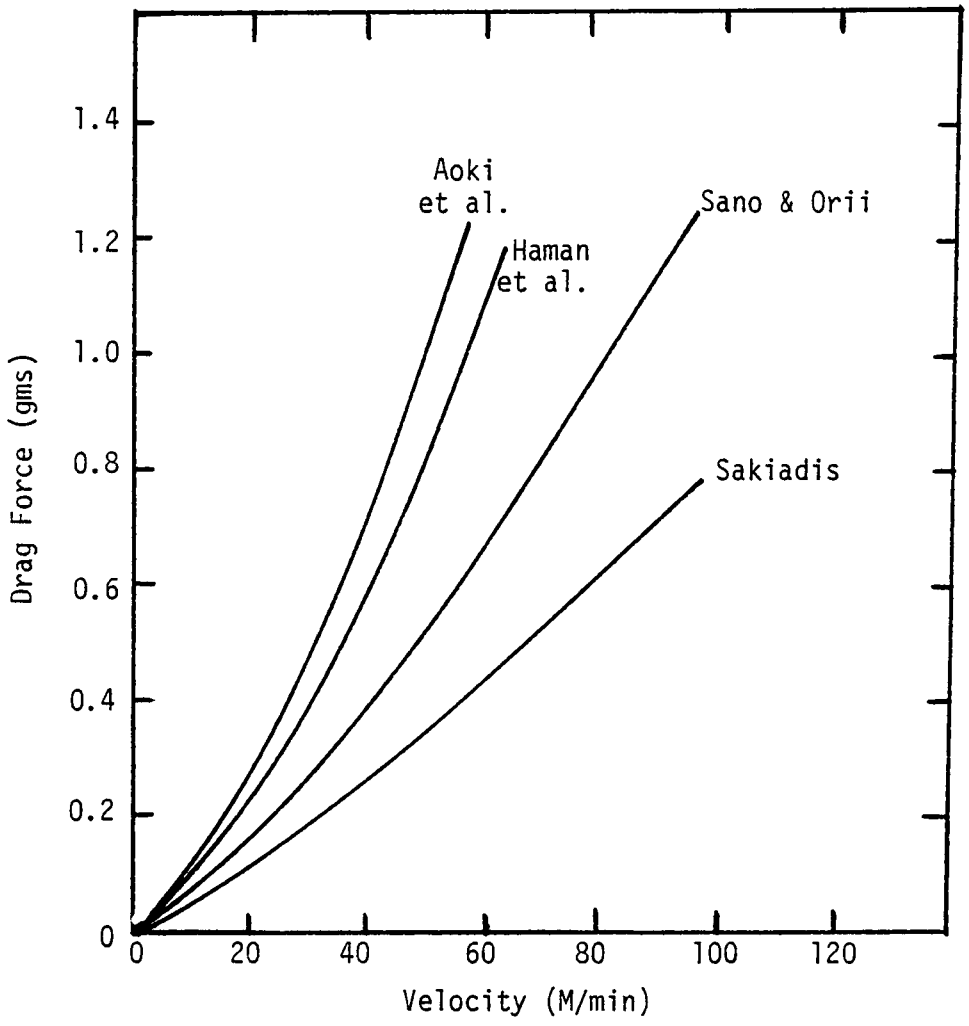

Figure IV-1. Drag force vs. fiber velocity from various correlations.

meters/minute was measured as 3 grams without any guide pins. Addition of one ceramic guide pin increased this to 4 grams. This is as opposed to the 0.1 gm predicted in the above paragraph by drag calculations. Based on this it is assumed that for the apparatus discussed in this thesis, the drag force is negligible.

In general, commercial wet spinning is carried out at much higher speeds than our experimental conditions and also multifilament yarns are spun. In a commercial wet spinning process fiber Reynolds numbers may be expected to vary from 10 to 600. It is not clear how these variables affect the significance of the drag force. If the total force is relatively independent of spinning speed, the drag force may become quite significant at higher spinning speeds. If we were to operate our apparatus at a velocity of 100 meters/minute, drag forces of order 1-2 grams would be predicted and at 500 meters/minute, 10 grams or more. This has been discussed by several authors but there is little agreement on the significance of drag forces.

Elongational Viscosity

Our force balance of Equation IV-1 may be rewritten:

$$F_{rheo} = A\sigma_{11} = A\chi_{eff}\frac{dV_1}{dx_1} = F_L - \int_0^L \pi D\sigma_f dx \qquad \text{(IV-3)}$$

where A = cross sectional area of the fiber

σ_f = frictional shear stress

χ_{eff} = the elongational viscosity

V_1 = fiber velocity

x_1 = distance from the spinneret

χ_{eff} is not a true reological property but is rather a parameter

χ_{eff} is not a true rheological property but is rather a parameter defined by Equation IV-3. It is three times the shear viscosity for a Newtonian fluid, but will be something more complex for polymer solutions.

The elongational viscosity of the filament as a function of distance from the spinneret is needed. In a filament being wet spun, the spinning dope solvent is being extracted as the fiber moves through the bath. This gives rise to both radial and axial concentration gradients and elongational viscosity gradients. It is very difficult in any case to even measure the elongational viscosity of a homogeneous polymer solution.

Han and Segal (72) have attempted the measurement of an elongational viscosity of PAN in DMAc during wet spinning using draw down and tension measurements. Coagulation was occurring during their experiments and such data cannot be relied upon because of the extraction process which induces changes in the filament (including variation of mass) during coagulation.

For Newtonian fluids, the elongational viscosity may be shown to be equal to three times the zero shear viscosity. This factor of three is known as the Trouton ratio.

For viscoelastic fluids, the various theories predict many kinds of behavior including that χ approaches infinity at modest elongation rates. Some authors (43, 44) emphasize that elongational flow is a transient process and steady state is often never achieved.

Dealy (42) some years back reviewed the area of extensional flow and listed two possible ways of measuring the elongational viscosity of relatively low viscosity solutions. One method is the inverse syphon which has been used by Astarita and Nicodemo (9) and the other method is that of converging flow used by Metzner and Metzner (116). A third method sometimes discussed is fiber spinning through air (without evaporation). Metzner and Metzner have performed experiments on aqueous solutions of polyacrylamide and reported Trouton ratios ranging from 270 to 29,000. These values are considerably higher than those for polymer melts. In studies on melts, Cogswell (37, 38), Laun and Munstedt (106), and Ide and White (87) report Trouton ratios of from less than three to thirty. They used constant elongation rate or stress devices which cannot be used for solutions. It is difficult to insure steady state elongational flow for solutions by such means. This is a primary reason for the sparcity of data in the area.

Experimental data for the elongational viscosities of our dopes are not available, but zero shear viscosity data is available. Since the Trouton ratio is not known very accurately, several values of it are used to estimate the elongational viscosity. As the concentration changes during coagulation so does the zero shear viscosity and elongational viscosity. The zero shear viscosity of several polymer solutions at various concentrations has been determined in our laboratory by Aoki et al. (5). The viscosity vs. concentration data for nylon-6 and nylon-66 in formic acid is shown in Figure IV-2 as well as Nomex® in

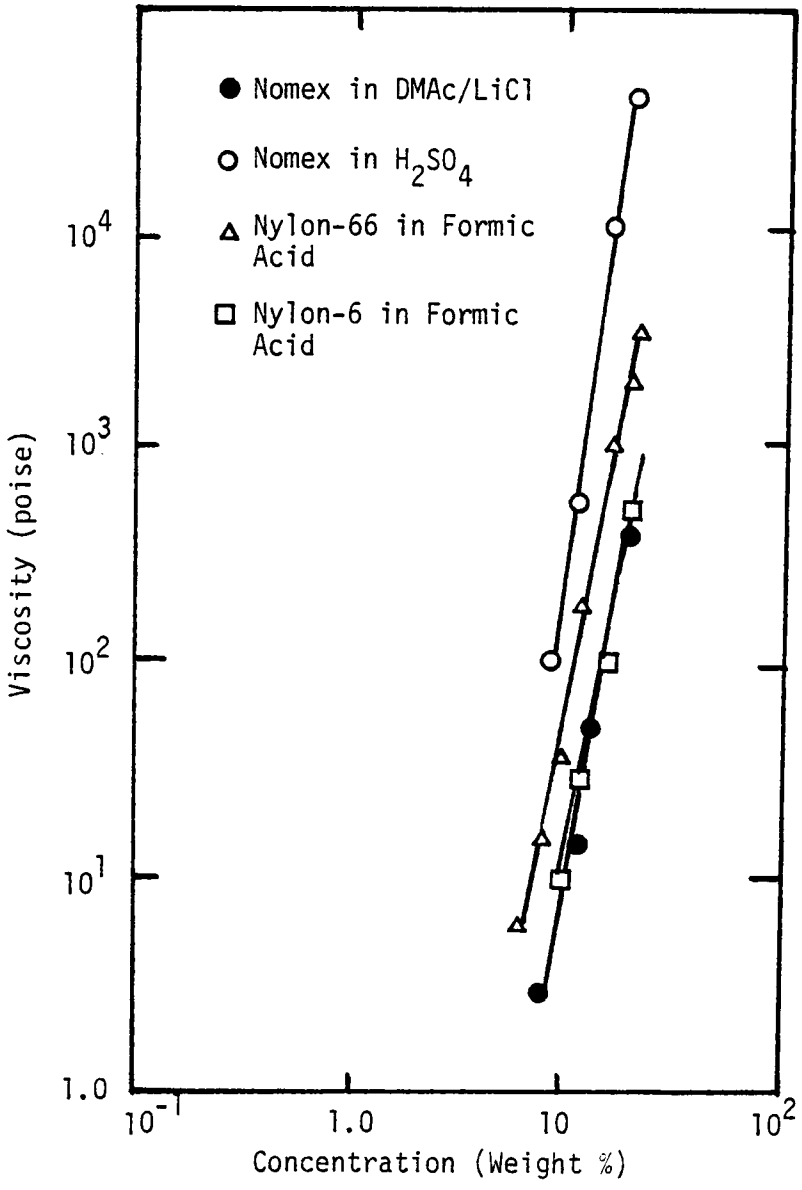

Figure IV-2. Shear viscosity vs. polymer concentration for several systems.

sulfuric acid and in DMAc/LiCl. When analyzed by the least squares method, the data fit Equations IV-4a,b,c,d.

Nylon-6 in formic acid: $\eta_o = (6.62 \times 10^{-5}) C^{5.2}$ (IV-4a)

Nylon-66 in formic acid: $\eta_o = (6.56 \times 10^{-4}) C^{5.0}$ (IV-4b)

Nomex® in DMAc/LiCl: $\eta_o = (2.76 \times 10^{-5}) C^{5.5}$ (IV-4c)

Nomex® in sulfuric acid: $\eta_o = (5.08 \times 10^{-7}) C^{8.43}$ (IV-4d)

An elongational viscosity profile is calculated and is used to obtain an average value for the elongational viscosity. This effective elongational viscosity may be defined in the following manner:

$$F = \left[\int_0^{R(x)} 2\pi r \chi(r) dr \right] \frac{dV}{dx} \qquad \text{(IV-5)}$$

$$F = \chi_{eff} \pi R^2(x) \frac{dV}{dx} \qquad \text{(IV-6)}$$

This averaging technique is carried out by calculating an elongational viscosity profile (based on the concentration) across the cross section and obtaining the mean elongational viscosity.

Mass Balances

The mass balance on solvent is given by:

$$\frac{d}{dx_f}[\bar{C} A V_f] = -\pi D K_{o'all} (\bar{C} - C_o) \qquad \text{(IV-7)}$$

where $\bar{C}$ = the average solvent concentration in the filament

D = diameter of the filament

$K_{o'all}$ = overall mass transfer coefficient

C_o = solvent concentration in the bath

Various relationships for overall continuity may be derived. The velocity V_1 may be written in terms of the area (A) and the volumetric flow rate (Q)

$$Q = AV_1 \tag{IV-8a}$$

$$\text{or } \frac{dV_1}{dx_1} = \frac{1}{A}\frac{dQ}{dx_1} - \frac{Q}{A^2}\frac{dA}{dx_1} \tag{IV-8b}$$

$\frac{dQ}{Dx_1}$ is from a mass balance

$$\rho\frac{dQ}{dx_1} = \frac{d}{dx_1}[\bar{C}AV_1] = -\pi DK_{o'all}(\bar{C} - C_\infty) \tag{IV-9}$$

which allows us to write $\frac{dV_1}{dx_1}$ in terms of $A(x_1)$ and $\bar{C}(x_1)$.

By continuity we also know that

$$\rho AV_1 = G_p + \bar{C}AV_1 \tag{IV-10}$$

where G_p = mass flow rate of polymer

ρ_p = density of polymer in solution

We now have three equations and three unknowns (i.e., A, V_1, and $\bar{C}$). Rewriting Equation IV-10, we obtain

$$V_1 = \frac{G_p}{(1-\bar{C})A\rho} \tag{IV-11}$$

Mass Transfer Rate

The volumetric flow rate changes as the filament proceeds through the bath. The change in flow rate is as we have shown the mass transfer rate,

$$\rho\frac{dQ}{dx} = j = -2\pi RK_{o'all}(\bar{C} - C^*) \tag{IV-12}$$

The overall mass transfer coefficient, $K_{o'all}$, is a combination of the external and internal mass transfer coefficients.

$$1/K_{o'all} = \frac{1}{k_{ext}} + \frac{1}{k_{int}} \tag{IV-13}$$

Following Giddings (66 , 67), we may write:

$$k_{int} = \frac{\mathcal{D}int}{\alpha R} \qquad \text{(IV-14)}$$

where α has a value of 0.25. (Bogue (23) has shown α to have a value of 0.20 for a sphere.)

The external mass transfer coefficient may be obtained by applying the Chilton-Colburn analogy (35) to a heat transfer coefficient or drag coefficient. If we write:

$$Nu = (CPr^{1/3})\ F(Re) \qquad \text{(IV-15)}$$

where $Nu = \frac{hD}{\kappa}$ = Nusselt number

$Pr = \frac{C_p \mu}{\kappa}$ = Prandtl number

$Re = \frac{VD\rho}{\mu}$ = Reynolds number

μ = viscosity of coagulation bath liquid

h = heat transfer coefficient

D = diameter of cylinder

κ = thermal conductivity

C_p = heat capacity

The analogy simply substitutes the Sherwood number for the Nusselt number and the Schmidt number for the Prandtl number. This means that:

$$Sh = (CSc^{1/3})F(Re) \qquad \text{(IV-16)}$$

where $Sh = \frac{k_{ext}D}{\mathcal{D}}$ = Sherwood number

$Sc = \frac{\mu}{\mathcal{D}\rho}$ = Schmidt number

This analogy has been substantiated experimentally. Data is reviewed by Friend and Metzner (62) who made a critical literature search. They

found quite good agreement in the range of 0.6 to 3,000 for the Schmidt number.

The other part of the analogy is used for correlation with the drag coefficient.

$$\left(\frac{Sh}{ReSc}\right)Sc^{2/3} = \frac{Cf}{2} \qquad \text{(IV-17)}$$

This too has been tested by various investigators experimentally and found to be reasonably accurate over a wide range of conditions.

A suitable heat transfer correlation was readily obtained from the melt spinning literature. Several groups have empirically or theoretically evaluated a heat transfer or drag coefficient. Equations for the mass transfer coefficient are listed in Table IV-2. By analogy with the Kase and Matsuo work Equation IV-18 is obtained.

$$Sh = 0.47\ RE^{1/3}Sc^{1/3} \qquad \text{(IV-18)}$$

This was used for our computations because it represented a correlation developed specifically for a spinning operation and because it was numerically in the middle of the range of the other values.

One Dimensional Model of Wet Spinning

A one dimensional model for wet spinning may be developed as a first approximation. This is equivalent to the Kaso and Matsuo melt spinning model (91,92). This would represent a first order model which accounts for mass transfer by way of an external mass transfer coefficient. Radial concentration variations are neglected.

The force balance neglecting drag is:

$$F_L = F_{rheo} = A\sigma_{11} = A\chi_{eff}(\bar{C})\frac{dV_1}{dx_1} \qquad \text{(IV-19)}$$

where χ_{eff} is a function of $\bar{C}$

TABLE IV-2

MASS TRANSFER COEFFICIENTS BY ANALOGY

Research Group	Correlation	Method
Kase & Matsuo (91, 92)	$Sh = 0.47\ Re^{0.334}\ Sc^{1/3}$	Empirical
Sakiadis (156, 157)	$\left(\frac{Sh}{ReSc}\right) Sc^{1/3} = \frac{Cf}{2}$	Theoretical
Sano & Orii (158)	$\left(\frac{Sh}{ReSc}\right) Sc^{1/3} = 0.34 Re^{-0.8}$	Empirical
Hamana et al. (71)	$\left(\frac{Sh}{ReSc}\right) Sc^{1/3} = \frac{Cf}{2}$	Theoretical
Aoki et al. (3)	$\left(\frac{Sh}{ReSc}\right) Sc^{1/3} = \frac{Cf}{2}$	Theoretical
Andrews (2)	$\left(\frac{Sh}{ReSc}\right) Sc^{1/3} = \frac{Cf}{2}$	Theoretical

The one dimensional mass balance neglecting internal mass transfer is:

$$\frac{d}{dX_1}[\bar{C}AV_1] = -\pi D k_{ext}(\bar{C}-C_o) \qquad \text{(IV-20)}$$

Substitution of Equation IV-11 into Equation IV-1 and IV-20 yields the following two equations.

$$F_L = X_{eff}\ A\ \frac{d}{dx_1}\left[\frac{G_p}{\rho(1-\bar{C})A}\right] \qquad \text{(IV-21)}$$

$$\frac{d}{dx_1}\left[\frac{\bar{C}G_p}{(1-\bar{C})\rho}\right] = -\ 2\sqrt{\pi A}\ k_{ext}(\bar{C}-C_o) \qquad \text{(IV-22)}$$

or

$$F_L = \frac{X_{eff}G_p}{\rho(1-\bar{C})^2}\ \frac{d\bar{C}}{dx_1} - \frac{X_{eff}G_p}{\rho A(1-\bar{C})}\ \frac{dA}{dx_1} \qquad \text{(IV-23)}$$

$$\frac{G_p}{\rho(1-\bar{C})^2}\ \frac{d\bar{C}}{dx_1} = -\ 2\sqrt{\pi A}\ k_{ext}(\bar{C}-C_o) \qquad \text{(IV-24)}$$

For the case in which there is no mass transfer

$$k_{ext} = \frac{d\bar{C}}{dx_1} = 0 \qquad \text{(IV-25a)}$$

and

$$\frac{A}{A_o} = \frac{D}{D_o} = e^{-\frac{F_L\,\rho(1-\bar{C})}{\chi_{eff}}\,x_1} \qquad \text{(IV-25b)}$$

More generally we must solve Equations IV-23 and IV-24 simultaneously with

$$k_{ext} = \frac{\mathcal{D}}{D}\,Sh = 1/2\sqrt{\frac{\pi}{A}}\,\mathcal{D}Sh \qquad \text{(IV-26)}$$

where the Sherwood number is given by Equation IV-18

$$Sh = 0.47\left[\frac{4Gp}{\pi D^2(1-\bar{C})}\right]^{1/3}\left[\frac{\cdot 1}{\rho\mathcal{D}}\right]^{1/3} \qquad \text{(IV-27)}$$

This leads to the set of equations

$$F_1 = \frac{\chi_{eff}G_p}{\rho(1-\bar{C})2}\,\frac{d\bar{C}}{dx_1} - \frac{\chi_{eff}G_p}{\rho A(1-\bar{C})}\,\frac{dA}{dx_1} \qquad \text{(IV-28)}$$

$$\frac{G_p}{\rho(1-\bar{C})^2}\,\frac{d\bar{C}}{dx_1} = -\,0.47\pi\mathcal{D}\left[\frac{2G_p}{\pi^{1/2}\rho\mathcal{D}}\right]^{1/3}\frac{1}{A^{1/6}}\,\frac{\bar{C}-C_o}{(1-\bar{C})^{1/3}} \qquad \text{(IV-29)}$$

which must be simultaneously solved.

Initial Conditions and Extrudate Swell

When polymer solutions emerge from a die, the fluid generally swells to a diameter "d" larger than the diameter "D" of the hole from which it emerged. Extrudate swell is defined as B = d/D. This has been studied by several authors (173, 155) and their work is reviewed in Chapter II. Generally B decreases with increasing die L/D ratio at constant shear rate. At constant L/D, B increases with increasing shear

rate. B also varies with polymer solution composition and concentration. For the wet spinning of acrylics B was found (57) to vary from 2.0 to almost 10 over a range of shear rates from 10^2 to 10^5 sec^{-1}.

The extrudate swell of nylon-66 spun from formic acid solution into water was photographically measured as 3.0 at 10^4 sec^{-1} shear rate. The die had an L/D of about one as is the case for most spinnerets.

Illustrative Numerical Solutions to One Dimensional Model

The equations must first be placed in dimensionless form

$$2\frac{d\ln D^*}{dx_1^*} = \left(\frac{\rho F_L D_o}{\chi_\infty G_p}\right)\left(\frac{\chi_o}{\chi}\right)(1-\bar{C}) + \frac{1}{(1-\bar{C})}\frac{d\bar{C}}{dx_1^*} \qquad \text{(IV-30)}$$

$$\frac{1}{(\bar{C}-C_o)(1-\bar{C})^2}\frac{d\bar{C}}{dx_1^*} = -\pi\left(\frac{k_{ext}D_o^2\rho}{G_p}\right)D^* = -\pi\left(\frac{k_{ext}D_o}{\mathcal{D}}\right)\left(\frac{\rho\mathcal{D}D_o}{G_p}\right)D^* \qquad \text{(IV-31)}$$

where by Equations IV-26 and IV-27 $G_p/\rho\mathcal{D}D_o$ is the Peclet Number, the product of the Reynolds and Schmidt Numbers and $k_{ext}D_o/\mathcal{D}$ is the initial Sherwood Number. The solutions C* and D* may be expressed in terms of the dimensionless groups

$$\left(\frac{\chi_o}{\chi}\right)\frac{\rho F_L D_o}{\chi_o G_p} \text{ and } \left(\frac{k_{ext}D_o}{\mathcal{D}}\right)\left(\frac{G_p}{\rho\mathcal{D}D_o}\right) \qquad \text{(IV-32a)}$$

If we introduce Equation IV-29, the right hand side of Equation IV-31 becomes

$$-0.47\,\pi\left(\frac{4}{\pi}\right)^{2/3}\left(\frac{\rho\mathcal{D}D_o}{G_p}\right)^{2/3}D^{*4/3} \qquad \text{(IV-32b)}$$

and the pertinent dimensionless groups are

$$\frac{\chi_o}{\chi}\left(\frac{\rho F_L D_o}{\chi_o G_p}\right) \text{ and } \frac{G_p}{\rho \mathcal{D} D} \qquad \text{(IV-32c)}$$

or by Equation IV-29

$$\left(\frac{\chi_o}{\chi}\right)\frac{\rho F_L D_o}{\chi_o G_p} \text{ and } \frac{\left(k_{ext}\right)_o D_o}{\mathcal{D}} \qquad \text{(IV-32d)}$$

We take χ/χ_o to vary with polymer concentration to the fifth power.

We show in Figure IV-3 calculations of $D^*(x_1)$ for various values of $\rho F_L D_o/\chi G_p$ and $G_p/\rho \mathcal{D} D_o$ (or $\left(k_{ext}\right)_o D_o/\mathcal{D}_o$) where we have used Equation IV-29. Decreasing $G_p/\rho \mathcal{D} D_o$ or increasing $\left(k_{ext}\right)_o D_o/\mathcal{D}$ decreases the extent of draw down. Increasing $\rho F_L D_o/\chi G_p$ increases the extent of draw down since this group represents a ratio of external force to rheological force.

The dimensionless diameter is seen to decrease very rapidly with distance from the spinneret. This occurs much more rapidly than is considered reasonable based on experimental observations.

The implications of this rapid decrease in diameter are that the fiber will essentially draw down to infinitely small diameters within the first five inches of the bath. This of course is not realistic. The discrepancy would appear due to inaccuracy on the prediction of the apparent elongational viscosity since this is the force that retards draw down. In this model these forces are predicted based on an average concentration across the fiber. This is a critical area since the apparent elongational viscosity varies as the fifth power of the concentration. For this reason, it makes a significant difference in how the average is arrived at (i.e., whether an average concentration

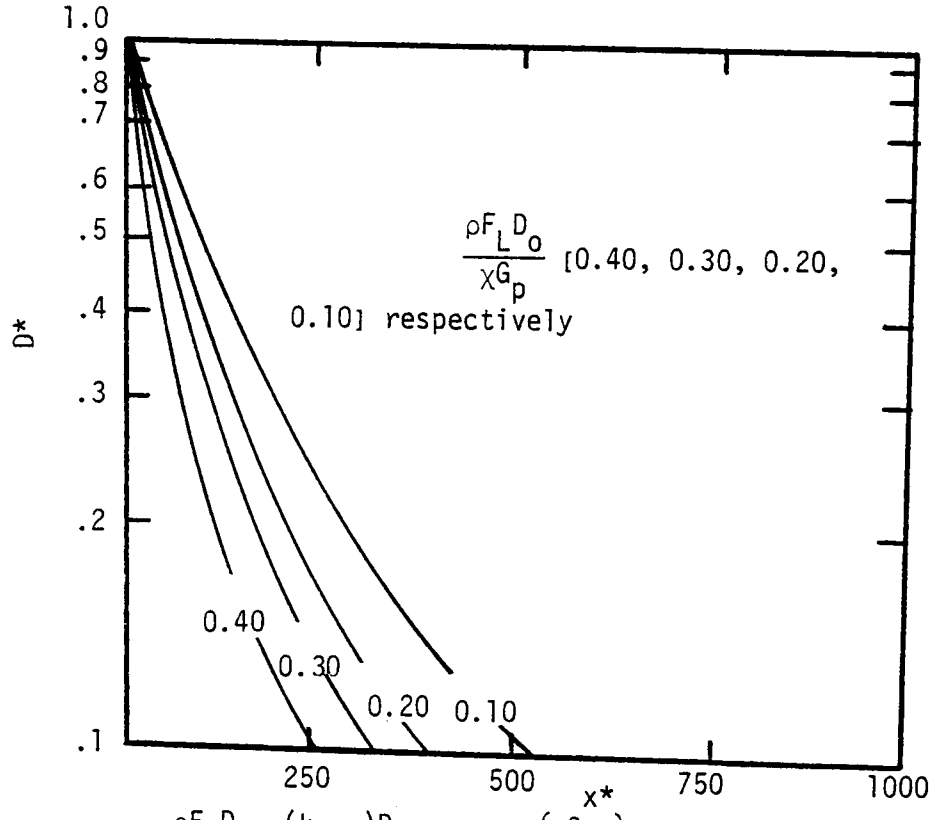

(a) with varying $\frac{\rho F_L D_o}{\chi G_p}$, $\frac{(k_{ext})_{D_o} D_o}{\mathcal{D}} = 8.0$, $\left(\frac{G_p}{\rho \mathcal{D} D_o}\right) = 1.9 \times 10^4$.

Figure IV-3. Log dimensionless filament diameter vs. dimension distance from the spinneret as calculated the one dimensional model of wet spinning.

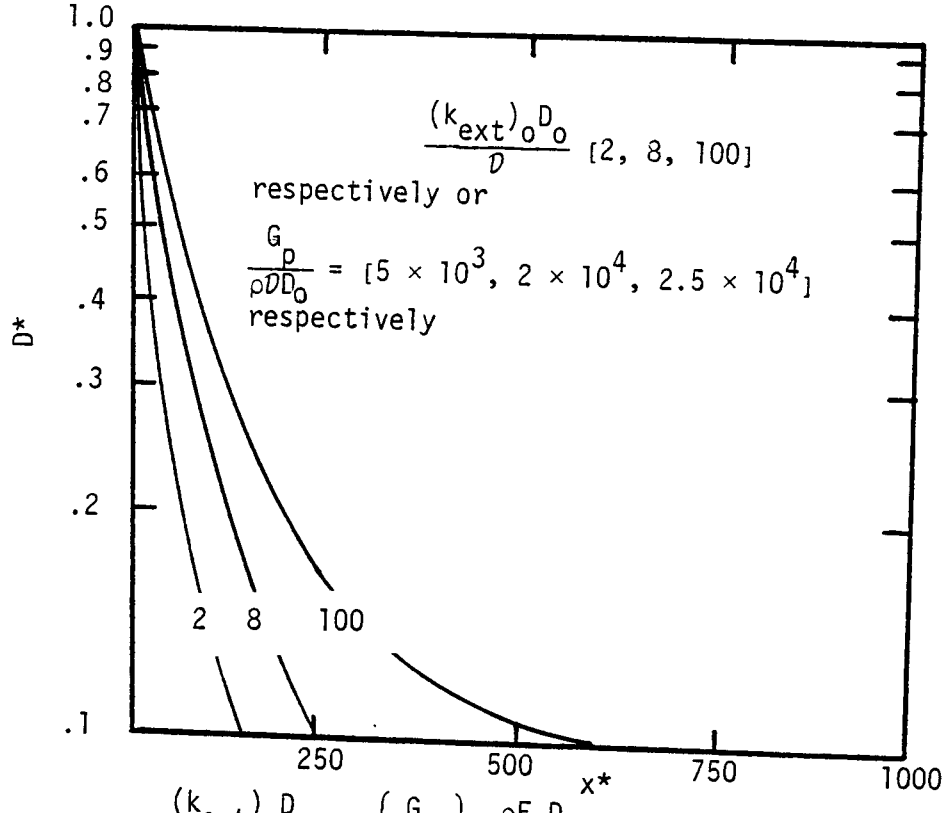

(b) with varying $\frac{(k_{ext})_o D_o}{\mathcal{D}}$ or $\left(\frac{G_p}{\rho \mathcal{D} D_o}\right)$, $\frac{\rho F_L D_o}{\chi G_p}$ = 0.20.

Figure IV-3. (Continued)

is used to compute the viscosity or the viscosity is computed at several points and averaged). Very high polymer concentrations near the filament/water interface cause the apparent elongational viscosity to increase sharply and result in a retarded draw down. To achieve this a concentration profile across the filament as a function of distance in the bath is necessary.

In our studies the actual values for $\rho F_L D_o/\chi_o G_p$ and $\left(k_{ext}\right)_o D_o/\mathcal{D}$ $(G_p/\rho D_o \mathcal{D}_{ext})$ were 0.19 and 24 respectively. The one dimensional model does not accurately predict the experimental result so a higher order model must be derived.

Higher Order Analysis

General. To improve the model the starting point must again be the basic balances in Equations IV-3 and IV-7. A similar development is carried out but Equations IV-19 and IV-20 are replaced with balances which consider radial concentration profiles in the filament during spinning. Specifically,

$$F_L = A\left[\int_0^1 2\frac{r}{R}\chi(C)d\frac{r}{R}\right]\frac{dV_1}{dx_1} \qquad \text{(IV-33)}$$

$$\frac{d}{dx_1}[\bar{C}AV_1] = -\left[\frac{\pi D}{\frac{1}{k_{ext}}+\frac{1}{k_{int}}}\right](\bar{C}-C_o) \qquad \text{(IV-34)}$$

These may be reduced to

$$F_L = \frac{\chi_{eff}G_p}{\rho(1-\bar{C})^2}\frac{d\bar{C}}{dx_1} \quad \frac{\chi_{eff}G_p}{\rho A(1-\bar{C})}\frac{dA}{dx_1} \qquad \text{(IV-35)}$$

$$\frac{G_p}{\rho(1-\bar{C})^2}\frac{d\bar{C}}{dx_1} = \frac{\pi}{\frac{1}{\alpha \mathcal{D}_{int}} + \frac{1}{\mathcal{D}Sh}}\ (\bar{C}-C_o) \qquad \text{(IV-36)}$$

where the integrals of χ are written as χ_{eff}

To evaluate these integrals one must know the concentration profile in the fiber as a function of position.

Concentration profile. A relationship between the change in concentration across the cross section of the fiber and the residence time or distance in the spin bath is needed. This relationship would open the way for defining the other unknown variables in Equations IV-35 and IV-36.

We may obtain the concentration profile from solving the diffusion equation (20). Equation IV-37 describes the radial transient diffusion in a cylinder.

$$V_1 \frac{\partial C}{\partial x} = \frac{\partial C}{\partial t_{res}} = \frac{1}{r}\frac{\partial}{\partial r}\left(\mathcal{D}_{int}\frac{\partial C}{\partial r}\right) \qquad \text{(IV-37)}$$

where C = concentration of solvent

t_{res} = residence time of fiber in bath

$\mathcal{D}_{int}$ = diffusivity

r = radial position

The initial and boundary conditions for this particular problem are:

$$C(o,r) = C_o$$

$$\left(\frac{\partial C}{\partial r}\right)_{(t,o)} = 0 \qquad \text{(IV-38a,b,c)}$$

$$-\mathcal{D}\left(\frac{\partial C}{\partial r}\right)_{(t,R)} = k_{ext}\ [C(R)-C_o^*]$$

where, R(t) = D/2 must be considered a function of bath residence time determined by Equation IV-37. The concentration profile is constant at time zero, the concentration is a maximum at the center of the fiber at all times, and at the surface of the fiber convective mass transfer is occurring.

Equation IV-36 is the solution of Equation IV-34 for the stated boundary conditions based on both a constant diffusivity and radius, R:

$$\frac{C - C_o}{C_\infty - C_o} = 1 - \sum_{n=1}^{\infty} \frac{2LJ_o(r\beta_n/R)}{(\beta_n^2+L^2)\, J_o(\beta_n)}\, e^{-\beta^2 n \mathcal{D}_{int} t/R^2} \qquad \text{(IV-39)}$$

where β_n's are roots of $\beta_n J_1(\beta_n) - LJ_o(\beta_n) = 0$

$L = Rk_{ext}/\mathcal{D}_{int}$ = internal Sherwood number = $\frac{1}{2}Sh$,

$\mathcal{D}_{int} t/R^2$ = diffusion Fourier number = F_o

The infinite series in Equation IV-36 may be numerically summed for various values of $X = \int V_1 dt_{res} = \int Q/A dt_{res}$. Detailed computations however require knowledge of the diffusivity, $\mathcal{D}$, and external mass transfer coefficient, k_{ext}.

Equation IV-39 should be realized to be only an approximate concentration profile as it does not consider the variation of D with t and r nor R with t.

Solutions of Special Cases of Higher Order Model

The ideal way to handle the preceding equations would be to solve them simultaneously. This means that the force balance and the

diffusion equation along with the terms in them would need to be solved together. This is not practical however and for simplification the force balance and mass balance are solved separately and then related back to each other. Several simplifications of the force balance may be used conveniently and may be handled more easily in dimensionless form.

We now introduce dimensionless variab les.

Let $D = \frac{D}{D_o}$

$x^* = \frac{x}{D_o}$

$V^* = \frac{V}{V_o}$

$C^* = \frac{C}{\rho}$

$L^* = \frac{L}{D_o}$

For our experimental apparatus the drag was found as shown in section II to be small. When drag is neglected, the following equation for the force balance results.

$$\frac{dD^*}{dX^*} = \frac{-(1-\bar{C}^*)D^*F_L}{2\chi_{eff}G_p} + \frac{(1-\bar{C}^*)D^*\pi D_o}{2G_p(\frac{1}{\alpha D_{int}} + \frac{1}{DSh})} \qquad \text{(IV-40)}$$

This equation is very similar to Equation IV-30 with some added terms. The higher order model involves a new way to evaluate χ_{eff} by using a concentration profile across the filament. The variation of $\bar{C}$ with x_1 is also included in this model necessitating the inclusion of an internal diffusivity. This results in the addition of another dimensionless to those listed in Equations IV-32c and IV-32d. This group is the internal Sherwood number

$$Sh_{int} = \frac{k_{ext} D_o}{\mathcal{D}_{int}} \qquad \text{(IV-41)}$$

or the ratio

$$\frac{\mathcal{D}_{int}}{\mathcal{D}_{ext}} \qquad \text{(IV-42)}$$

Equations IV-40 and IV-39 were solved by an iterative technique.

The finite difference scheme, which was implemented to solve the equations, divides the total length of the coagulation bath into small increments. At each of these small segments, the diameter is assumed to be constant as well as the elongational viscosity.

Beginning at a point very near the spinneret, a concentration profile is computed from Equation IV-39 for the initial diameter. The average concentration and average elongational viscosity may be computed directly at this point. Using this information and an initial value for flow rate and diameter, Equation IV-40 is solved for a new value for diameter. This new value then is used to compute a new flow rate for the next increment of X. Equation IV-39 is again solved, but this time for the new diameter. Equation IV-40 is solved using the new values for diameter, average elongational viscosity, and flow rate. This procedure is continued down the spin line until the end of the spin bath is reached.

Figure IV-4 shows the diameter of the filament versus distance from the spinneret at several initial Sherwood numbers. The initial Sherwood number is perhaps the key dimensionless group in this analysis since it contains both the maximum external mass transfer coefficient and the diffusivity.

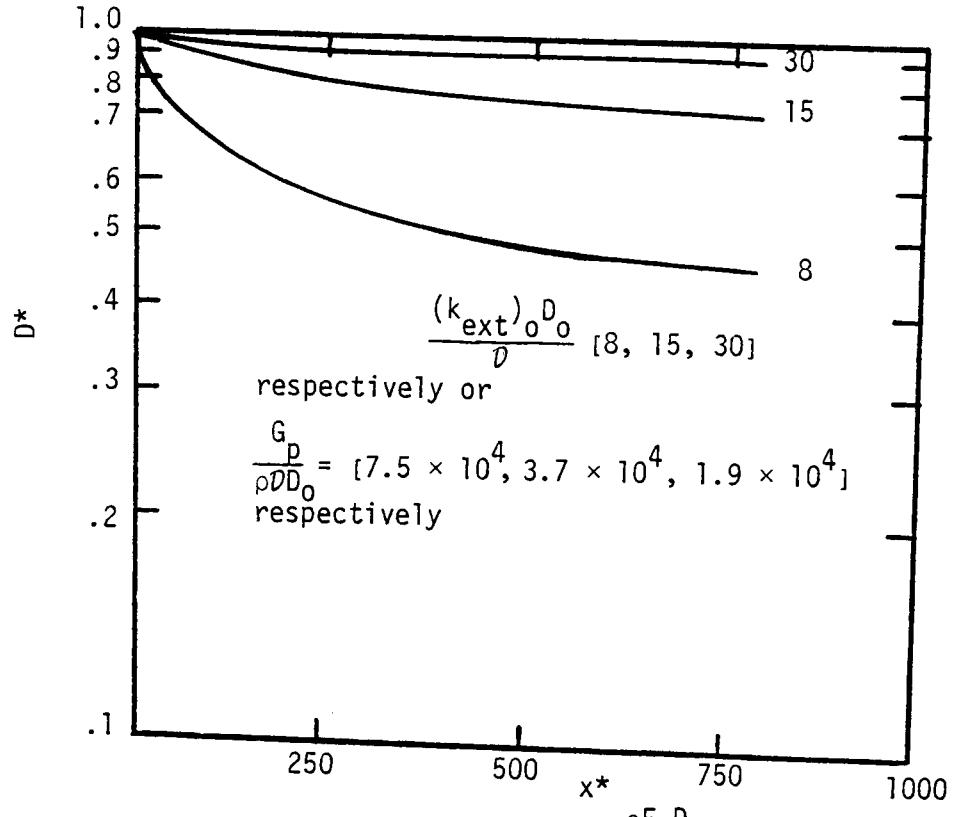

(a) various initial external Sherwood numbers $\frac{\rho F_L D_o}{\chi G_p} = 0.20$,

$\frac{\mathcal{D}_{int}}{\mathcal{D}_{ext}} = 10^{-5}$.

Figure IV-4. Log dimensionless filament diameter vs. dimensionless distance from the spinneret at (a), (b), (c).

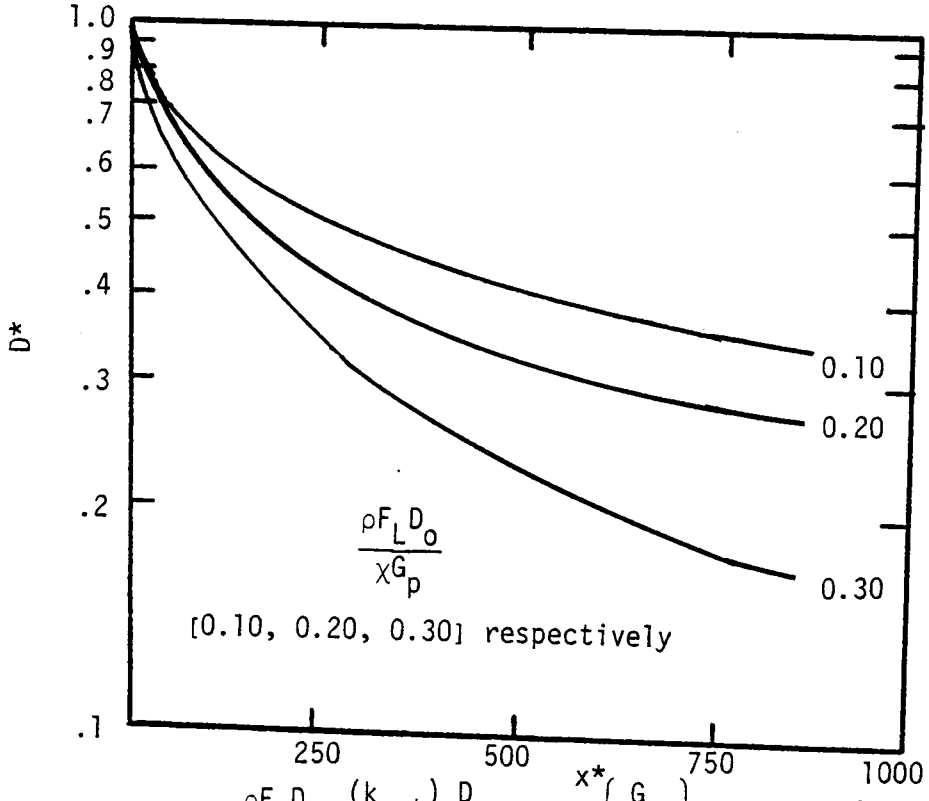

(b) various values of $\frac{\rho F_L D_o}{\chi G_p}$, $\frac{(k_{ext})_o D_o}{\mathcal{D}} = 8.0$, $\left(\frac{G_p}{\rho \mathcal{D} D_o}\right) = 1.9 \times 10^4$, $\frac{\mathcal{D}_{int}}{\mathcal{D}_{ext}} = 10^{-5}$.

Figure IV-4. (Continued)

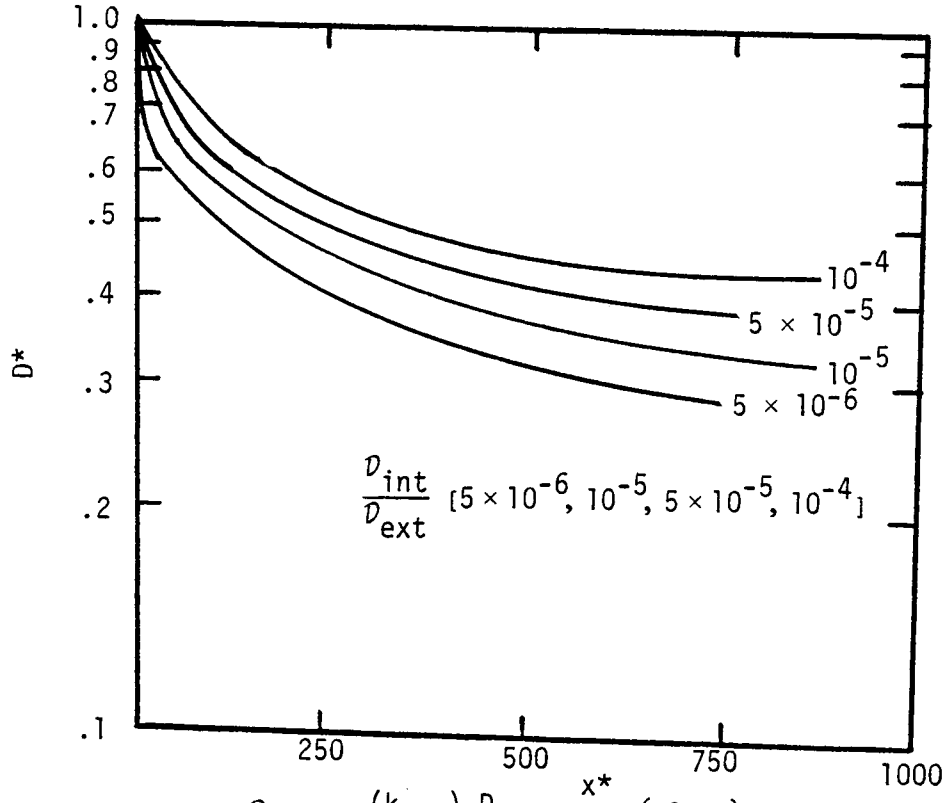

(c) various values of $\frac{\mathcal{D}_{int}}{\mathcal{D}_{ext}}$, $\frac{(k_{ext})_o D_o}{\mathcal{D}} = 8.0$, $\left(\frac{G_p}{\rho \mathcal{D} D_o}\right) = 1.9 \times 10^4$, $\frac{\rho F_L D_o}{\chi G_p} = 0.20$.

Figure IV-4. (Continued)

Figure IV-4 shows that for initial Sherwood numbers greater than 20 very little draw down occurs. A large initial Sherwood numbers means a very rapid coagulation and thus little draw down. To achieve this high initial Sherwood number the initial mass transfer coefficient must be very high.

Consider the quantities

$$\frac{k_{o'all}}{V_o} = \frac{\text{radial convective mass flux}}{\text{axial mass flux}} \tag{IV-43}$$

$$\frac{F_L}{\chi_{eff} D_o V_o} = \frac{\text{axial tension}}{\text{draw down resistance}} \tag{IV-44}$$

For the systems investigated in this thesis the value of Equation IV-43 (the ratio of radial convective mass flux to axial mass flux) is of order 10^{-4}. The value of $F_L/\chi_{eff} D_o V_o$ of Equation IV-42 (the ratio of the axial tension to the draw down resistance) ranges from 10^{-5} to 10^{-7}, depending upon the point at which the effective elongational viscosity is considered. The ratio of frictional drag to draw down resistance for our system is between 10^{-7} and 10^{-9}. In all cases this group is two orders of magnitude smaller than the other groups. This supports the assumption to neglect the drag force.

Table IV-3 shows numerical values for the mass transfer coefficient of our system obtained by various analogies. Table IV-4 shows other specific conditions in our system and Figures IV-5, IV-6, and IV-7 show the results of the preceding equations for our experimental conditions. No provision is made for coagulation via skin formation (i.e., no provision for a phase change). The draw down does cease as a

TABLE IV-3

MASS TRANSFER COEFFICIENTS BY ANALOGY FOR OUR EXPERIMENTAL CONDITIONS

K_{ext} [cm/sec]	Group	Method
0.00875	Kase & Matsuo (91, 92)	{heat transfer empirical}
0.00190	Sakiadis (156, 157)	{drag coefficient theoretical}
0.00252	Sano & Orii (158)	{drag coefficient empirical}
0.00278	Hamana et al. (71)	{drag coefficient empirical}
0.00278	Aoki et al. (3)	{drag coefficient empirical}
0.0113	Andrews (2)	{drag coefficient empirical}

TABLE IV-4

EXPERIMENTAL CONDITIONS

Q	= 2 cm^3/min
K_{ext}	= 0.00875 cm/sec
α	= 0.25
$\mathcal{D}$	= 0.0000140 cm^2/sec
L	= 12.2
R_o	= .01905 cm
C_o^*	= 0.0
C_o	= .70
F_L	= 2 gms or 1960 dynes

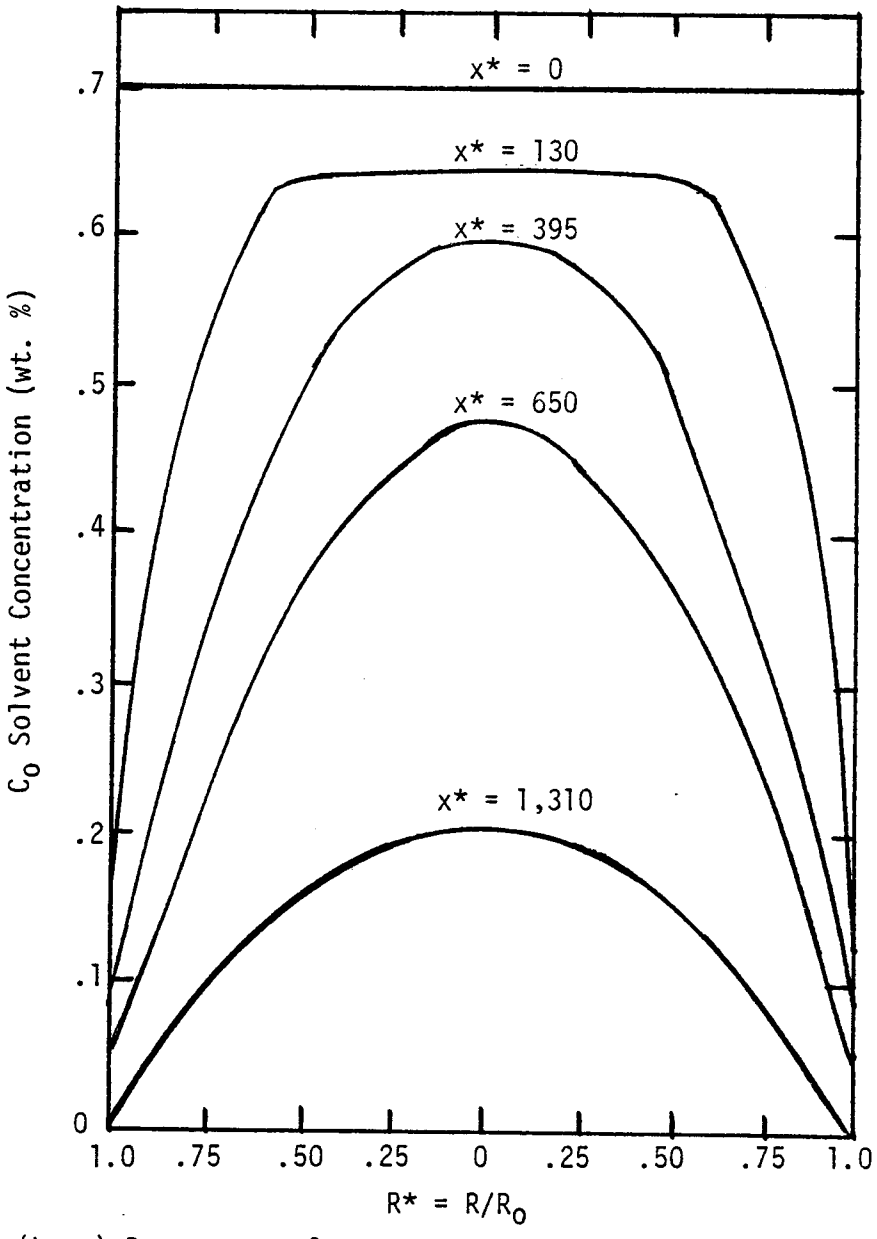

$$\frac{\rho F_L D_o}{\chi G_p} = 0.20, \frac{(k_{ext})_o D_o}{\mathcal{D}} = 10.0 \text{ or } \frac{G_p}{\rho D D_o} = 2.5 \times 10^4, \frac{\mathcal{D}_{int}}{\mathcal{D}_{ext}} = 10^{-5}.$$

Figure IV-5. Solvent concentration profiles across the filament cross-section for water coagulant.

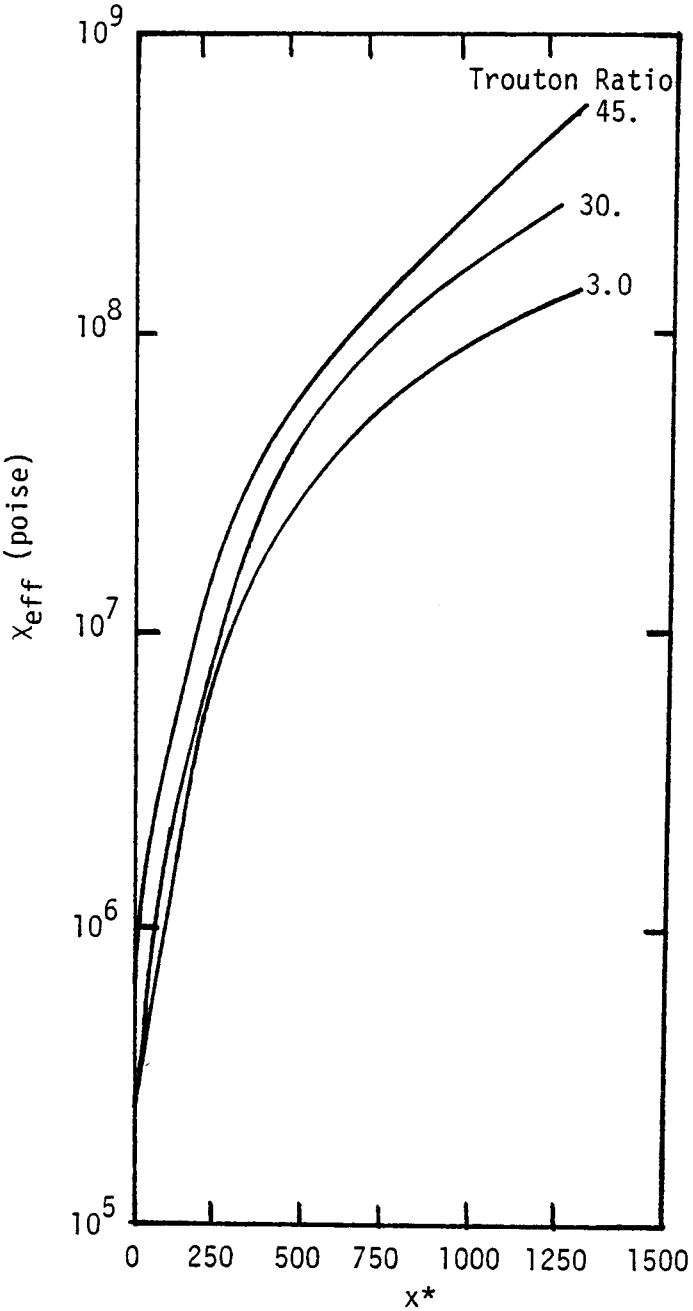

$$\frac{(k_{ext})_o D_o}{\mathcal{D}} = 10.0 \text{ or } \frac{G_p}{\rho \mathcal{D} D_o} = 2.5 \times 10^4, \quad \frac{\mathcal{D}_{int}}{\mathcal{D}_{ext}} = 10^{-5}, \quad \frac{\rho F_L D_o}{\chi G_p} = 0.020, 0.20, 0.30.$$

Figure IV-6. Effective elongational viscosity vs. distance.

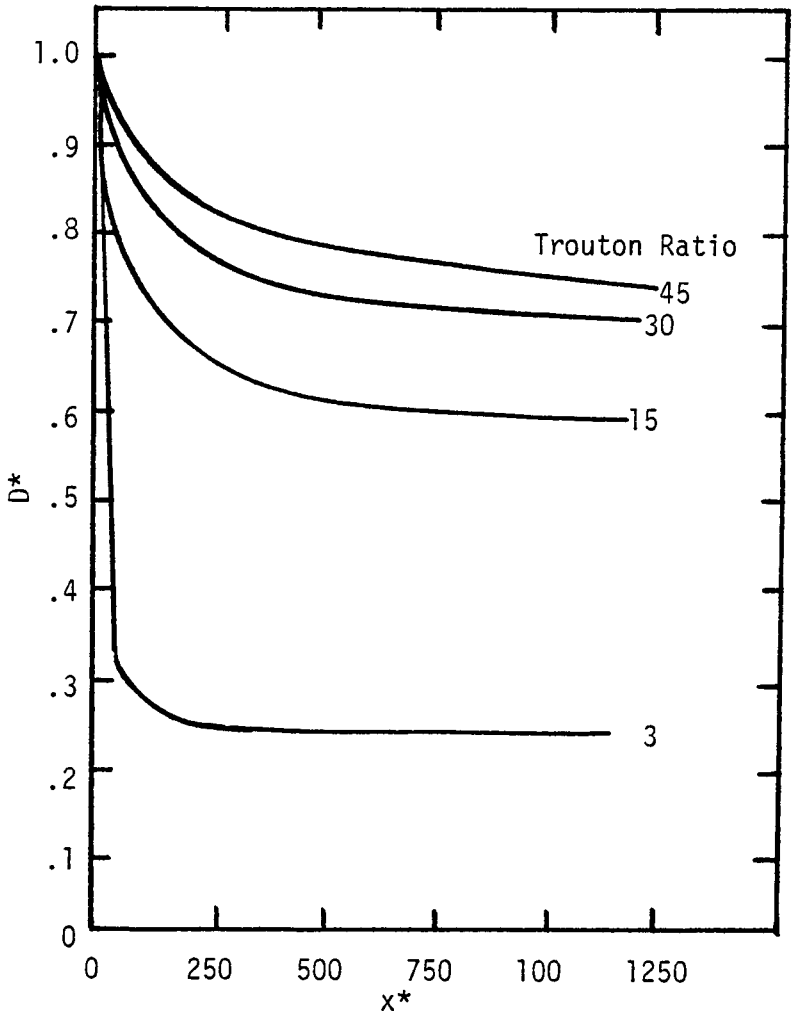

$$\frac{(k_{ext})_o D_o}{\mathcal{D}} = 10.0 \text{ or } \frac{G_p}{\rho \mathcal{D} D_o} = 2.5 \times 10^4, \quad \frac{\mathcal{D}_{int}}{\mathcal{D}_{ext}} = 10^{-5}, \quad \frac{\rho F_L D_o}{\chi G_p} = .30, .20, .10, .020.$$

Figure IV-7. Dimensionless filament diameter vs. dimensionless distance from the spinneret at various Trouton ratios.

result of extremely high elongational viscosity values and this final diameter is compared to experimental data.

II. EXPERIMENTAL

Systems Studied

Nylon-6, redissolved Nomex®, and PAN/VA copolymer were the three major polymers used in this study.

Nylon-6 was chosen because of the abundance of information developed earlier by the author (41, 42) on its superstructure when dissolved in formic acid and coagulated with water or alkaline or acid solutions. The coagulation bath composition used, varied from strongly basic to strongly acidic. The baths are summarized in Table IV-5.

Nomex® is commercially solution spun. Redissolved Nomex® solutions were spun from sulfuric acid and from DMAc with 5% LiCl. This polymer was also considered in our earlier work (41, 42). The fibers spun from these solutions had considerably different superstructures than those of the nylon-6 or nylon-66 fibers. There were also marked differences between fibers spun from the two solvents. Coagulation baths were varied from strongly basic to strongly acidic. This is summarized in Table IV-5.

The acrylic polymers are the most commercially significant wet spun fibers of recent years. A copolymer made up of 97.5% PAN and 2.5% VA was used in this study and dissolved in DMAc. The resulting fiber superstructures were very similar to those found in the Nomex-

TABLE IV-5

WET SPINNING SYSTEMS STUDIED

Polymer	Solvent	Coagulant
Nylon-6	Formic Acid	5% NaOH in water
		Water
		5% Formic acid in water
		10% Formic acid in water
		15% Formic acid in water
Nomex®	DMAc/5%LiCl	Water
		5% DMAc in water
		10% DMAc in water
		15% DMAc in water
		40% DMAc in water
	Sulfuric Acid	50% NaOH in water
		30% NaOH in water
		5% NaOH in water
		Water
		10% H_2SO_4 in water
		25% H_2SO_4 in water
		50% H_2SO_4 in water
97.5% PAN -2.5% VA copolymer	DMAc	MeOH
		Water
		5% DMAc in water
		10% DMAc in water
		15% DMAc in water
		40% DMAc in water
		60% DMAc in water

DMAc system. Coagulation bath compositions varied from water to high concentrations of DMAc in water. This is summarized in Table IV-5.

Polystyrene solutions were also examined. A number of solvents and a few other polymers (Nylon-66, Kevlar, and Bisacid A-2) were also examined. This will be discussed in later chapters.

Types of Fiber Superstructures Observed

Results. The fiber superstructures observed in this study can be divided into three categories: (1) hollow core, (2) fluted core, and (3) sponge-like fiber. These superstructures may exist in the same fiber under different conditions. All fibers not distinguished as (1) or (2) are classified as (3), sponge-like fibers. The voids in fibers of type (3) vary in size from fiber to fiber.

An example of a hollow core superstructure is shown in Figure IV-8. The hollow core was found in nylon-6 fibers spun from formic acid into caustic coagulation baths. Other polymer-solvent systems such as nylon-66 in formic acid, nylon-66 in sulfuric acid, and Nomex® in sulfuric acid exhibited a similar structure in caustic coagulation baths.

The fluted core superstructure is particularly intriguing. The fiber core resembles a wagon wheel with eliptical spokes. An example of this structure is shown in Figure IV-9. The following are some of the systems in which the fluted structure is seen: Nomex® in DMAc with 5% LiCl spun into water, PAN/VA in DMAc spun into water, and Nomex® in sulfuric acid spun into water.

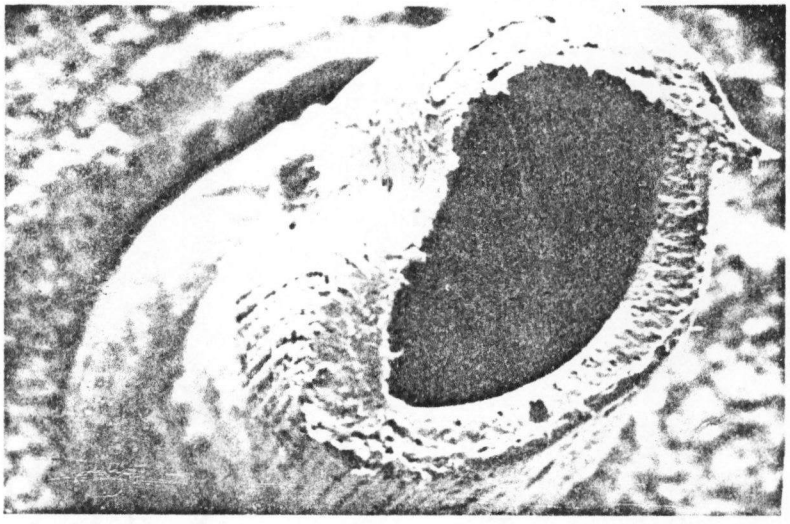

Figure IV-8. SEM photomicrograph of nylon-6 fiber spun from formic acid into 5% NaOH in water (100X).

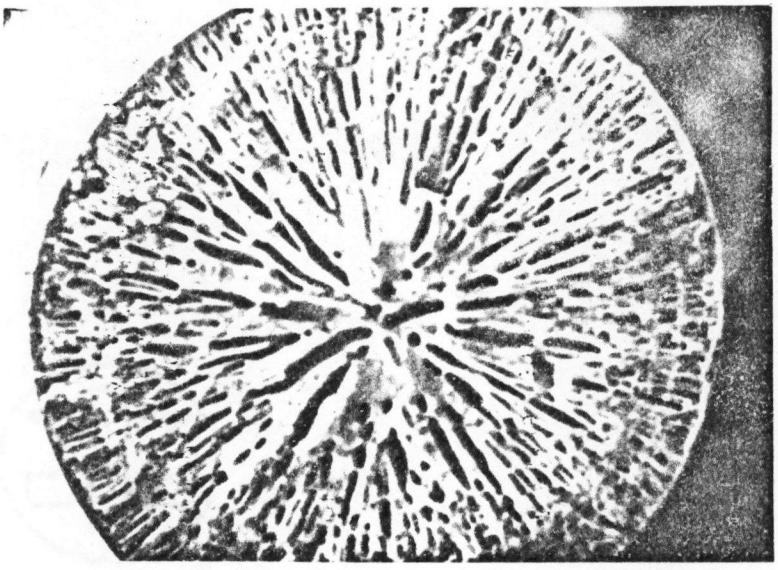

Figure IV-9. SEM photomicrograph of Nomex fiber spun from sulfuric acid into water (200X).

Discussion. Commercial fibers contain very small voids and therefore come under this category. All of the systems studied which were successfully spun exhibited some type of sponge-like structure at the optimum spinning conditions (Figure IV-10). It should be remembered that sponge-like fibers with voids resolvable in the SEM are not commercially acceptable and that the SEM examples include large diameter fibers which show large voids for discussion purposes. Better quality fibers have voids discernable only by SAXS or some type of absorption method.

The mechanisms by which these three types of superstructures are formed will be discussed in the following chapters. Experimental observations are listed in Table IV-6.

Comparison of theory and experiment. The nylon-66/formic acid system was chosen to study most carefully and compare to the theory because the fiber superstructure is simple and the mass transfer does not involve any instabilities. The dimensionless groups from Equations IV-32d and IV-42 are calculated from parameters given in Table IV-4, page 62. For this specific solvent system the values are as follows:

$$\frac{\rho F D_o}{\chi G_p} \cong 0.20$$

$$\frac{(k_{ext})_o D_o}{\mathcal{D}} \cong 12.2$$

$$\frac{\mathcal{D}_{int}}{\mathcal{D}_{ext}} \cong 10^{-5}$$

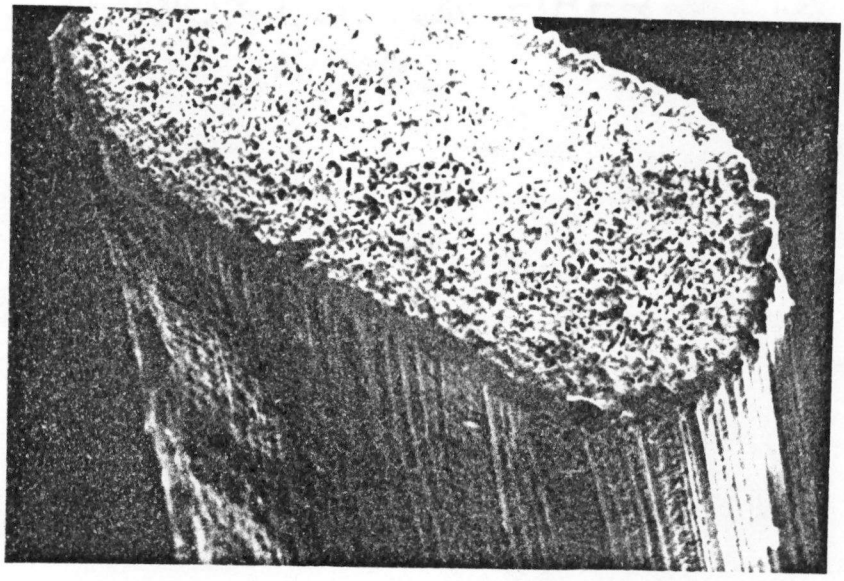

Figure IV-10. SEM photomicrograph of nylon-6 fiber spun from formic acid into 4% methanol in water (200X).

TABLE IV-6

FIBER SUPERSTRUCTURES RESULTING FROM WET SPINNING

Polymer	Solvent	Coagulant	Superstructure
Nylon-6	Formic acid	5% NaOH	Hollow core
		Water	Sponge-like
		5% formic acid	Sponge-like
		10% formic acid	Sponge-like
		15% formic acid	Sponge-like
Nylon-66	Formic acid	5% NaOH	Hollow core
		Water	Hollow core
		5% formic acid	Sponge-like
		10% formic acid	Sponge-like
		15% formic acid	Sponge-like
Nomex®	DMAc/LiCl	Water	Fluted
		5% DMAc	Fluted
		10% DMAc	Fluted
		15% DMAc	Fluted
Nomex®	Sulfuric acid	30% NaOH	Hollow core
		5% NaOH	Hollow core
		Water	Fluted
		10% sulfuric acid	Fluted
		25% sulfuric acid	Fluted
		50% sulfuric acid	Sponge-like
Kevlar®	Sulfuric acid	5% NaOH	Sponge-like
		Water	Sponge-like
		5% sulfuric acid	Sponge-like
		10% sulfuric acid	Sponge-like
		15% sulfuric acid	Sponge-like
97.5%PAN/ 2.5%VA	DMAc	Water	Fluted
		20% DMAc	Fluted
		30% DMAc	Fluted
		40% DMAc	Fluted
		60% DMAc	Sponge-like

The elongational viscosity is calculated from the data shown in Figure IV-2, page 42 and an assumed Trouton ratio of 30. Figure IV-11 shows the theoretical predictions at the experimental condition for the first order model and the higher order model with a die swell of 1.5 as measured experimentally. Two extreme coagulation baths are shown, water and 15% formic acid in water.

As expected the prediction of the higher order model is much superior to that of the first order model when compared to actual experimental results. The experimental results are obtained by measuring the final fiber diameter after removal from the coagulant and therefore they are one point measurements which may be compared with the theory only at the end of the coagulation bath (@ $X^* = 1000$).

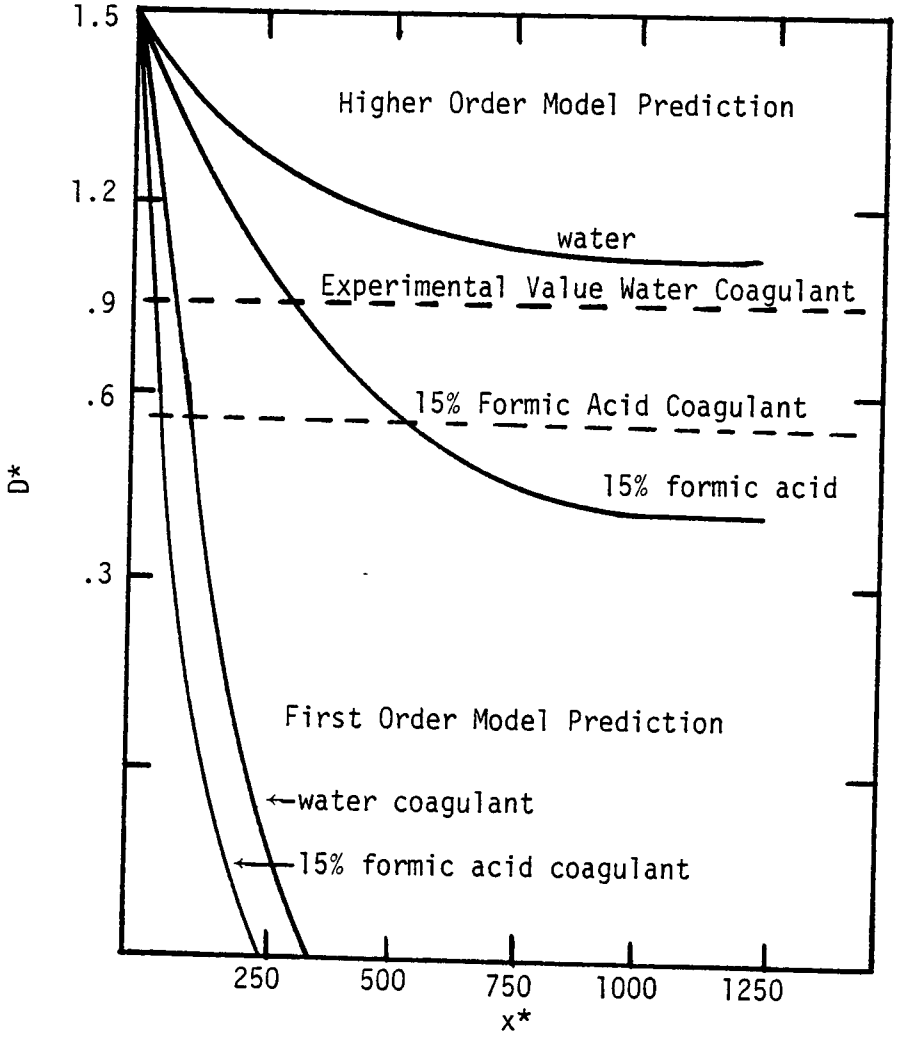

$$\frac{(k_{ext})_o D_o}{\mathcal{D}} = 12.0 \text{ or } \frac{G_p}{\rho \mathcal{D} D_o} = 2.0 \times 10^4, \frac{\mathcal{D}_{int}}{\mathcal{D}_{ext}} = 10^{-5}, \frac{\rho F_L D_o}{\chi G_p} = 0.20.$$

Figure IV-11. Dimensionless filament diameter vs. dimensionless distance from the spinneret—theoretical predictions compared to experimentally measured final fiber diameters.

CHAPTER V

MECHANISMS CAUSING HOLLOW CORE FIBERS

I. INTRODUCTION

The fibers discussed in this study were all spun through a round spinneret. The hollow core fibers were first observed with filaments formed from aliphatic nylons (i.e., nylon-6 and nylon-66) dissolved in Formic Acid. When these polymer solutions were spun into caustic (5% NaOH in water) coagulation baths, a hollow fiber was formed. In the case of nylon-66 in formic acid a hollow fiber was also produced when spun into pure water, but the relative size of the hollow core was much smaller. SEM photomicrographs of some nylon-6 and nylon-66 hollow fibers are shown in Figure V-1. The hollow core extends the entire length of the fiber forming a tube.

It was desireable to find a polymer solution which, when spun into different coagulants, would exhibit all three types of void structures. This was found in the 16% Nomex® dissolved in sulfuric acid system. Hollow fibers were formed with coagulation in 5% NaOH in water (Figure V-2). It was found in this system that for the same dope and coagulant, a large diameter (0.127 cm) (Figure V-2) spinneret produced the hollow fibers while a smaller (0.038 cm) one did not.

In almost all cases resulting in a hollow fiber, a chemical reaction at the interface was involved. The chemical reaction at

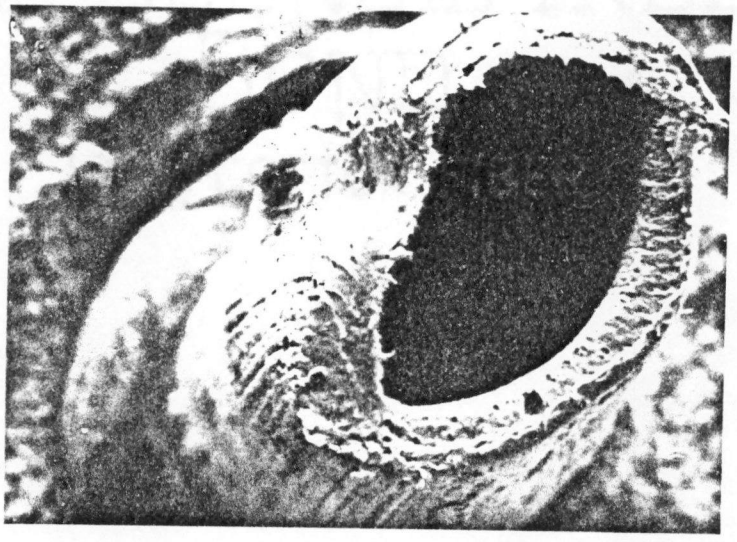

(a) 100X

Figure V-1. SEM photomicrograph of nylon-6 fiber spun from formic acid into 5% NaOH in water; (a) 100X, (b) 200X.

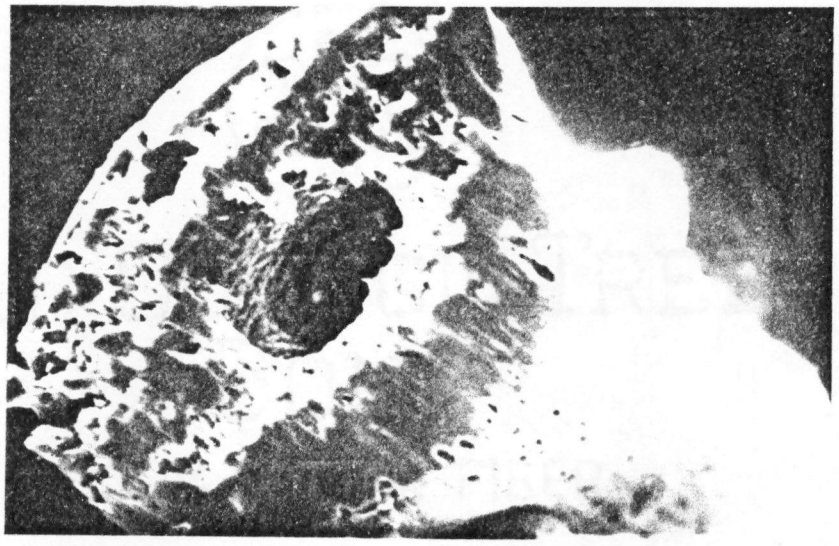

(b) 200X

Figure V-1. (Continued)

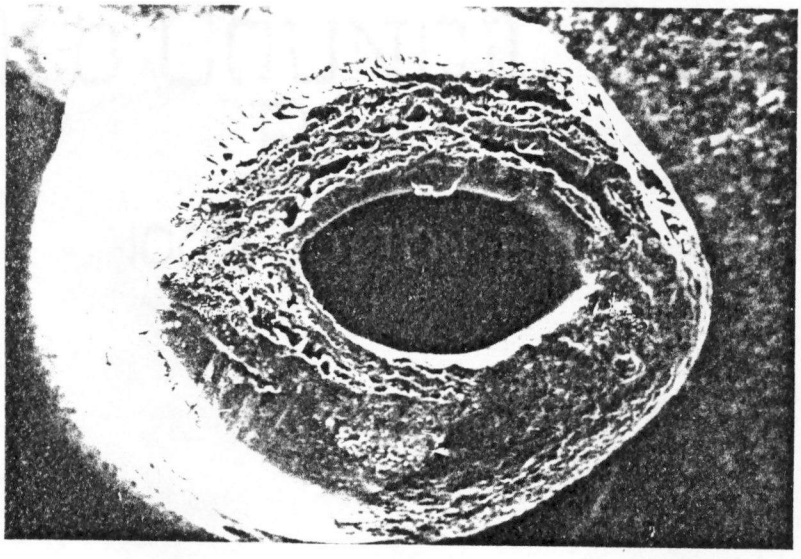

Figure V-2. SEM photomicrograph of Nomex fiber spun from sulfuric acid into 5% NaOH in water (50X).

the interface in the instances described above is essentially an acid-base neutralization reaction. The coagulant contains a very strong base such as sodium hydroxide and completely surrounds the filament. The following mechanism would seem probable. As soon as a molecule of acid diffuses to the filament surface, it is neutralized by the caustic coagulant. This drastically increases the coagulation rate because the surface remains at zero acid concentration and increases the driving force for diffusion. The formation of hollow fibers thus appears dependent on high mass transfer rates induced by a chemical reaction between solvent and coagulant at the interface. The neutralization reaction at the interface keeps the concentration of solvent at the interface quite low and gives an increased driving force for diffusion. A high diffusion rate and interfacial reaction means that the filament will coagulate very rapidly.

II. MICROSCOPIC OBSERVATIONS

An effective way of observing and measuring the speed of coagulation is described in Chapter III as the static observation of coagulation. Video tapes were made of the coagulation process for various combinations of dopes and coagulants. The systems studied are listed in Table V-1.

Still photographs from these tapes are shown in Figure V-3. From these photographs it is clear that the coagulation front is moving much more quickly for caustic coagulants than for acidic ones. This may be seen in Figure V-4 where the advance of the coagulation front is plotted against time.

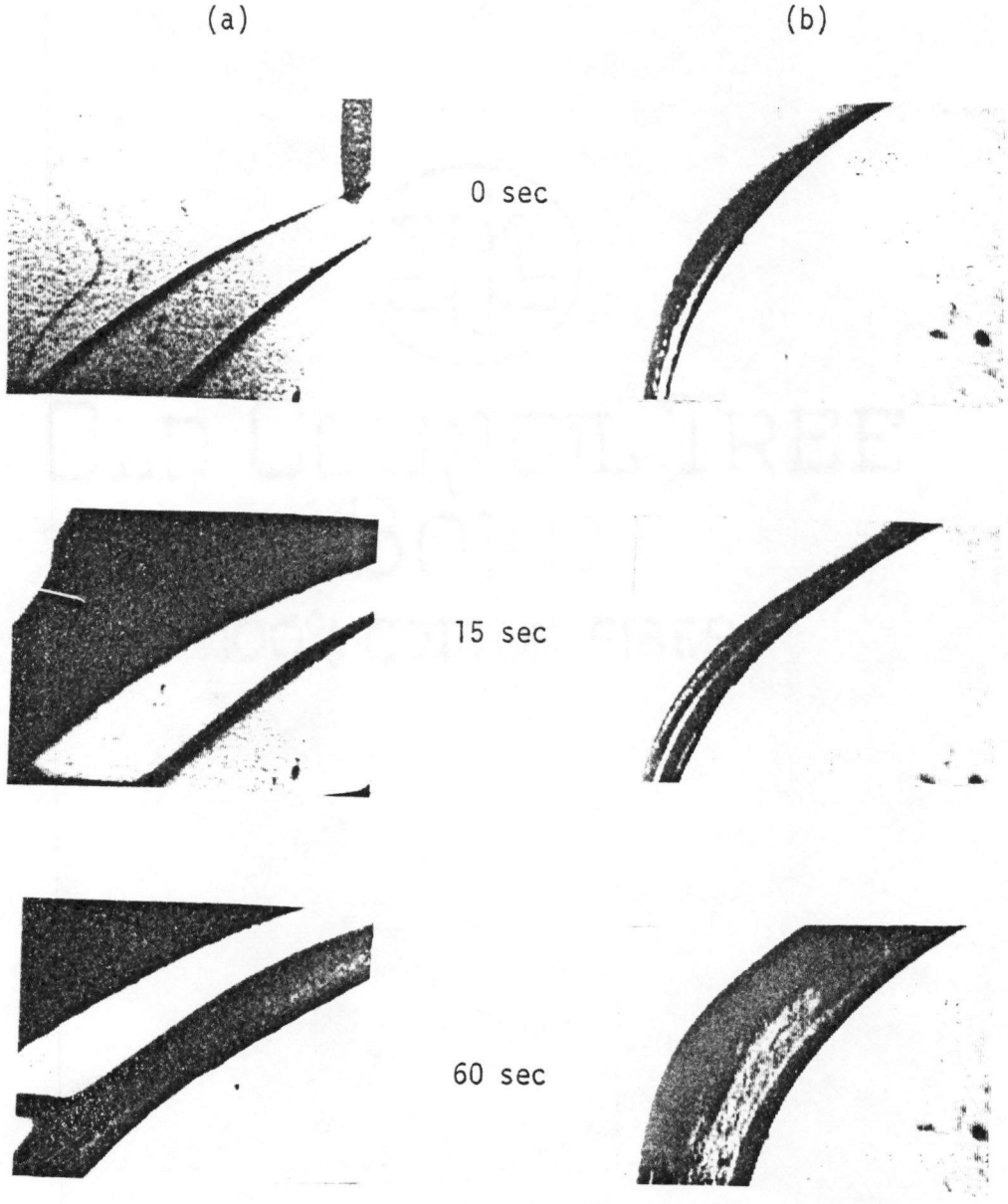

Figure V-3. Optical micrographs of static coagulation of nylon-6 in formic acid with (a) water coagulant (b) 5% NaOH in water coagulant.

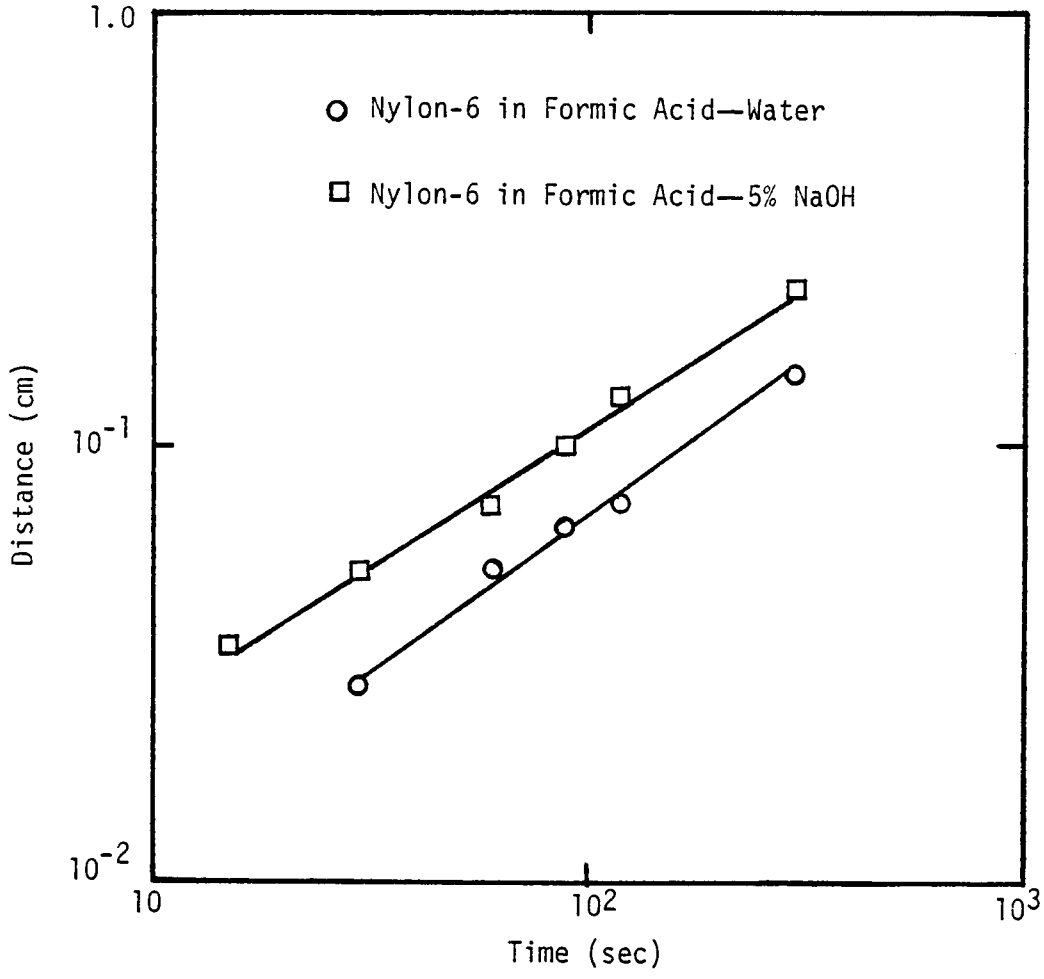

Figure V-4. Skin growth vs. time for static coagulation of nylon-6 in formic acid with various coagulants.

TABLE V-1

STABLE INTERFACES STUDIED UNDER MICROSCOPE

Polymer	Solvent	Coagulant
Nylon-6	Formic acid	5% NaOH in water
Nylon-6	Formic acid	Water
PAN	DMAc	40% DMAc in water
---	Formic acid	Water

It is interesting to note that the slope of the lines for 5% NaOH in water and pure water are approximately the same. The equations of these lines by a least squares fit are respectively: $X = 0.00632t^{0.612}$ and $X = 0.00316t^{0.687}$. From the transient diffusion equation with constant diffusivity one would expect: $X \alpha t^{0.5}$. Of course in this situation the proportionality is complicated by the coagulation phenomena. At some critical concentration the phase change occurs and changes the diffusivity. Both exponents on time are greater than 0.5 which indicates that the mass transfer is faster than expected from a constant diffusivity diffusion model. The accuracy of the measurements may not be sufficient to test this hypothesis.

From Equation IV-13, it is seen that there are two mass transfer coefficients, the internal and external mass transfer coefficient, which combine to form the overall mass transfer coefficient. One can also include an interfacial mass transfer resistance. Initially the external mass transfer would be controlling and then as the process continues the internal mass transfer increase would increase to the

point that it is controlling. This is probably due to the variation of diffusivity with concentration.

$$D \alpha \frac{1}{C^5} \qquad \text{(V-1)}$$

Thus as the concentration of the polymer increases due to diffusion of solvent out, the diffusivity quickly decreases to the point of being the rate determining step.

The coagulation process is a two-step mass transfer process. The solvent must first diffuse through the polymer solution and then diffuse through the interface between the polymer solution and coagulant. This may be discussed in terms of an internal mass transfer coefficient and and external mass transfer coefficient. The overall mass transfer coefficient may be defined as:

$$K_{o'all} = \frac{1}{\frac{1}{k_{ext}} \quad \frac{1}{k_{int}}} \qquad \text{(V-2)}$$

It is suspected that during some very brief initial period that the external mass transfer is the rate controlling step. After this initial period, the internal mass transfer would become the rate controlling step. From Equation V-2 it is seen that $K_{o'all}$ is dominated by the smaller value of k_{ext} or k_{int}. The difference between the coagulation rate of the 5% NaOH solution and pure water should show up in k_{ext} only because of the acid-base reaction involved. This means that for the period that k_{ext} is important in the process the two coagulants behave differently. After this instant they behave similarly. In viewing the data in Figure V-4 this must be kept in mind. The figure begins at a

time equal 15 seconds. This means that the brief instant where k_{ext} is the rate controlling step has already transpired before the data could be taken. The first data point is influenced by k_{ext} and therefore this point is higher for the 5% NaOH coagulant than for the water coagulant. This appears in Figure V-4 as an offset between the two curves because data is not available for the complete coagulation process. So even though the curves appear to have different y-intercepts and similar slopes, they may not extrapolate. This would involve ignoring the initial step in the mass transfer process.

In summary, our static coagulation studies are applicable only after the internal mass transfer coefficient has become controlling due to the greatly decreased diffusivity because the measurements may only be taken after 15 sec. These observations lead to the statement of a two step coagulation mechanism and an explanation for hollow core fibers.

III. PROPOSED MECHANISM FOR THE FORMATION OF HOLLOW FIBERS

It has been shown in the previous chapter that hollow fibers are formed when caustic coagulants and acidic solvents are used in wet spinning. Based on these observations and the preceeding static coagulation studies, we will attempt to describe the process by hollow fibers form.

The filament emerges from the spinneret as a homogeneous polymer solution. The solvent begins to diffuse into the coagulant thus effectively raising the polymer content in the filament. When the

polymer concentration increases to a point above the equilibrium solubility, the polymer forms a gel-like skin at the periphery of the filament. Of course kinetics also plays an important role in the coagulation and the polymer concentration will necessarily reach a value significantly above the equilibrium solubility so that coagulation will appear in a short time scale.

A thin polymer skin forms on the periphery of the filament and grows inward as the solvent continues to diffuse out (Figure V-5). As the diffusion of solvent is occurring, the filament is being drawn down by the take-up force. When about 10% of the radius is coagulated, this draw down ceases because the load is carried by the solid polymer skin. This means that a very rapid coagulation would result in large diameter fiber since the coagulated skin is formed before significant draw down can occur.

When the draw down ceases, the fiber radius is fixed and this fixes the volume per unit length of the fiber. At this point the fiber still contains 50-60% solvent which is continually diffusing out into the coagulant during the remainder of the bath.

The solvent has a density near unity and occupies a considerable amount of volume. When it is removed, the polymer left does not have sufficient volume to fill the total volume fixed by the early coagulation. The fiber must either collapse or voids will form within it. If the polymer skin is sufficiently sturdy, it cannot collapse but rather forms a large void in the center of the fiber making it hollow.

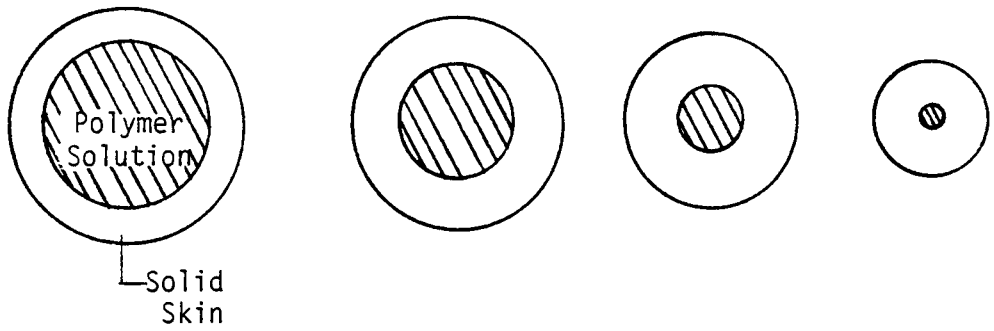

Figure V-5. Schematic of skin growth in coagulating filament.

The mechanism then is simply that the volume is fixed by rapid coagulation and the polymer cannot fill the entire volume provided.

IV. RADIUS PREDICTIONS

General

The radius prediction is based upon the equations developed in Chapter IV. Equation IV-40, the force balance neglecting drag, was used in conjunction with Equation IV-39, the solution of the diffusion equation. In Chapter IV these equations were also solved, but the formation of a rigid skin (i.e., a phase change) which stops all draw down was neglected. This is included here.

When the polymer concentration increases to a certain point, due to diffusion of solvent out, a polymer gel forms. This certain concentration for gelation is the solubility limit for the polymer, solvent, and coagulant, but it is not necessarily the equilibrium solubility since kinetics are certainly involved. When the solubility limit is reached at a point perhaps of order 10% of the radius into the filament, a skin which is capable of supporting the entire load is formed and draw down ceases.

To form a hollow fiber a very high external mass transfer coefficient is necessary. Very high values may be best achieved with a chemical reaction at the interface which changes the diffusing species and thereby lowers its concentration drastically. To fit the previously developed equations this interfacial diffusion and reaction must be represented by a mass transfer coefficient.

The area of mass transfer with chemical reaction has long been a subject of interest to chemical engineers. Many simplified relations between reaction rate, concentration, and mass transfer have been derived.

Hatta (78) has treated the simplified case of a stagnant film theoretically. Although the interface between the fiber and bath is not stagnant, the following relationship may be useful to estimate an order of magnitude mass transfer coefficient with chemical reaction.

$$k_L = - \mathcal{D}\left(\frac{dC}{dr^*}\right)_{r^*=1} = \sqrt{2\mathcal{D}\int_0^{C_{ai}} R(c)\,dC} \qquad \text{(V-3)}$$

where C = concentration of diffusing substance

C_{ai} = concentration of diffusing substance A at interface

$R(c) = K_n C^n$ = reaction rate

K_n = rate constant

n = reaction order

k_L = mass transfer coefficient with reaction

upon substitution of K_n

$$k_L = \sqrt{2\mathcal{D}K_n\int_0^{C_{ai}} C^n dC} \qquad \text{(V-4)}$$

and finally

$$k_L = \sqrt{\frac{2}{n+1}\,\mathcal{D}K_n\,C_{ai}^{n-1}} \qquad \text{(V-5)}$$

This relationship gives the mass transfer coefficient as a function of the reaction parameters.

The preceding work was based on reaction controlled conditions, but it is possible that the interfacial reaction occurs so rapidly that it

is not rate controlling. If this occurs the depletion of one of the reactants limits the reaction and the diffusion of that reactant becomes the controlling step. Again simplifying this by considering a stagnant film model, the governing equations are (8):

$$\frac{1}{r} \mathcal{D}_1 \frac{\partial}{\partial r} \left(r \frac{\partial C}{\partial r}\right) = \frac{\partial C}{\partial t} = V \frac{\partial C}{\partial r} \qquad \text{(V-6)}$$

$$\frac{1}{r} \mathcal{D}_2 \frac{\partial}{\partial r} \left(r \frac{\partial b}{\partial r}\right) = \frac{\partial b}{\partial t} = V \frac{\partial b}{\partial r} \qquad \text{(V-7)}$$

with boundary conditions of:

at $t = 0$ $\quad C = 0 \quad b = b_o$

$r = R \quad C = C_o'$

$b = b_o \quad \frac{\partial b}{\partial r} = 0$

$r = \lambda \quad b = c = 0$

$$\frac{d\lambda}{dt} = - \left[\frac{\partial C/\partial t}{\partial C/\partial r}\right]_{r=\lambda}$$

and a stoichiometric condition at the reaction radius ($r = \lambda$)

$$-\mathcal{D}_1 \left[\frac{\partial C}{\partial r}\right]_{r=\lambda} = \frac{1}{q} \mathcal{D}_2 \left[\frac{\partial b}{\partial r}\right]_{r=\lambda} \qquad \text{(V-8)}$$

where q = the stoichiometric coefficient

Again using the simple film theory (which gives an order of magnitude estimate), the film thickness is divided into two parts of width λ and $(\delta-\lambda)$ such that the stoichiometric balance at the reaction plane is fulfilled as follows.

$$\mathcal{D}_2 \frac{b_o}{\delta-\lambda} = q \mathcal{D}_1 \frac{C_o'}{\lambda} \qquad \text{(V-9)}$$

This is then solved for λ and

$$\frac{k_L}{k_o} = \frac{\delta}{\lambda} = 1 + \frac{\mathcal{D}_2 b_o}{\mathcal{D}_1 q C_o'} \qquad \text{(V-10)}$$

is the result where k_L is the mass transfer coefficient with reaction and k_o is the coefficient without reaction.

Perhaps the best way to handle the specific problem of a fiber moving through a bath and the corresponding flow fields is by empirical correlation. Experiments (7) concerning a laminar jet of one fluid into another have been performed and used to develop the following correlation.

$$\frac{k_L}{k_{L_o}} = N_1 \left(\frac{a}{b}\right)^{N_2} \qquad \text{(V-11)}$$

The constants N_1 and N_2 must be defined for each system and their specific values are discussed under detailed calculations.

It has been found that the formation of hollow fibers is related to high initial mass transfer rates and this is reflected in a high value for the initial Sherwood number. From Figure IV-4, page 58, it is seen that for initial Sherwood numbers of 20 or higher very little draw down occurs. This is necessary for the formation of hollow fibers as seen in the following equation.

From a simple material balance between the spinneret and the take-up roll the final fiber diameter may also be predicted.

$$\phi_p Q = \rho\phi_p \frac{\pi D^2}{4} V_o = (1-\varepsilon)\ \frac{\pi D^2_{final}}{4}\ V_L \rho' \qquad \text{(V-12}$$

where ϕ_p = weight fraction polymer

Q = volumetric flow rate of solution

ρ = solution density

V_o = average velocity at spinneret

ε = void fraction in final fiber

V_L = take-up velocity

ρ' = density of fiber

In this matter a void fraction may be calculated using the experimental conditions.

$$\varepsilon = 1 - \frac{4\phi_p Q}{\pi D^2_{final} V_L \rho'} \qquad \text{(V-13)}$$

Thus the void fraction is purely a function of the total volume per unit length of the fiber which is fixed by coagulation and the total volume of polymer per unit length of the fiber which is fixed by the rate of extrusion. Using these relationships a critical void fraction can be calculated which signals the beginning of the formation of hollow fibers. Above some critical void fraction, a hollow core is thought to form to accommodate the excess volume brought on by rapid coagulation. This critical void fraction is near 0.75-0.80 or higher.

Illustrative Calculations

Equations IV-39 and IV-40 were solved by an iterative technique to yield the final fiber diameter for a series of conditions. The same dimensionless groups (Equations IV-32c, IV-32d, and IV-42) are appropriate for this discussion. Similar results to those shown in Figures IV-4a, b, and c, pages 58, 59, and 60, are obtained for this case except that draw down is terminated when 10% of the filament radius has reached a solvent concentration of about twice the equilibrium solubility limit. Figure V-6 shows the results. The termination of draw down results in 20-30% higher final fiber diameters than those shown

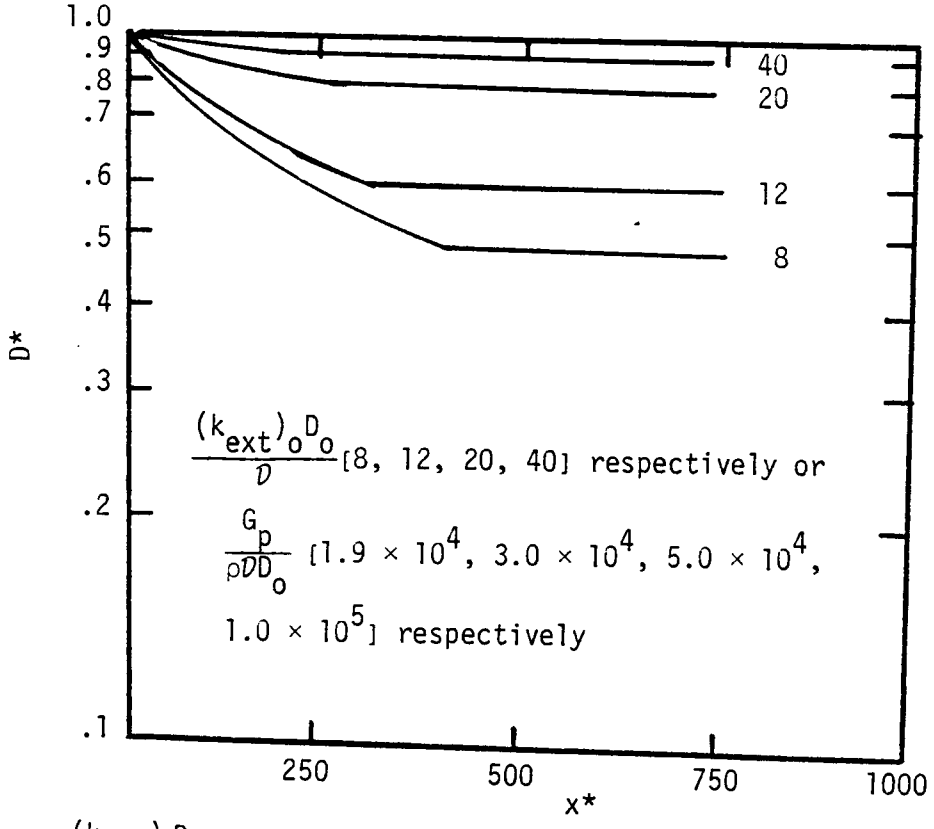

(a) various $\frac{(k_{ext})_o D_o}{\mathcal{D}}$ or $\frac{G_p}{\rho \mathcal{D} D_o}, \frac{\rho F_L D_o}{\chi G_p} = 20, \frac{\mathcal{D}_{int}}{\mathcal{D}_{ext}} = 10^{-5}$.

Figure V-6. Log dimensionless filament diameter vs. dimensionless distance from the spinneret at (a), (b), (c).

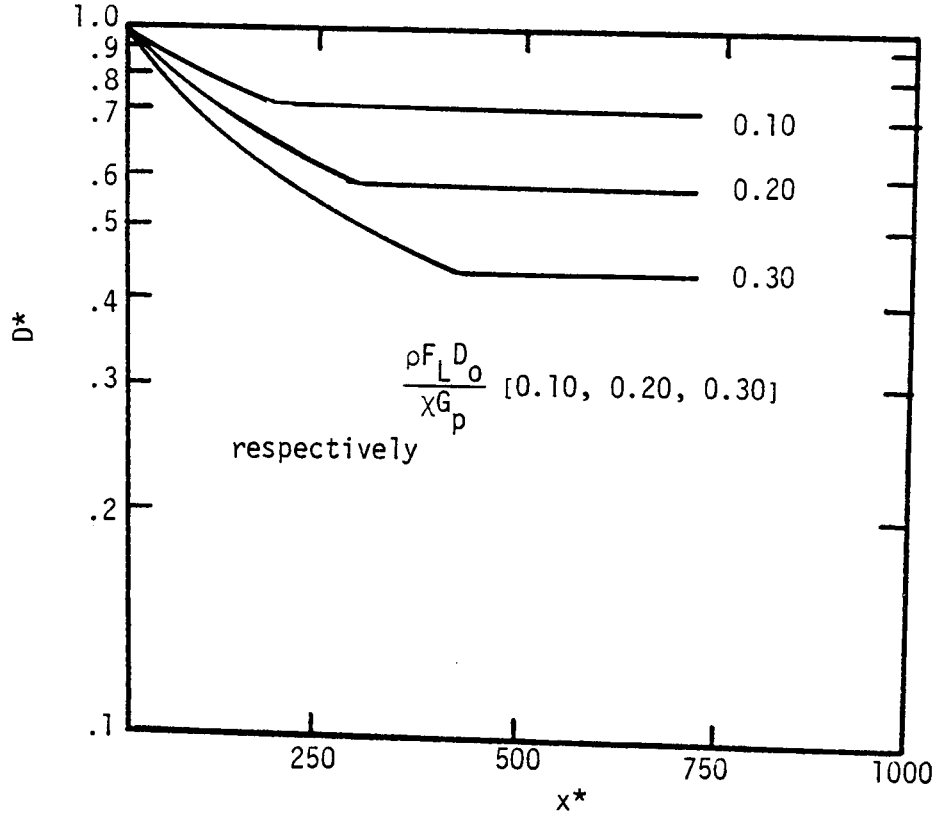

(b) various values of $\frac{\rho F_L D_o}{\chi G_p}$, $\frac{(k_{ext})_o D_o}{\mathcal{D}} = 20$ or $\frac{G_p}{\rho \mathcal{D} D_o} = 5.0 \times 10^4$,

$\frac{\mathcal{D}_{int}}{\mathcal{D}_{ext}} = 10^{-5}$.

Figure V-6. (Continued)

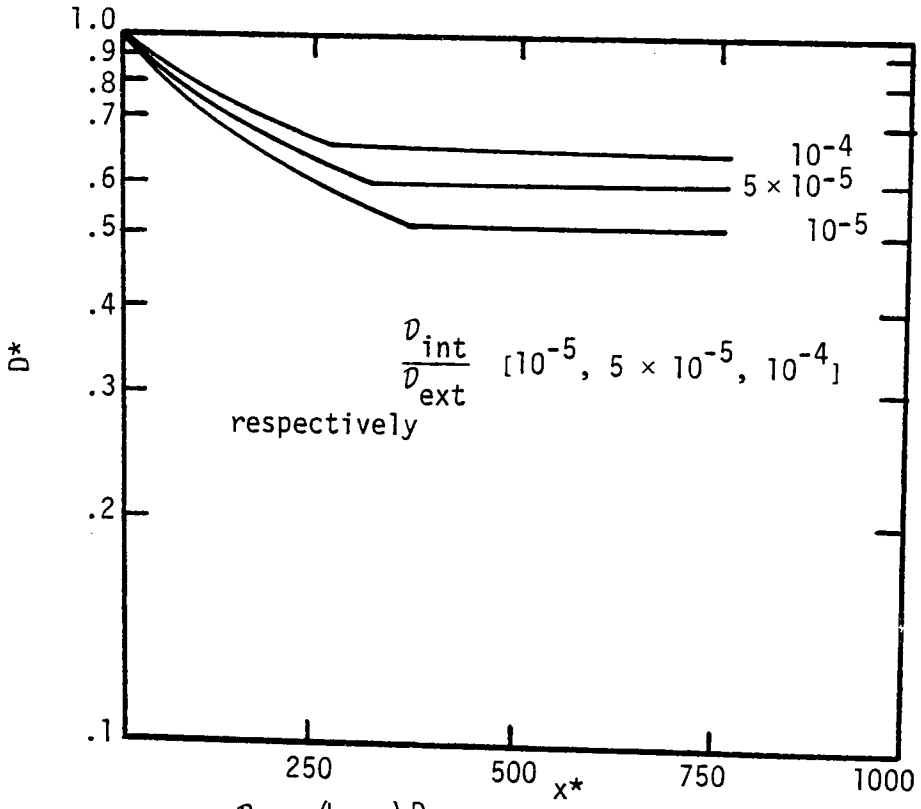

(c) various values of $\frac{\mathcal{D}_{int}}{\mathcal{D}_{ext}}$, $\frac{(k_{ext})_o D_o}{\mathcal{D}} = 20$ or $\frac{G_p}{\rho \mathcal{D} D_o} = 5.0 \times 10^4$,

$\frac{\rho F_L D_o}{\chi G_p} = 0.20$.

Figure V-6. (Continued)

previously in Chapter IV. It is effectively a discontinuity in the diameter vs. distance curve brought on by a phase change and the difference in final diameter is sufficient in some cases to cause hollow fibers. Note that as the initial Sherwood number increases the final fiber diameter increases. Also increasing $\frac{c^{F_L} D_o}{\chi G_p}$ causes a decreasing final fiber diameter. The variation of $\mathcal{D}_{int}/\mathcal{D}_{ext}$ is not nearly as large as seen in results without chemical reaction because the diffusivity is now not the rate controlling step. Some variation is still seen but this is primarily due to changes in the $\mathcal{D}_{int}$ rather than $\mathcal{D}_{ext}$.

Detailed Calculations and Comparison with Experiments

Equation IV-39 was used to calculate a dimensionless concentration profile, ϕ.

$$\phi = \frac{C - C_o}{C_o^* - C_o} \qquad \text{(V-14)}$$

where C = solvent concentration at r, t

C_o = initial solvent concentration (gm/cm^3)

C_o^* = solvent concentration in bath (gm/cm^3)

For the nylon-6-formic acid system, the value for C_o^* is obviously 0, 0.05, 0.10, and 0.15 for water, 5%, 10%, and 15% formic acid in water coagulation baths. The external mass transfer coefficient from the convection boundary condition (Equation IV-38) was obtained by analogy with a heat transfer coefficient determined by Kase and Matsuo (92) for melt spinning of a fiber. Using their correlations and inserting our experimental conditions an initial external mass transfer coefficient of

0.00875 cm/sec was obtained. This value was chosen because it was obtained experimentally for a melt spinning model and because it represents a value which is of the same order of magnitude as the others and in the middle of the range. The diffusivity used was that of formic acid in water and again was thought to be a reasonable value at 1.37×10^{-5} cm^2/sec. Using the spinneret hole radius as the characteristic dimension, these values yield an initial Sherwood number of 12.2. The filament was assumed to be a solid when the polymer concentration reached a level of 80% by weight (about twice the equilibrium value) at a distance equal to 10% of the radius from the surface. This value allows for supersaturation before coagulation and allows for 20 weight percent of residual solvent after coagulation. Figure V-7 shows the diameter predictions versus distance from the spinneret for the water and sodium hydroxide baths.

The hollow fibers were formed in a caustic coagulant of 5% NaOH in water. The chemical reaction at the interface causes a greatly increased mass transfer coefficient. Mass transfer rates with this type of chemical reaction have been described by Sherwood, Pigford, and Wilke (164) and by Astarita (8).

The interfacial reaction is a neutralization of hydronium ions with hydroxyl ions:

$$H^+ + OH^- \rightarrow H_2O$$

The reaction rate may be expressed as:

$$R = K_1 [H^+][OH^-] \qquad \text{(V-15)}$$

but it is assumed that $[OH^-]$ is essentially constant because of the large excess present so:

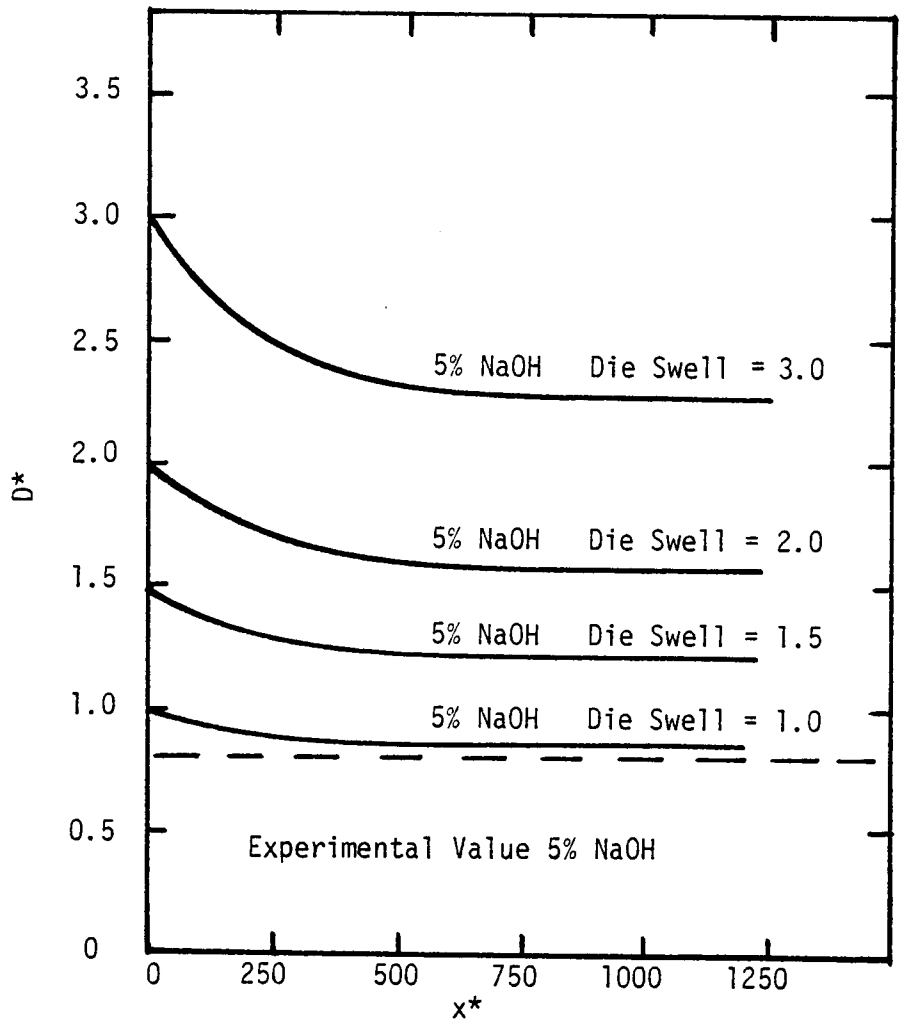

$\frac{(k_{ext})_o D_o}{\mathcal{D}} = 12.2$ or $\frac{G_p}{\rho \mathcal{D} D_o} = 3.0 \quad 10^4$, $\frac{\rho F_L D_o}{\chi G_p} = 0.20$, $\frac{\mathcal{D}_{int}}{\mathcal{D}_{ext}} = 10^{15}$.

Figure V-7. Dimensionless filament diameter vs. dimensionless distance from the spinneret for various coagulants and die swells.

$$R = K_2 [H^+] \tag{V-16}$$

where $K_2 = K_1[OH^-]$. $[H^+]$ may be determined from the equilibrium relationship: $HCOOH \rightleftarrows H^+ + COOH^-$. The equilibrium constant for this dissociation is 1.77×10^{-4}. The concentration of hydronium ions may then be expressed as:

$$(H^+) = \left[(1.77 \times 10^{-4})\ [HCOOH]\right]^{1/2} \tag{V-17}$$

When this is substituted back into the rate equation, we obtain:

$$R = K_2\left[(1.77 \times 10^{-4})\ [HCOOH]\right]^{1/2} \tag{V-18}$$

or $$R = K_3[HCOOH]^{1/2} \tag{V-19}$$

where $K_3 = K_2\ (1.77 \times 10^{-4})^{1/2} = K_1[OH^-](1.77 \times 10^{-4})^{1/2}$

This is now obviously a half order reaction and according to Sherwood et al. (164) the mass transfer coefficient in terms of the Hattat theory with chemical reaction is:

$$k_L = \sqrt{\frac{2}{1.5}\mathcal{D}K_3[HCOOH]^{-1/2}} \tag{V-20}$$

Using the previously stated diffusivity, a value of $1.4 \times 10^{11}\ M^{-1}$ sec^{-1} for K_1, and a 1.25 M solution of NaOH (5 weight percent), k_L becomes

$$k_L = \frac{206.2}{[HCOOH]^{1/4}} \tag{V-21}$$

For our purposes the concentration of formic acid at the interface varies between 70% initially to 20% finally or in terms of gm-moles/liter 35.1 to 25.7. If the value 25.7 is used for the concentration, a k_L of 90 cm/sec results. This value is larger than the mass transfer coefficient without reaction by four orders of magnitude. This is extraordinarily high and suggests that the reaction rate is not the

controlling factor. The rate constant for the neutralization is of order 10^{11} which is certainly close to an instantaneous reaction. In the case of an instantaneous reaction the depletion of one or both reactants becomes the controlling factor as previously described. When the depletion of one or both reactants becomes the controlling factor, the diffusion process of the reactants to the reaction plane may be used to describe the process.

The assumption that excess NaOH is present at the interface may not be valid because of the very rapid reaction rate. From film theory it has been shown that:

$$k_L = k_L^o \left(1 + \frac{\mathcal{D}_{NaOH}\, C_{NaOH}}{\mathcal{D}_{HCOOH} C_{H^+}}\right) \qquad \text{(V-22)}$$

The diffusivity of NaOH and formic acid in water are approximately the same within the confidence limits of their determination. The concentration of NaOH is 1.25M and the concentration of H^+ ions is 0.0519M. k_L is 0.22 cm/sec by this method. This value is the theoretical value, but specific experimental work with weak acids reacting with caustic solutions have shown this to be somewhat high. The experimental data was obtained by Astarita (7) using a laminar jet of aqueous monoethanolamine passing through CO_2. The CO_2 was absorbed forming carbonic acid which reacted with the monoethanolamine. The ratio of the liquid phase mass transfer coefficient with reaction to that without was empirically shown to vary as:

$$\frac{k_L}{k_L^o} = 0.875 \left(\frac{C_{NaOH}}{C_{H^+}}\right)^{0.67} \qquad \text{(V-23)}$$

For our conditions this yields a mass transfer coefficient of 0.065 cm/sec which is 7.4 times the value without reaction. The higher theoretical value simply shifts the curve for caustic coagulant closer to the spinneret and increases the final diameter of the fiber. If an initial external mass transfer coefficient of greater than 0.16 cm/sec is used, the model predicts an instantaneous skin formation and does not allow any draw down. This points to the experimental fact that very high concentrations of caustic in the bath can reduce the draw down to zero or in some cases make it impossible to spin fibers.

The final diameter as determined experimentally is compared to theoretical predictions in Table V-2. Theoretical predictions which include several possible die swells of 1.5, 2.0, and 3.0 are also given. The spinneret had an L/D of about one and showed a die swell of about 3.0 for the nylon-6 system spun into water. This was measured photographically and coincided with findings for acrylic fiber extrusion (57) at our shear rate of 10^4 sec^{-1}.

The theoretical predictions are compared to experimentally determined final fiber diameters in Table V-2. There seems to be reasonable agreement within the range of possible die swells.

TABLE V-2

FINAL FIBER DIAMETERS OF NYLON-6 IN FORMIC ACID

Coagulant	Experimental (cm)	Theoretical Diameters @ Die Swell (cm)				Sherwood Number	Super-structure
		1.0	1.5	2.0	3.0		
5%NaOH	.028	.017	.024	.031	.044	90	Hollow
Water	.023	.014	.020	.025	.037	12	Sponge-like
5% formic	.020	.014	.019	.023	.035	12	Sponge-like
10% formic	.020	.013	.018	.022	.034	12	Sponge-like
15% formic	.021	.012	.016	.021	.032	12	Sponge-like

CHAPTER VI

MECHANISMS CAUSING FLUTED FIBERS

Fluted fibers are fibers which contain long, lobe-like voids which extend from the outer surface of the fiber toward the center (Figure VI-1). These voids are formed during the coagulation step and remain intact in the solid fiber. It is the purpose of this chapter to explain why these voids are formed and how they may be avoided. Several examples of fluted fibers have been discovered. These systems are listed in Table VI-1 and examples are shown in Figure VI-2.

TABLE VI-1

SYSTEMS EXHIBITING FLUTING

Spinning Dope	Coagulant
20% Nomex in DMAc/5%LiCl	Water, 5%, 10%, 15% DMAc in water
20% Bisparamide A2 in DMAc	Water
25% PAN/VA copolymer in DMAc	Water
20% PS in DMAc	Water
16% Nomex in sulfuric acid	Water, 5% NaOH in water

I. CHARACTERIZATION OF FIBERS EXHIBITING FLUTING

The systems which were used to form the fluted fibers in this study are listed in Table VI-2. The diameter of the fiber, number of flutes in the cross section, and the average length of the flutes is also given. The fibers were spun from round spinnerets of diameters

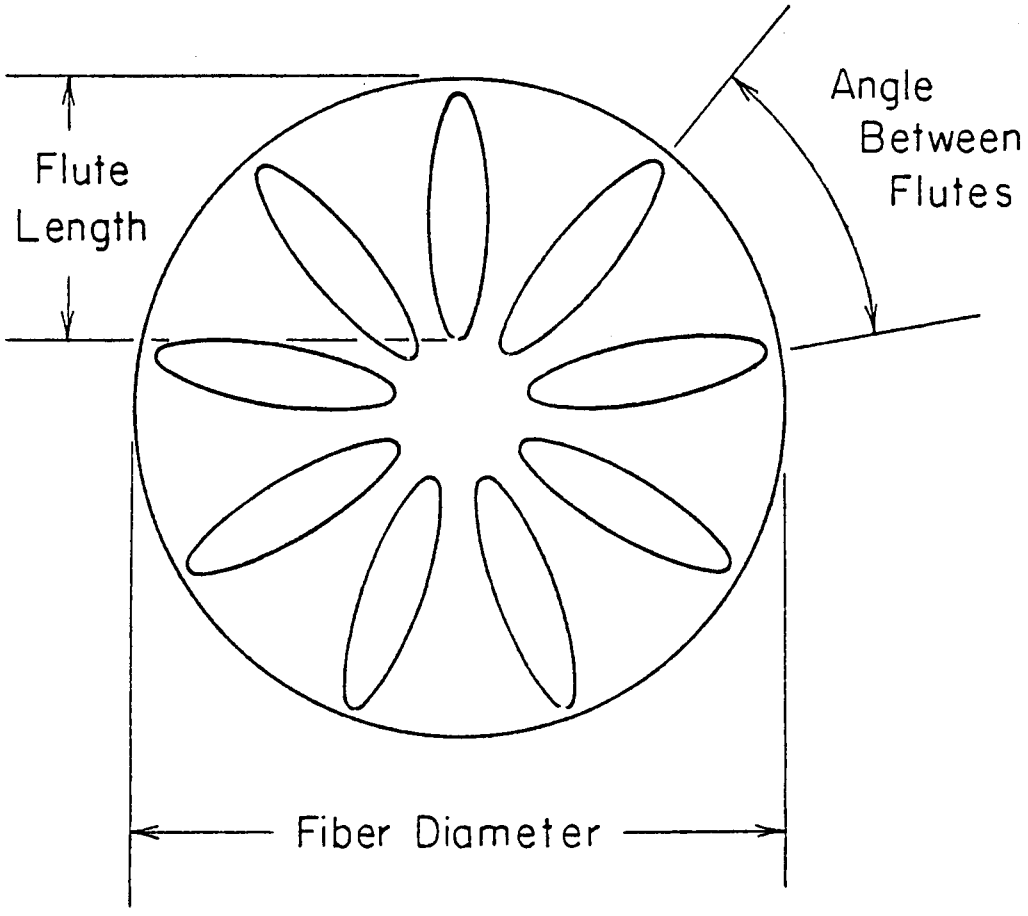

Figure VI-1. Schematic of fluted fiber.

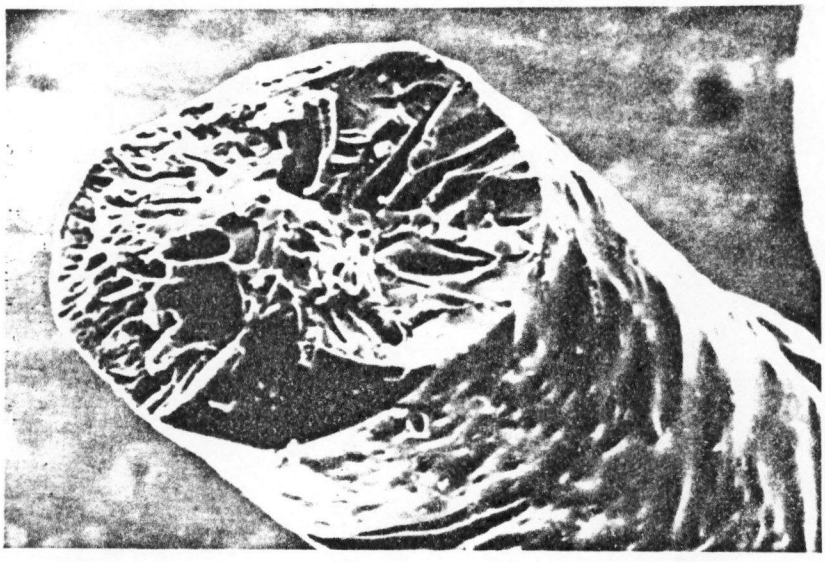

(a)
(200X)

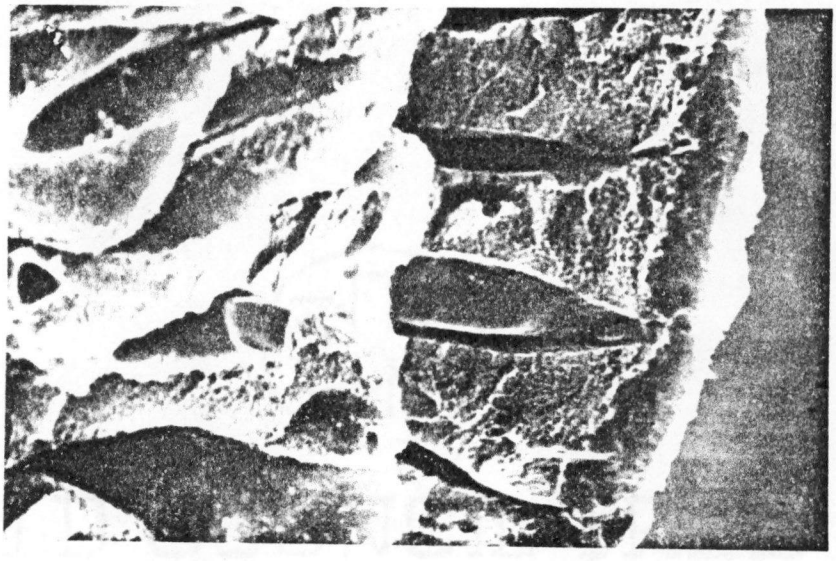

(b)
(2000X)

Figure VI-2. SEM photomicrographs of wet spun fibers; (a) 25% PAN/VA copolymer in DMAc water coagulation (200X), (b) 25% PAN/VA copolymer in DMAc water coagulation (2000X), (c) 20% Nomex in DMAc water coagulation (200X), (d) 16% Nomex in sulfuric acid water coagulation (200X).

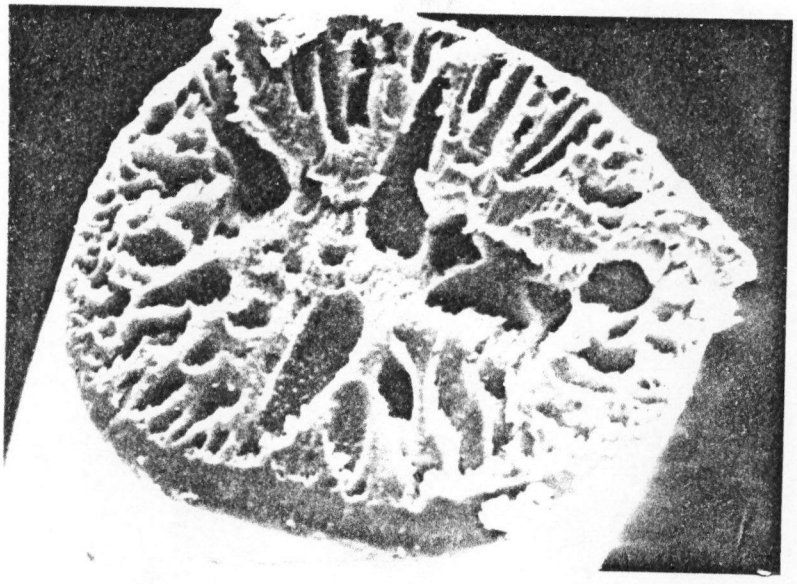

(c)
(200X)

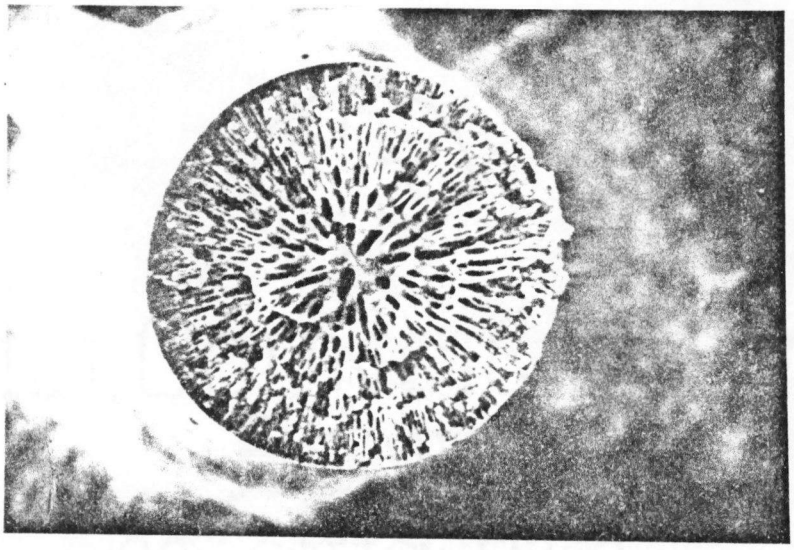

(d)
(200X)

Figure VI-2. (Continued)

TABLE VI-2

CHARACTERIZATION OF FLUTED FIBERS

Polymer	Solvent	Coagulant	Diameter (cm)	Void Fraction	Angle between Flutes	Length of Flutes (cm)	Reduced Length of Flute
Nomex	DMAc	Water	0.039	0.38	8.2°	0.01	0.26
		5% DMAc	0.039	0.57	9.0°	0.008	0.21
		10% DMAc	0.043	0.64	12.0°	0.008	0.19
		15% DMAc	0.043	0.64	18.0°	0.008	0.19
Nomex	H_2SO_4	5% NaOH	0.053	0.67	1.5°	0.0035	0.07
		Water	0.045	0.65	1.5°	0.0055	0.12
		10% H_2SO_4	0.064	---	6.0°	0.007	0.11
		25% H_2SO_4	0.105	---	4.7°	0.012	0.11
		50% H_2SO_4	0.0625	---	None	None	0---
PAN/VA	DMAc	Water	0.025	0.09	15.0°	0.01	0.40
		30% DMAc	0.012	0	90.0°	0.003	0.25
		40% DMAc	0.011	0	None	None	---
		Methanol	0.089	0	None	None	---

0.127, 0.038, and 0.0152 cm. The fiber diameter variations for a given spinneret are caused by die swell and draw down. The void fraction was calculated from Equation VI-1.

$$\varepsilon = 1 - \frac{M}{LA\rho} \qquad \text{VI-1}$$

where ε = void fraction

M/L = denier

A = cross sectional area

ρ = density of polymer

The void fraction values give an indication of the porosity of the fibers, but their absolute value is so dependent on accurate measurement of the dimensions that it is uncertain. Some of the fibers are elliptical and diameter measurement for such samples was obtained by averaging two dimensions.

The length of the flutes seems to remain near 0.01 cm or below for most systems. The angle between the flutes seems to be larger in systems with large amounts of spinning dope solvent in the bath.

II. OBSERVATIONS OF MECHANISM OF FLUTING

Microscopic Studies

The static observation of coagulation, discussed previously, provides a means of watching the flutes form. Epstein and Rosenthal (54) have used a microscopic coagulation technique to observe the interface during coagulation. They filmed the sequence and observed the disruption of the interface by flutes. A similar technique was used in this thesis and was described in Chapter III. By this method

many systems were studied which could not be wet spun into fibers. Table VI-3 shows the systems examined. Polystyrene was chosen for many of these studies because it is easily soluble in a number of different solvents.

The polymer solutions which formed fluted fibers also showed fingering when examined under the microscope during coagulation. PAN dissolved in DMAc was one such system which exhibited fingering. Still photographs of this coagulation are seen in Figure VI-3. Figure VI-4 shows a similar set of photographs for polystyrene dissolved in DMAc and H_2O. The interface starts moving smoothly and suddenly begins to break up into a series of finger-like intrusions. These intrusions grow inward towards the center of the drop of polymer solution.

It was found that when DMAc was the solvent, fingering occurred no matter what polymer was present. These same polymers in other solvents did not show fingering and indicated that some property inherent to the solvent was causing the fingering.

At this point the interface between pure solvent and coagulant with no polymer present was examined. DMAc and water showed fingering (Figure VI-5) which was even more pronounced in the absence of polymer than it was with polymer present. Since the effect occurred without polymer being present, the interaction between solvent and coagulant was considered to be of primary importance. The presence of the polymer increased the viscosity and probably acts as a damping force when the fingering begins. Several systems were studied to determine the onset of the fingering. These are listed in Table VI-4.

TABLE VI-3

SYSTEMS EXAMINED BY STATIC COAGULATION TECHNIQUE

Polymer	Solvent	Coagulant	Heat of Solution Cal/gm sol'n.	Observations
PAN	DMAc	Water	11.4	Fingers
PS	DMAc	Water	11.4	Fingers
Nomex	DMAc	Water	11.4	Fingers
Nylon-6	Formic Acid	Water	4.5	Smooth
Nomex	H_2SO_4	Water	55.5	Fingers
PS	p-xylene	MeOH	Small	Smooth
		n-Heptane	Small	Smooth
		Acetone	Small	Smooth
		Water	Small	Smooth
	Benzene	MeOH	Small	Smooth
		n-Heptane	Small	Smooth
		Acetone	Small	Smooth
	MEK	MeOH	Small	Smooth
		n-Heptane	Small	Smooth
		Acetone	Small	Smooth
		Water	Small	Smooth
	EtAc	MeOH	Small	Smooth
		n-Heptane	Small	Smooth
		Acetone	Small	Smooth

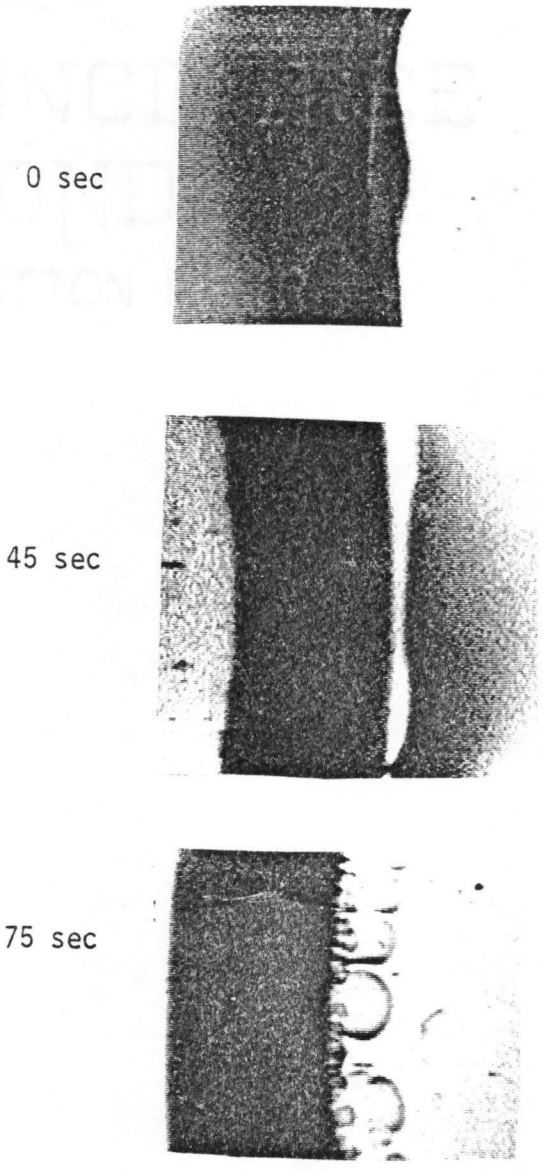

Figure VI-3. Static coagulation studies of PAN/VA in DMAc and water coagulant.

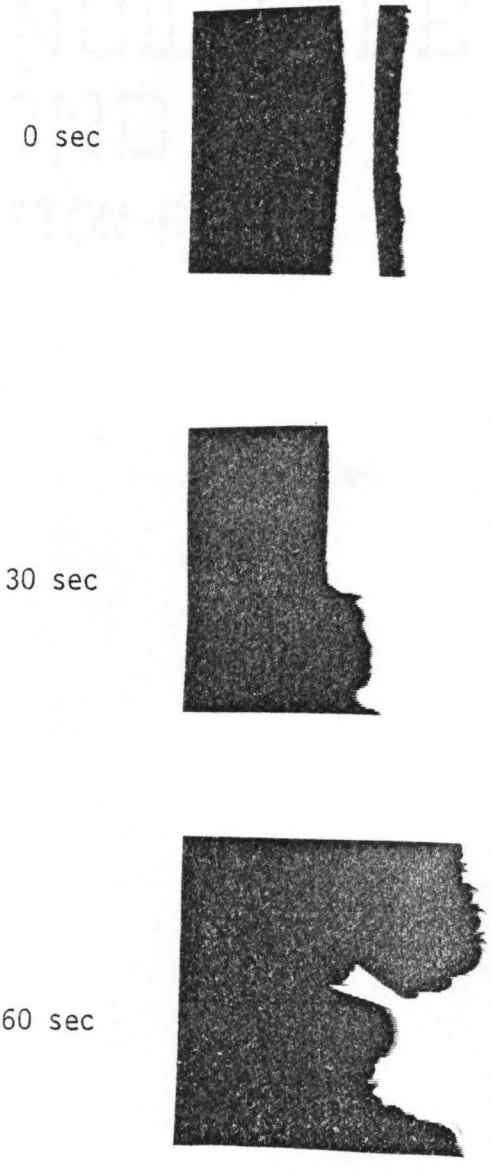

Figure VI-4. Static coagulation studies of polystyrene in DMAc and water coagulant.

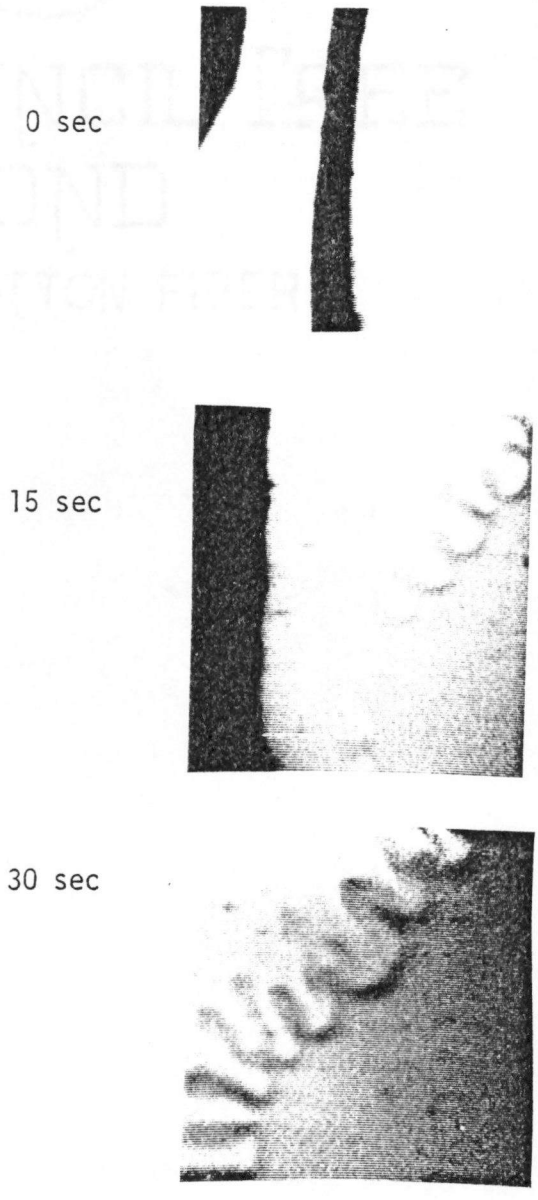

Figure VI-5. Static interfacial studies between DMAc and water.

TABLE VI-4

STUDIES OF THE ONSET OF FINGERING

Solution	Coagulant	Heat of Solution cal/gm sol'n.	Observation
DMAc	Water	11.4	Fingers
	15% DMAc	8.0	Fingers
	30% DMAc	6.0	Fingers
	40% DMAc	5.2	Smooth
	60% DMAc	3.0	Smooth
30% NaOH	Water	8.9	Fingers
	10% NaOH	5.6	Fingers
	20% NaOH	1.9	Smooth
100% H_2SO_4	Water	117	Fingers
	50% H_2SO_4	60	Fingers
	70% H_2SO_4	42	Fingers
	80% H_2SO_4	22	Fingers
	90% H_2SO_4	1	Smooth

Studies of system interaction in these liquid pairs turned up that a primary variable with these systems is the heat of solution. Those systems in Table VI-3, page 110, with a high heat of solution exhibit fingering while those with a low heat of solution do not. This is further shown in Table VI-4 where the onset of the fingering is studied.

It was desireable to quantify the heat of mixing necessary to produce fingering. Pure solvent and various concentrations of solvent in coagulant were combined and observed to determine the onset of fingering. Fingering did not occur when pure DMAc and 40/60 (DMAc/water) were mixed, but fingering did occur when pure DMAc and 30/70 (DMAc/water) were mixed. The heats of mixing of the above two cases based on data by DiCave and Carli (45) are 5.2 cal/gm solution and 6.0 cal/gm solution respectively. Liquids other than the typical wet spinning solvents show this phenomena also such as concentrated sodium hydroxide in water. Fingering did not occur when 30% NaOH in water and 20% NaOH in water were mixed, but fingering did occur when 30% NaOH in water and 10% NaOH in water were mixed. According to data from McCabe (114) the heats of solution are 1.9 cal/gm solution and 5.6 cal/gm solution respectively. The onset of fingering seems to occur at about 5.6-6.0 cal/gm solution. The interface between sulfuric acid and water-acid solutions shows similar fingers. The onset of fingering occurs at some point between a heat of solution of 22 and 1.0 cal/gm. This value is in the same area that the fingering began for the two previous systems. This data seems to indicate a correlation between fingering and the value of the heat of solution.

Movement of the Interface

The static coagulation technique has been used for measurement of the interfacial position. This is similar to that used for results presented in Chapter V for smooth interfaces, but the position of the interface is not easily judged. As shown in Figure VI-3, page 111 the coagulation front follows the fingered interface. The movement of this coagulation front was measured with the calibrated microscope.

It was seen, as predicted, that the coagulation was much more rapid, due to increased surface area, when the instability was present. Figure VI-5 shows that the lower viscosity dopes have more rapid interfacial movement (e.g., Polystyrene initially coagulated more slowly than PAN but soon overtook and surpassed PAN with similar solvent and coagulant). This may be changed by the addition of surfactants to the bath as shown for the polystyrene-DMAc-water + soap coagulation. The most rapid interfacial movement was Polystyrene in DMAc, next was PAN in DMAc, and slowest was polystyrene in DMAc with water plus surfactant as coagulant. The surfactant used was about 1% liquid detergent. All of these were more rapid than the Nylon-6 in formic acid system shown in Figure IV-4, page 58.

III. DISCUSSION

Comparison to Observations on Films

For many years membranes have been prepared by casting a film from solution and coagulating the polymer or allowing the solvent to evaporate. Membranes used for desalination of salt water are produced by casting

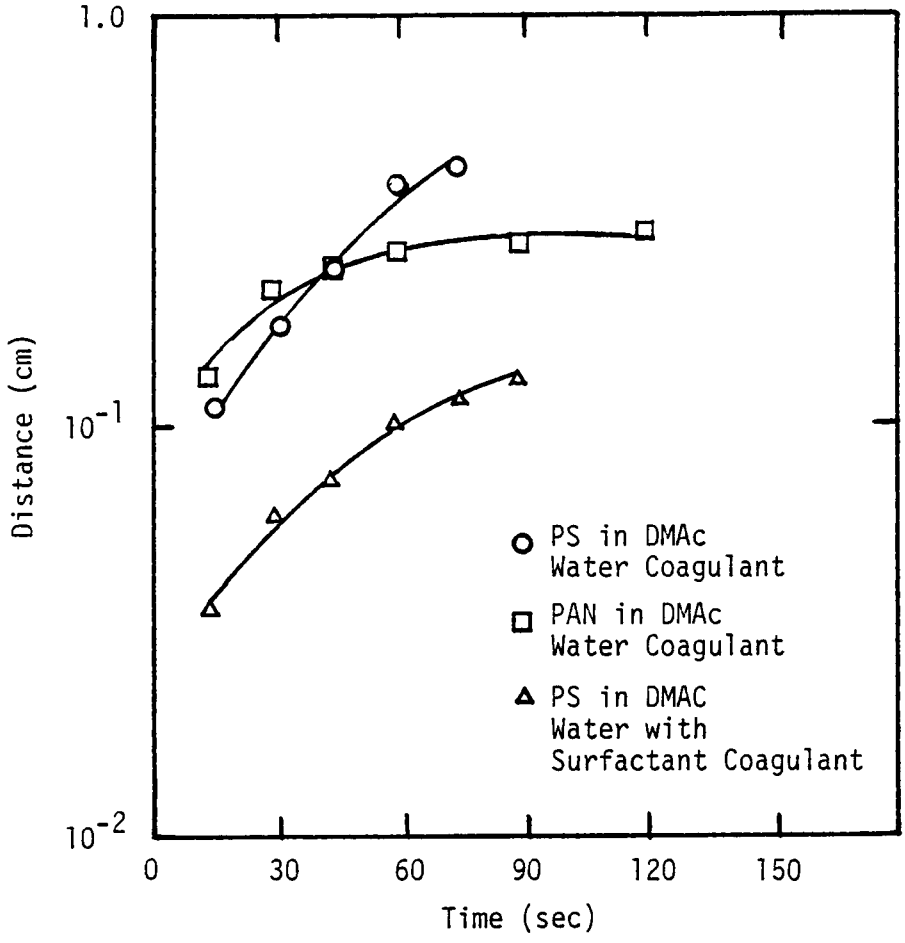

Figure VI-6. Coagulated distance vs. time.

films of cellulose acetate from DMAc solutions. Matz (112, 113), Frommer and Messalem (63), and Strathmann, Kock, and Amar (171) have shown that these finger-like intrusions are present in the membranes. They predicted that the intrusions occurred during coagulation and proved this by observing partially coagulated membranes under the SEM. They stopped the coagulation at various stages and saw that the intrusions became larger with increasing coagulation time. The fingering created pores in the final membrane. The size of these pores was crucial since they caused the semipermeable nature of the membrane. They offered no mechanistic explanation for the formation of the pores, but the solvents producing fingering used in their studies had high heats of solution.

Statement of Mechanism

The preceding experimental evidence leads to the conclusion that fluted fibers are caused by a hydrodynamic instability. This instability is the result of a high heat of mixing between solvent and coagulant. The heat generated at the interface causes a local temperature increase which occurs suddenly. This temperature increase causes a point decrease in interfacial tension. As a result of the decreased interfacial tension a fluctuation of the interface occurs and grows into a macroscopic disturbance. This disturbance grows into an intrusion with a smaller and smaller radius of curvature.

The instability causes a very rapid coagulation because it generates additional surface area for diffusion. The lobes that are formed during

coagulation dry to form voids of similar shape in the final fiber. These voids are the flutes seen under SEM examination of the fiber cross-sections.

The interfacial tension fluctuations may be damped by physical properties such as viscosity and addition of surfactants. A highly viscous spinning dope would not show the instability even if the solvent and coagulant had a high heat of solution. The viscous forces over power the forces causing the interfacial fluctuations. It is also true that a lower viscosity dope with the same solvent-coagulant pair exhibits more flutes per 360°. This was shown in the system of DMAc/ Bisparamide A2 (6) and DMAc/Nomex. The Bisparamide A2 solution had a lower viscosity than the Nomex solution and showed many more flutes. Another example of the effects of viscosity is the Kevlar/sulfuric acid system. This system never exhibits any flutes even though it obviously has a high heat of solution. Nomex dissolved in sulfuric acid shows flutes, but the Kevlar dopes are much more viscous and simply damp out the instability. Another possible way to eliminate the instability is to add a surfactant to the bath. It was found that the use of methanol as a coagulant or the addition of small amounts of methanol to water eliminated the instability. This was also true for the addition of liquid soap in water. These two means by which the instability may be damped are specifically excluded from the stability analysis.

Hydrodynamic Stability Interpretation

The appearance of an intrusion or finger is reminiscent of some sort of hydrodynamic instability. When the fingers are viewed as an

instability, two classical types come to mind: (1) Rayleigh instability (density driven), and (2) Marangoni instability (interfacial tension driven). The Rayleigh instability has been examined by numerous authors (149, 14, 15), but all are in general agreement that for depths less than one centimeter, the density driven instability is not significant. Numerous authors have examined the Marangoni instability and its implications (143, 41), but the most useful treatment for our purposes was carried out by Sternling and Scriven (169). They have quantified the instability and used a perturbation type analysis to predict the necessary conditions for a stable interface. They solved simultaneously the equations of motion and diffusion to obtain a growth constant which was then subjected to a perturbation analysis. Their analyses involve an interfacial instability caused by a local fluctuation in surface tension during mass transfer which builds up into a macroscopic disturbance. Their equations predict that this will be promoted if the solute transfers from the phase of higher viscosity and lower diffusivity, if there are large differences in diffusivity, and also in kinematic viscosity between the two phases, if there are steep concentration differences near the interface, if $d\gamma/dc$ is large negatively, if surface active agents are absent, and if the interface is large in extent. Sternling and Scriven were analyzing an instability due to interfacial tension fluctuation as a result of mass transfer or concentration changes.

The fingering instability while having many features of the Sternling-Scriven mechanisms has certain differences. The wet spinning

instability is associated with heats of mixing and local temperature changes rather than concentration changes and only two components are present. Further work by Sawistowski and his coworkers (11, 145, 190) has modified the Sternling-Scriven analysis to apply to partially miscible liquid pairs. This analysis discusses instabilities resulting from thermal effects due to heats of solution rather than from mass transfer of a third component. This is directly applicable to the instability occurring in wet spinning.

IV. STABILITY ANALYSIS FOR COAGULATING FILAMENT

The fiber was assumed to be a cylinder in contact with an infinite sea of coagulant. The problem was treated in a two-dimensional fashion neglecting disturbances along the fiber axis. As a first approximation we neglect the non-Newtonian viscoelastic characteristics of the filaments. The applicable equations of motion for a Newtonian fluid are:

$$\frac{\partial v_r}{\partial t} + v_r \frac{\partial v_r}{\partial r} + \frac{v_\theta}{r}\frac{\partial v_r}{\partial \theta} - \frac{v_\theta^2}{r} = -\frac{1}{\rho}\frac{\partial P}{\partial r} + \nu\left[\frac{\partial}{\partial r}\left(\frac{1}{r}\frac{\partial}{\partial r}(rv_r)\right) + \frac{1}{r^2}\left(\frac{\partial^2 v_r}{\partial \theta^2}\right) - \frac{2}{r^2}\frac{\partial v_\theta}{\partial \theta}\right] \tag{VI-2}$$

$$\frac{\partial v_\theta}{\partial t} + v_r \frac{\partial v_\theta}{\partial r} + \frac{v_\theta}{r}\frac{\partial v_\theta}{\partial \theta} + \frac{v_r v_\theta}{r} = -\frac{1}{\rho r}\frac{\partial P}{\partial \theta} + \nu\left[\frac{\partial}{\partial r}\left(\frac{1}{r}\frac{\partial}{\partial r}(rv_\theta)\right) + \frac{1}{r^2}\frac{\partial^2 v_\theta}{\partial \theta^2} + \frac{2}{r^2}\frac{\partial v_r}{\partial \theta}\right] \tag{VI-3}$$

The nonlinear inertial terms are neglected because they are of secondary importance in comparison with the other terms. The pressure terms are eliminated by cross differentiation and subtraction of Equation VI-3 from Equation VI-2 to obtain:

$$\frac{\partial^2 v_r}{\partial t \partial \theta} - r\frac{\partial^2 v_\theta}{\partial t \partial \theta} = \nu\left[\frac{\partial^2}{\partial \theta \partial r}\frac{1}{r}\frac{\partial}{\partial r}(rv_r) + \frac{1}{r^2}\frac{\partial^3 v_r}{\partial \theta^3} - r\frac{\partial^2}{\partial r^2}\left(\frac{1}{r}\frac{\partial}{\partial r}(rv_\theta)\right) - \frac{1}{r}\frac{\partial^3 v_\theta}{\partial \theta^2 \partial r} - \frac{2}{r}\frac{\partial^2 v_r}{\partial r \partial \theta} + \frac{2}{r^2}\frac{\partial v_r}{\partial \theta}\right] \tag{VI-4}$$

The stream functions for polar coordinates are:

$$v_r = \frac{-1}{r}\frac{\partial \psi}{\partial \theta} \tag{VI-5}$$

$$v_\theta = \frac{\partial \psi}{\partial r} \tag{VI-6}$$

When Equation VI-4 is written in terms of the stream function, Equation VI-7 is obtained.

$$-\frac{1}{r}\frac{\partial^3 \psi}{\partial t \partial \theta^2} - r\frac{\partial^3 \psi}{\partial t \partial r^2} = \nu\left[-\frac{1}{r}\frac{\partial^4 \psi}{\partial r^2 \partial \theta^2} + \frac{1}{r^2}\frac{\partial^3 \psi}{\partial r \partial \theta^2} - \frac{1}{r^3}\frac{\partial^4 \psi}{\partial \theta^4} - \frac{\partial^3 \psi}{\partial r^3} + \frac{2}{r}\frac{\partial^2 \psi}{\partial r^2} - \frac{2}{r^2}\frac{\partial \psi}{\partial r} - r\frac{\partial^4 \psi}{\partial r^4} - \frac{1}{r}\frac{\partial^4 \psi}{\partial \theta^2 \partial r^2} + \frac{2}{r^2}\frac{\partial^3 \psi}{\partial \theta^2 \partial r} - \frac{4}{r^2}\frac{\partial^2 \theta}{\partial \theta^2}\right] \tag{VI-7}$$

Let the stream function, $\psi = \phi(r)e^{i\alpha\theta}e^{\beta t}$, where α is the wave number of the perturbation and β is the growth constant. Upon substitution of this into Equation VI-7, simplifying, and putting into dimensionless form Equation VI-8 is obtained.

$$\phi'''' + \frac{1}{\delta}\phi''' - \left(\frac{2\alpha^2 + 1}{\delta^2}\right)\phi'' - \left(\frac{\alpha^2 - 2}{\delta^3}\right)\phi' - \left(\frac{4\alpha^2 - \alpha^4}{\delta^4}\right)\phi = \frac{\alpha^2 \beta R^2}{\nu \delta^2}\phi + \frac{\beta R^2}{\nu}\phi'' \qquad \text{(VI-8)}$$

where $\delta = r/R$

$$\phi' = \frac{\partial \phi}{\partial \delta}$$

The boundary conditions are as follows:

1. & 2. $\phi_A = \phi_A' = 0$ at $\delta = \infty$

3. & 4. $\phi_B = \phi_B' = 0$ at $\delta = 0$

5. & 6. $\phi_A = \phi_B = 0$ at $\delta = 1$

7. $\phi_A' = \phi_B'$ at $\delta = 1$

8. $\gamma_{r\theta_A} - \gamma_{r\theta_B} = \frac{\partial \gamma_\theta}{\partial \theta}$ at $\delta = 1$

Now let us examine the perturbed equations of energy and concentration for this system. The two-dimensional diffusion equation in polar coordinates is given in Equation VI-9.

$$\frac{\partial C}{\partial t} + v_r \frac{\partial C}{\partial r} + \frac{v_\theta}{r}\frac{\partial C}{\partial r} = \mathcal{D}\left[\frac{\partial^2 C}{\partial r^2} + \frac{1}{r}\frac{\partial C}{\partial r} + \frac{1}{r^2}\frac{\partial^2 C}{\partial \theta^2}\right] \qquad \text{(VI-9)}$$

The perturbed concentration may be written as:

$$C = C^\circ + \hat{C}\,(r,\theta,t)$$

where $C^\circ = C_i^\circ + r\varepsilon_D$

$\hat{C} = H(r)e^{i\alpha\theta}e^{\beta t}$

C_i° = interfacial concentration

ε_D = concentration gradient at the interface

$$v_r = \frac{-i\alpha}{r}\,\phi e^{i\alpha\theta} e^{\beta t}$$

$$v_\theta = \phi'\, e^{i\alpha\theta} e^{\beta t}$$

When this perturbation is introduced into Equation VI-9, the second order terms are neglected, and the result is put into dimensionless form, Equation VI-10 results.

$$H'' + \frac{1}{\delta} H' - \left(\frac{\alpha^2}{\delta^2} + \frac{\beta R^2}{D}\right) H = \frac{-i\alpha R}{\delta D}\,\phi\varepsilon_D - \frac{\varepsilon_D R}{\delta} \qquad \text{(VI-10)}$$

Similarly for the energy equation, the temperature perturbation takes the form:

$$T = T^\circ + \hat{T}\,(r,\theta,t)$$

where $T^\circ = T_i^\circ + \varepsilon_T r$

$\hat{T} = P(r)e^{i\alpha\theta} e^{\beta t}$

T_i° = interfacial temperature

ε_T = temperature gradient at the interface

The final dimensionless energy equation is:

$$P'' + \frac{1}{\delta} P' - \left(\frac{\alpha^2}{\delta^2} + \frac{\beta}{K}\right) P = \frac{i\alpha R\varepsilon_T}{\delta K}\,\phi - \frac{\varepsilon_D R}{\delta} \qquad \text{(VI-11)}$$

The boundary conditions for Equations VI-10 and VI-11 are:

9. & 10. $P_A = H_A = 0$ at $\delta = \infty$

11. & 12. $P_B' = H_B' = 0$ at $\delta = 0$

13. $P_A = P_B$ at $\delta = 1$

14. $H_A = \left(\frac{\partial C_\delta^*}{\partial \bar{T}}\right) P_A = R_A P_A$ at $\delta = 1$

15. $H_B = \left(\frac{\partial C_\delta^*}{\partial \bar{T}}\right) P_B = R_B P_B$ at $\delta = 1$

16. $$-\mathcal{D}_A Q_A^\circ \frac{dH_A}{d\delta} + \mathcal{D}_B Q_B^\circ \frac{dH_B}{d\delta} = -\kappa_A \frac{dP_A}{d\delta} + \kappa_B \frac{dP_B}{d\delta} \quad \text{at } \delta = 1$$

Boundary condition (16.) may be rewritten in dimensionless form as:

16.A $$-F_A \frac{dH_A}{d\delta} + F_B \frac{dH_B}{d\delta} = \frac{dP_A}{d\delta} + \frac{dP_B}{d\delta}$$

where $$F_A = \frac{DQ\mathring{A}}{\kappa} \text{ and } F_B = \frac{DQ\mathring{B}}{\kappa}$$

The group F_A of F_B has dimensions of temperature however and in order to make them stand alone as dimensionless groups, they must be combined with a group having units of reciprocal temperature. Since H is the perturbed concentration profile, any dimensionless group must also contain concentration units, but in this case concentration is expressed as a mass fraction and is therefore dimensionless. It follows that the dimensionless group F should be defined as $\frac{DQC}{\kappa T}$ and that the characteristic value of this group is $\frac{DQ}{\kappa}\left(\frac{dC}{dT}\right)$ equilibrium where $\frac{dC}{dT}$ is the rate of change of equilibrium interfacial concentration with temperature. This also includes the assumption that the diffusivity and thermal conductivity of each phase is equivalent to that of the other phase, which seems reasonable due to the similarity of the solvents and coagulants.

The preceding analysis was carried out using the Navier-Stokes equations and thus assuming Newtonian fluid behavior. The polymer solutions involved are viscoelastic, but very near the interface the movement is very slight and probably may be presumed Newtonian. Use of a viscoelastic model would predict linearly viscoelastic response and probably erroneously predict that the instability would grow at a more rapid rate than that for the Newtonian model. This is inherent in linear stability analyses of quiescent fluids and is directly opposite

to experimental findings which show that the instabilities are damped out quickly in a highly viscoelastic fluid.

The stability equations may be solved in a similar manner to the Sternling and Scriven solution for a planar interface. The purpose of this work is to predict when an instability will occur and grow. At this point several dimensionless groups may be obtained from Equations VI-8, VI-10, and VI-11 and from boundary condition (16.). The equation of motion contains dimensionless groups with a characteristic length and kinematic viscosity. The equations of energy and concentration contain groups with thermal and mass diffusivity, temperature and concentration gradients at the interface, and a characteristic length. The dimensionless group originating in boundary condition (16.) is perhaps the most interesting for our particular case since it contains the mass diffusivity, thermal conductivity, and the heat of solution. These three terms are the parameters which control the temperature and concentration gradients at the interface. Their combination provides an effective way of stating the problem of stability with material properties. The group $\frac{DQ}{\kappa}\left(\frac{dC}{dT}\right)$ for most liquid systems is a stronger function of Q, heat of solution, than of diffusivity or thermal conductivity although both are important at times. The diffusivity controls the rate at which solvent and coagulant mix to yield a heat of solution and the thermal conductivity controls the temperature buildup at the interface due to the heat of solution.

Even though the dimensionless group containing heat of solution may be the primary one for our systems, other dimensionless groups are

present and must interact in determining the onset of the instability. One such group is the Marangoni number:

$$M = \mu\alpha/\sigma_T\varepsilon_T \qquad \text{(VI-12)}$$

where μ = interfacial viscosity

α = thermal diffusivity

σ_T = rate of change of interfacial tension with temperature

ε_T = gradient of temperature profile

The instability is driven by heat of solution effects but may either be promoted or retarded by hydrodynamic considerations. The viscosity or magnitude of the surface tension gradient can retard a prospective in stability to enhance it. The absolute value of the interfacial tension or its gradient with temperature is not well known and can only be interpreted qualitatively.

VI. INTERPRETATION FOR FIBER STRUCTURE

The parameters in the dimensionless group, F, are given for several systems in Tables VI-5 and VI-6. In order to obtain a value for F for a system the value of ΔT must be known. This value requires the solution of the problem unless a satisfactory assumption can be made.

The value of $(\frac{dC}{dT})_{equil}$ was assumed to be 0.1. and was used in the calculations to obtain a numerical value for F. The assumption is thought to be reasonable because of the relatively high heats of solution involved. The onset of the instability is seen to

TABLE VI-5

PHYSICAL PARAMETERS OF SOLVENT AND COAGULANTS

Two-Component System	Diffusivity $\times 10^5$ cm^2/sec	Thermal Conductivity $\frac{cal}{sec\ cm\ 2\ (\frac{°C}{cm})}$	Heat of Solution cal/gm sol'n.	F at $(\frac{dC}{dT})_{equil}$ =0.1
Low Molecular Weight Systems				
Sulfuric acid-water	1.97	0.0009	117.0	0.258
DMAc-water	1.19	0.0004	11.4	0.035
DMAc-30% DMAc	1.19	0.0004	6.0	0.018
DMAc-40% DMAc	1.19	0.0004	5.2	0.015
Formic acid-water	1.37	0.0004	4.5	0.015
30%NaOH-water	1.4	~0.0004	8.9	0.033
30%NaOH-10%NaOH	1.4	~0.0004	5.6	0.020
30%NaOH-20%NaOH	1.4	~0.0004	1.9	0.007

TABLE VI-6

PHYSICAL PARAMETERS OF POLYMER SOLUTIONS AND COAGULANTS

Two-Component System	Diffusivity $\times 10^5$ cm^2/sec	Thermal Conductivity $\frac{cal}{sec\ cm^2\ (\frac{°C}{cm})}$	Heat of Solution cal/gm sol'n.	F at $(\frac{dC}{dT})_{equil}$ =0.1
Polymer Solutions				
Nomex in H_2SO_4/water	1.97	0.0009	117	0.258
Nomex in H_2SO_4/ 20% H_2SO_4	1.97	0.0009	90	0.198
Nomex in H_2SO_4/ 50% H_2SO_4	1.97	0.0009	60	0.125
PAN in DMAc/water	1.19	0.0004	11.4	0.035
PAN in DMAc/30% DMAc	1.19	0.0004	6.0	0.018
PAN in DMAc/40% DMAc	1.19	0.0004	5.2	0.015
PS in DMAc/water	1.19	0.0004	11.4	0.035
PS in DMAc/30% DMAc	1.19	0.0004	6.0	0.018
PS in DMAc/40% DMAc	1.19	0.0004	5.2	0.015

occur at values of F higher than 0.018 for the low molecular weight combinations. This means that for systems in which formic acid is the solvent, no instability can occur. Experimentally this has been verified. DMAc-water mixtures do show an instability as expected at coagulant concentrations lower than 40% DMAc.

Fibers spun from these solvents may be characterized in a similar manner. None of the fibers spun from formic acid solutions showed any fluting. Both PAN and polystyrene spun from DMAc showed fluting at bath concentrations lower than 40% DMAc. Nomex® solutions in sulfuric acid did not follow this criteria as well, probably because of their high viscosity. The diffusivity varies with the inverse of the viscosity. This means that the diffusivity for a polymer solution is somewhat lower than that of the solvent without polymer and this would tend to decrease F and make the interface stable at lower concentrations of acid in the bath.

Table VI-2, page 107, shows that the angle between flutes generally increases with increasing solvent in the bath. This follows from our analysis since the frequency of instabilities around the circumference of the fiber should increase with increasing F (i.e., decreasing solvent in the bath). This is a qualitative observation however due to the inaccuracy in the measurements involved.

VI. CONCLUSIONS

The process during coagulation of polymer solutions which causes flutes in fibers and membranes is basically the same. The interaction

between solvent and coagulant is the determining factor in flute formation and the polymer present is of secondary importance. The mechanism by which the flutes are formed is a hydrodynamic instability brought about by fluctuations in interfacial temperature fluctuations due to high heats of solution between solvent and coagulant.

The interface has been modeled using a perturbation stability analysis. After the governing equations and their respective boundary conditions were assembled, a dimensionless group consisting of the product of diffusivity and heat of solution divided by the thermal conductivity and multiplied by the rate of change of concentration with temperature at steady state. For values of this group of 0.018 or higher the instability is promoted and for lower values the instability is damped.

The object of this work was to define the mechanism by which the macroscopic voids called flutes are formed. With a basic understanding of the mechanism, the phenomena may be avoided in commercial fiber processing. The occurrence of any void is detrimental to the mechanical properties of an industrial fiber. It has been shown that if a system exhibits the fingering instability in static coagulation tests, it will form fluted fibers. A rough idea of whether a potential instability will manifest itself may be obtained from simply combining the solvent and coagulant and observing the interface. An unstable interface would indicate a high probability of fluted fiber formation. This procedure forms a recipe for wet spinning research on new systems.

If flutes do become evident, they may be damped by adding surfactant to the bath or by increasing the viscosity of the solution. There are two possible explanations for this. According to Sternling and Scriven (169), the addition of surfactants increases the magnitude of the surface viscosity (μ). This in turn increases the Marangoni number (Equation VI-12, page 127) by (1) increasing the viscosity and (2) by lowering the interfacial tension gradient. An increase in solution viscosity would have similar effects. This is a condition where the hydrodynamic considerations are controlling and damp out the instability initiated by the heat of solution.

Another possible explanation is that the addition of surfactant or increase in dope viscosity simply decreases the mass transfer rate or the effective diffusivity. It has been shown that diffusivity varies inversely with viscosity. In this case, a decreased diffusivity would result in lower local heating and less likelihood for initiation of instability. Either explanation is possible and it is not clear whether one or the other is correct or some combination is true. Lowering the effective heat of mixing between the solvent and coagulant by adding solvent to the bath will also eliminate the flutes. It has been reported (90) that flute formation is related to take-up velocity. This was not found in our work but could be related to residence time in the bath.

These findings mean that for commercial wet spinning the dopes should be very viscous and should be spun into baths containing solvent (to lower the heat of solution) and surfactants (to stabilize the

interface). The fibers should have small diameters to speed coagulation and allow shorter residence times in the bath. This is a good description of the commercial wet spinning process as it exists today after having been developed empirically over many years.

CHAPTER VII

MECHANISMS CAUSING SPONGE-LIKE FIBERS

I. SYSTEMS WHICH EXHIBIT SPONGE-LIKE FIBERS

All solution spun fibers contain voids. These voids may be very small or quite large depending on coagulation conditions. It is usually desireable to minimize the size of these voids so that fiber properties will be maximized. The voids act as stress concentrators and weaken the fiber. When the voids are large, they may be seen with the SEM as in Fibure VII-1. These photomicrographs show the sponge-like character of some fibers with large voids and generally represent the situation for fibers with smaller voids. The SEM cannot be used for study of these small voids, but small angle x-ray scattering (SAXS) is a very effective tool for this. A SAXS pattern of such a fiber is shown in Figure VII-2. The dense area near the center of the pattern indicates microvoids in the range of 50-100 A°.

The nylon-6 and nylon-66 in formic acid systems show a sponge-like structure for all coagulants except those involving a chemical reaction at the interface. These systems may even have a sponge-like structure in the skin of the hollow core fiber which is picked up by SAXS. Melt spun fibers from these polymers contain no voids discernable by SEM or SAXS. This indicates that the coagulation process is responsible for void formation.

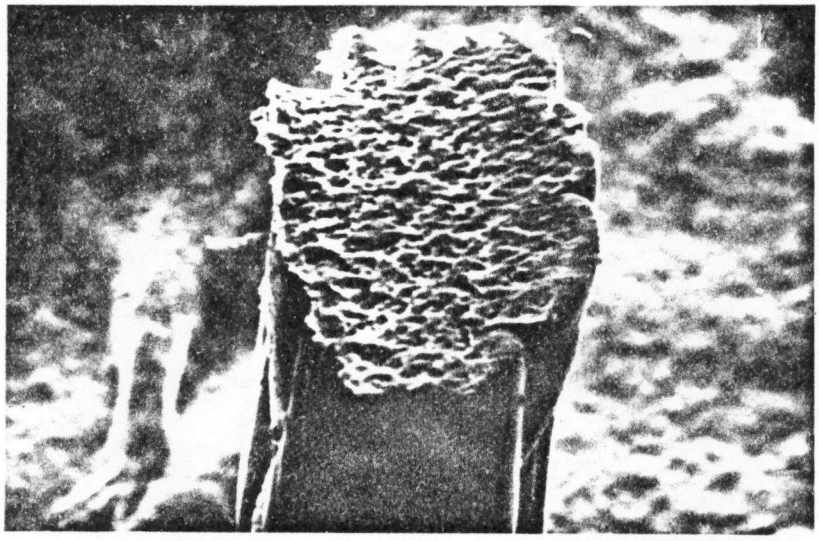

(a)
(100X)

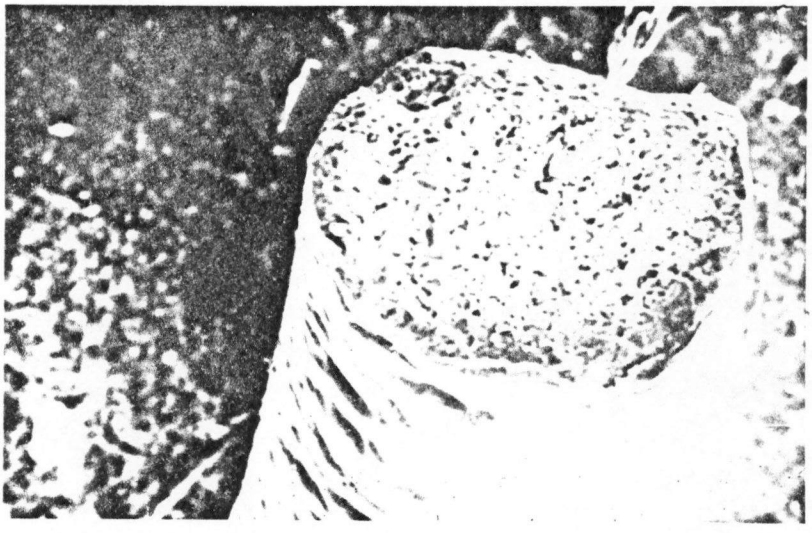

(b)
(100X)

Figure VII-1. SEM photomicrographs of (a) nylon-6 spun from formic acid into 10% formic acid; (b) nylon-66 spun from formic acid into 25% formic acid; (c) nylon-6 spun from formic acid into 4% methanol in water; (d) nylon-6 spun from formic acid into 4% methanol in water. (Note higher magnification.)

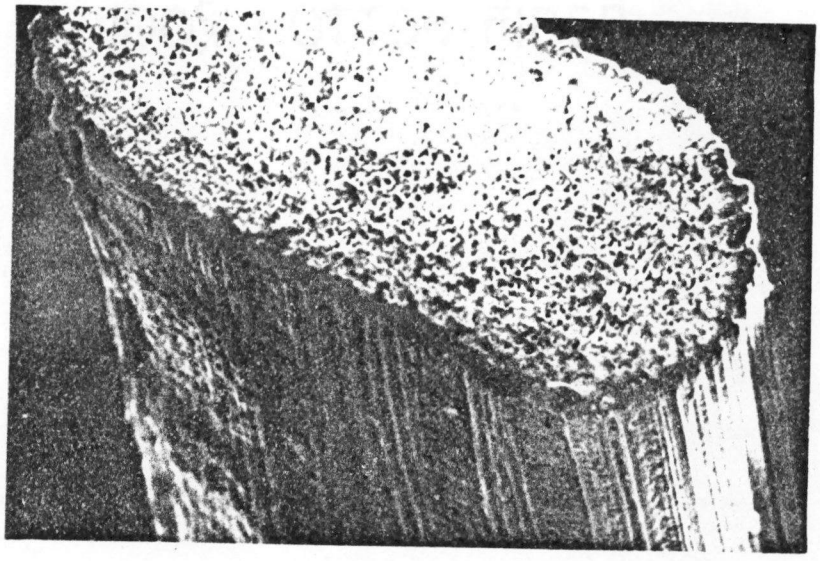

(c)
(200X)

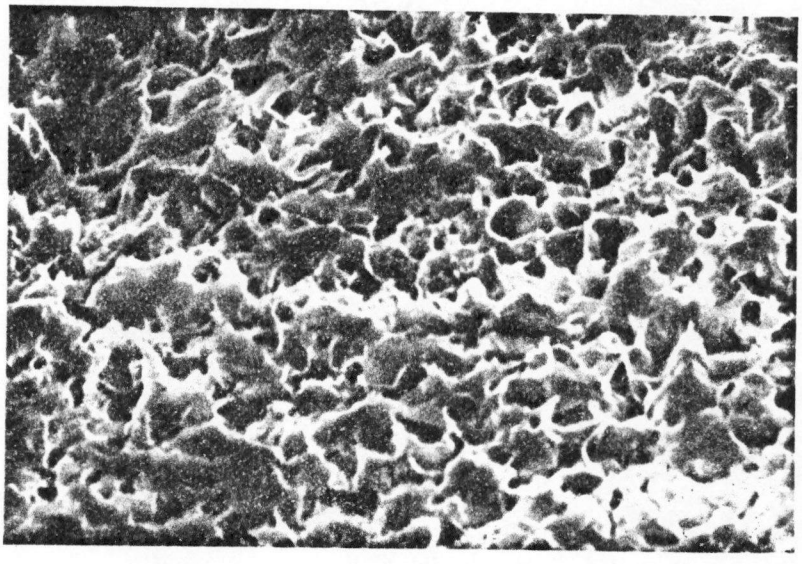

(d)
(1000X)

Figure VII-1. (Continued)

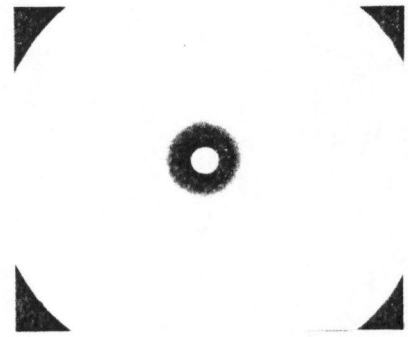

(a)

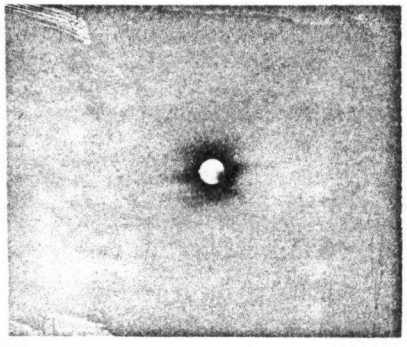

(b)

Figure VII-2. SAXS pattern of (a) wet spun nylon-6 from formic acid into 15% formic acid/water coagulant; (b) melt spun nylon-6.

Wet spun fibers which exhibit the hydrodynamic instability discussed in Chapter VI also contain microvoids, but they are elliptical in shape and are oriented in the radial direction. These voids result from the instability. When systems such as Nomex or PAN in DMAc are examined in coagulants which do not promote the instability, sponge-like microvoids are seen.

The sponge-like void is present when other forms of voids are not and sometimes even mixed with other types of voids. This category seems to account for the majority of industrial processes since they are designed to avoid other more drastic void types.

II. MICROSCOPIC OBSERVATIONS

The static coagulation technique described in Chapter III was used to observe the coagulation which produces sponge-like fibers. One such system observed was nylon-6 in formic acid with water as the coagulant (Figure VII-3). The coagulation proceeds slowly and with a regular interface. There are no step changes in the front movement as seen with the same dope and alkaline coagulant. Figure VII-4 shows the movement of the coagulation front vs. time and also the interfacial front movement between formic acid and water vs. time. The front in the polymer solution obviously moves more slowly than that between only the solvent and coagulant because its viscosity is considerably higher. It is expected that viscosity would impede the mass transfer process. The fact that the interface is smooth and unbroken makes the entire coagulation process uneventful and this is exactly what is needed for commercial wet spinning.

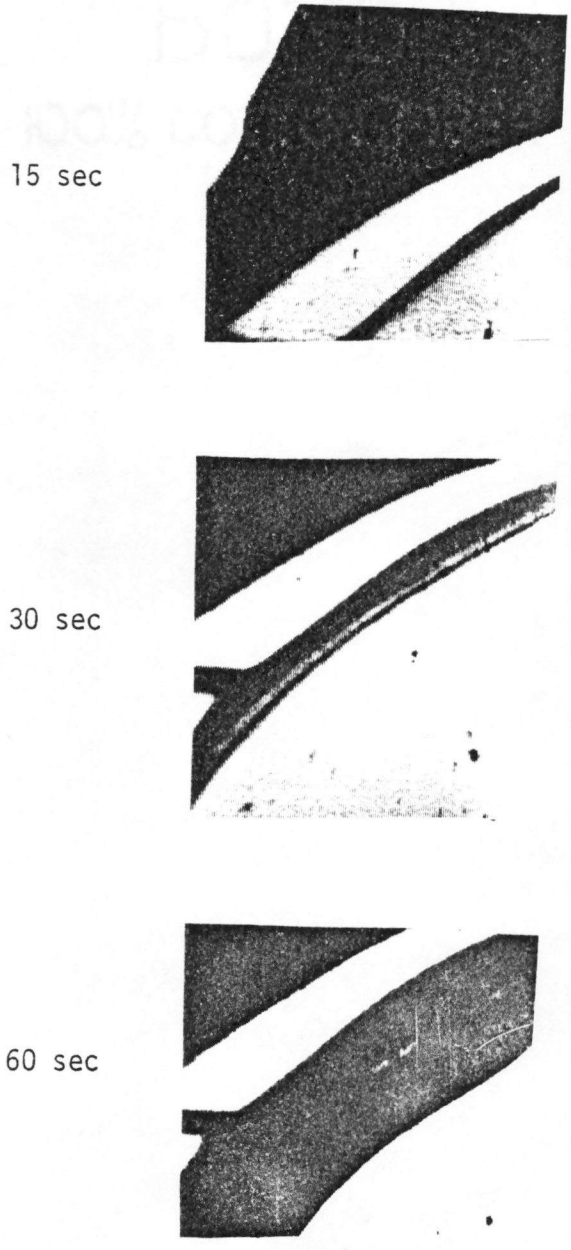

Figure VII-3. Static coagulation studies of nylon-6 in formic acid with water coagulant.

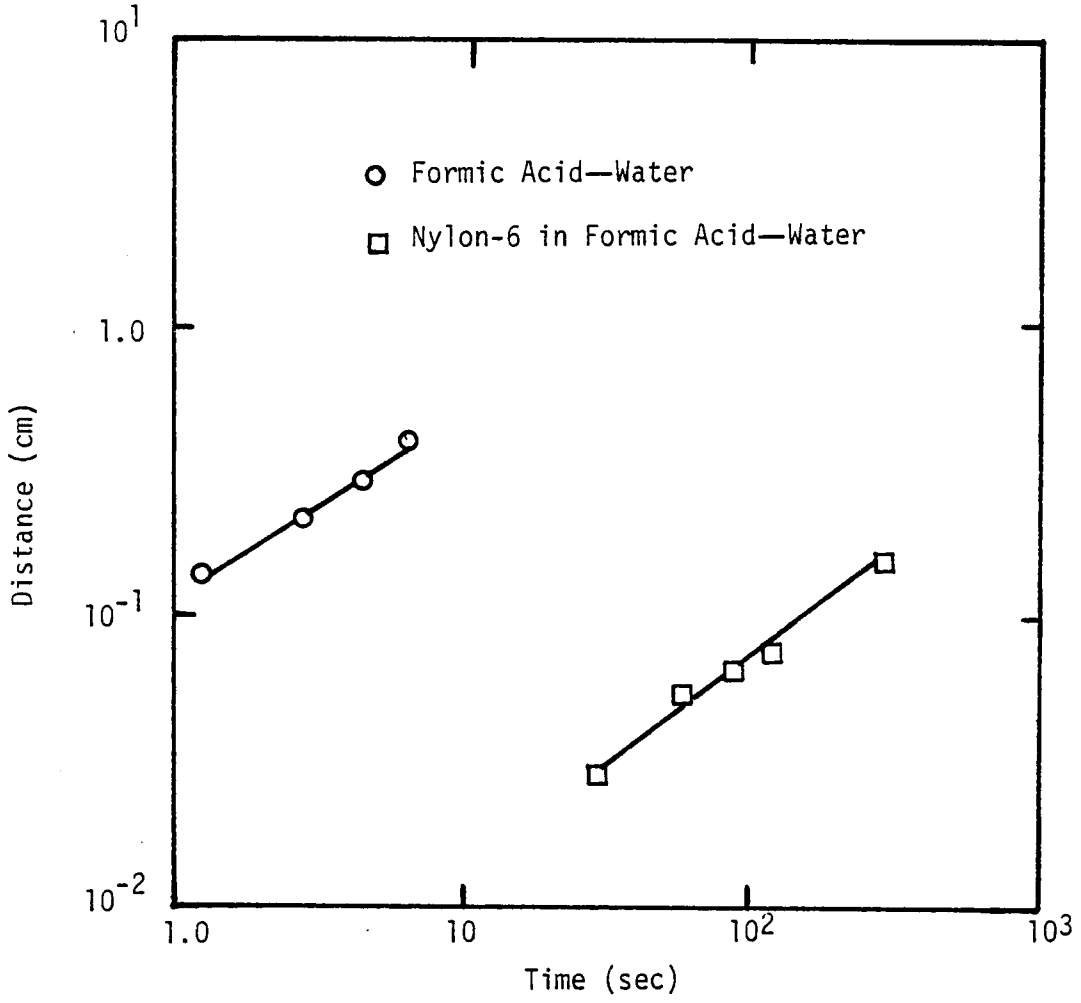

Figure VII-4. Static coagulation or interfacial movement for formic acid.

III. PROPOSED MECHANISM

Sponge-like fibers are the broadest of the three categories and include all fibers not in the other two. The size of the voids vary greatly and are obviously a function of coagulation conditions. Commercial fibers belong to this class and have very small voids (50-100 A°). Fibers spun in our experimental apparatus generally have much larger voids. For example, nylon-6 fibers spun from formic acid into methanol have voids of order 5 microns, and into 15% formic acid have voids of order 1 micron. The Nomex fibers have voids of order 1 micron when no fluting occurs. The acrylic fibers have much smaller voids of order 0.1 micron when no fluting occurs. These data can only be used qualitatively because of the experimental error involved in their determination. Equipment to sufficiently quantify these results was not available and consequently only a general mechanism was proposed. The specifics are left as a recommendation for future work.

The coagulation may be pictured as a simple diffusion problem where solvent is diffusing out of the filament and causing the polymer to coagulate. The coagulation occurs in local gel pockets which shrink to form voids after all of the solvent is leached out. This explains why the voids have no preferred orientation.

The size of these voids varies as a result of the size of gel pockets formed and of course this size is minimized if they are formed slowly and uniformly. This means that the entire fiber is coagulating uniformly and will contain only small voids.

The voids range in size from of order a few angstroms to four orders of magnitude larger. This represents quite a range and the cause for this is not well understood. It was noted that the voids are smaller in commercial fibers than in any of our experimental fibers. This would seem to indicate that small diameter, very viscous filaments which are coagulated slowly and very uniformly have the smallest voids. More drastic coagulation with nonuniformities obviously yields larger voids. Also larger diameter fibers have larger voids with all other parameters constant. As the concentration of polymer in the dope increases, the viscosity increases, and the void size decreases. This is quite logical because the smaller the quantity of solvent which must be removed the smaller the void. This is the reason that melt spun fibers have no voids.

CHAPTER VIII

CONCLUSIONS AND RECOMMENDATIONS

The major conclusions resulting from this study are summarized here.

1. The formation of macro or micro voids is inherent to any coagulation process. For wet spun fibers, the geometrical superstructure of these voids may be classified as: (1) hollow core, (2) fluted core, or (3) sponge-like.

2. Models of varying sophistication were developed and applied to the wet spinning process. Models including radial diffusion within the fiber gave a much better representation than one dimensional models analogous to the Kase-Matsuo melt spinning analyses.

3. When a chemical reaction occurs at the interface, the mass transfer rate is greatly increased. This shortens the period of time during which the filament is pliable and may be drawn down. When the initial external Sherwood number is greater than 20, it is predicted that hollow fibers are formed as a result of the decreased time available for draw down.

4. If the solvent and coagulant used in a wet spinning operation have sufficiently high heats of mixing, an instability can occur at the interface. The instability is a result of a fluctuation in interfacial tension which is induced by local temperature variations. It was analyzed by a perturbation type analysis which yielded a key dimensionless group $F = \frac{\mathcal{D}QC}{K\bar{T}}$. The characteristic value of this group is

$\frac{\mathcal{D}Q}{\kappa}\left(\frac{dC}{dT}\right)_{equil}$. Assuming that $\left(\frac{dC}{dT}\right)_{equil}$ is 0.1, fluted fibers are formed for values of F greater than 0.018.

5. All fibers not classified in the other two categories fall into the sponge-like class, but there are large variations in the size of the voids as a result of coagulation conditions.

6. Many of the empirically developed techniques used in commercial wet spinning were verified and the mechanisms by which they work were explained.

We conclude with recommendations for future work.

1. An experimental procedure to measure filament diameter, concentration, and tension on line should be devised to obtain experimental data for further testing of our models.

2. A further analysis of the skin growth during coagulation is needed; experimental data should be gathered to test such a model.

3. Equipment should be obtained to measure void size frequency distribution in the sponge-like fibers and this should be related to coagulation conditions.

4. Further work is needed to seek to control the formation of the lobe like voids for application to membranes and perhaps filtration media.

BIBLIOGRAPHY

BIBLIOGRAPHY

1. Addison, C. C. and T. A. Elliott. J. Chem. Soc., 2789 (1949).

2. Andrews, E. H. Cited by A. B. Thompson in Fiber Structure, J. W. S. Hearle & R. H. Peters, eds. Buterworth and the Textile Institute, Manchester-London, 1962.

3. Aoki, H., Y. Suzuki and A. Ishimoto. Unpublished work.

4. Aoki, H., D. Harwood, Y. Lee, J. F. Fellers, and J. L. White. PSE report 95 (1978).

5. Aoki, H., J. L. White and J. F. Fellers. PSE report 107 (1978).

6. Aoki, H., D. R. Coffin, T. A. Hancock, D. Harwood, R. S. Lenk, J. F. Fellers, and J. L. White. PSE report 108 (1978).

7. Astarita, G. Chem. Engr. Sci., 16, 202 (1961).

8. Astarita, G. Mass Transfer with Chemical Reaction. Elsevier Publishing Company, New York, 1965.

9. Astarita, G. and L. Nicodema. Chem. Engr. J., 1, 57 (1970)

10. Atkin, R. J., and F. M. Leslie. Q. J. Mech. and Appl. Math., XXIII Pt. 2 S3 (1970).

11. Austin, L. J., W. E. Ying, and H. Sawistowski. Chem. Engr. Sci., 21, 1109 (1966).

12. Bair, T. I. U.S. Patent 3,817,941, 1974.

13. Baird, B. R. U.S. Patent 3,819,569, 1974.

14. Berg, J. C. and A. Acrivos. Chem. Engr. Sci., 20, 737 (1965).

15. Berg, John C. and Carl R. Morig. Chem. Engr. Sci., 24, 937 (1969).

16. Black, W. B., J. Macro. Sci. Chem., A7-1, 3 (1973).

17. Black, W. B., J. Preston, and W. L. Hofferbert, Jr. J. of Macro. Sci. Chem., A7-1, 45 (1973).

18. Black, W. B., J. Preston, and W. L. Hofferbert, Jr. J. of Macro. Sci. Chem., A7-1, 67 (1973).

19. Black, W. B., J. Preston, H. S. Morgan, G. Raumann, and M. R. Liyquist. J. of Macro. Sci. Chem., A7-1, 137 (1973).

20. Black, W. B., and J. Preston. Man-Made Fibers, 2, 292 (1968).

21. Blades, H. U.S. Patent 3,767,756, 1973.

22. Blair, T. J., and P. W. Morgan. U.S. Patent 3,673,143, 1972.

23. Bogue, D. C. Anal. Chem., 32, 1777 (1960).

24. Bolton, E. K. Ind. Engr. Chem., 34, 53 (1943).

25. Booth, J. R. App. Poly. Symp., 6, 89 (1967).

26. Boger, C. U.S. Patent 2,955,017, 1960.

27. Brandrup, J., and E. H. Immergut. Polymer Handbook. Interscience Publishers, 1966.

28. Brazinsky, Irving, Albert G. Williams, and H. Leslie LaNieve. Poly. Engr. and Sci., 15, 834 (1975).

29. Brill, R., Z Physik. Chem., B53, 61 (1943).

30. Brinnegar, W. C. and M. E. Epstein. Appl. Poly. Symp., 6,99 (1967).

31. Carothers, W. H., and J. W. Hill. J. Amer. Chem. Soc., 54, 1579 (1932).

32. Cave, A. and A. Carli. British Chem. Engr. Process Technology, 17, 439 (1972).

33. Cernia, E. "Acrylic Fibers," in Man Made Fibers Science and Tech. 1-3, 135 (1967).

34. Chappel, F. P., M. F. Culpin, R. G. Gosden, and T. C. Tranter. J. App. Chem., 14, 12 (1964).

35. Chilton, T. H., and A. P. Colburn. Ind. Engr. Chem., 26, 1183 (1934).

36. Ciferri, A. Poly. Engr. and Sci., 15, 191 (1975).

37. Cogswell, F. N. Rheol. Acta, 4, 187 (1969).

38. Cogswell, F. N. Trans Soc. Rheology, 16, 405 (1972).

39. Crank, J. The Mathematics of Diffusion. Clarendon Press, Oxford, 1967.

40. Craig, J. P., J. P. Knudsen, and V. F. Holland. Tex. Res. J., 32-6, 435 (1962).

41. Davies, J. T., and E. K. Rideal. Interfacial Phenomena. Academic Press, New York, 1961.

42. Dealy, J. M. Poly. Engr. and Sci., 11, 433 (1971).

43. Denn, M. M., and G. Marrucci. A. I. Ch. E. J., 17, 101 (1971).

44. Denn, M. M., C. J. S. Petrie, and P. J. Avenas. A. I. Ch. E. J., 21, 791 (1975).

45. DiCave, S., and A. Carli. Brit. Chem. Engr. Proc. Tech., 17, 439 (1972).

46. Efimova, S. G., A. V. Volokhima, A. I. Koretskaya, M. M. Novleva, T. S. Sokolova, and S. P. Napkov. Journal of Theoretical and Experimental Chemistry and Physics of Compounds of High Molecular Weight, 14, 1523 (1959).

47. Elliott, A. and J. Ambrose. Disc. of Far. Soc., 9, 246 (1950).

48. Ericksen, J. L., Phys. of Fluids, 9 #6, 1205 (1966).

49. Ericksen, J. L. J. App. Math and Phys., 20, 383 (1969).

50. Ericksen, J. L., Trans Soc. Rheology, 13:1, 9 (1969).

51. Ericksen, J. L. Mol. Crystals and Liq. Crystals, 7, 153 (1969).

52. Ericksen, J. L. Liq. Crystals and Ordered Fluids, 181 (1970).

53. Ericksen, J. L. J. Mech. and App. Math, XXVII #2, 213 (1974).

54. Epstein, M. E., and A. J. Rosenthal. Tex. Res. J., 36-9, 813 (1966).

55. Ferguson, J. and K. M. Ibrahim. Polymer, 10, 135 (1969).

56. Ferguson, A. W., and R. G. Scott. Tex. Res. J., 26, 284 (1956).

57. Fitzgerald, W. E., and J. P. Craig. Appl. Poly. Symp., 6, 67 (1967).

58. Flory, P. J. J. Chem. Phys., 10, 51 (1942).

59. Flory, P. J. Proc. Roy. Soc., A234, 73 (1956).

60. Foldi, V. and J. C. Shivers. U.S. Patent 3,622,545, 1971.

61. Frank F. C. Disc. of Far. Soc., 25 (1958).

62. Friend, W. L., and A. B. Metzner. A. I. Ch. E. J., 4, 393 (1958).

63. Frommer, Moshe A. and Rami M. Messalem. Ind. Engr. Chem. Prod. Res. Develop., 12, 328 (1973).

64. Gainer, F. H., and P. Mina. Trans. Faraday Soc., 55, 1607 (1959).

65. Geoghan, M. DuPont Magazine, 71, 15 (1977).

66. Giddings, J. C. J. Chromatography, 5, 46 (1961).

67. Giddings, J. C. Dynamics of Chromatography. Marcel Dekker, Inc., New York, 1965.

68. Goldin, M., J. Yerushalmi, R. Pfeffer, and R. Shinnar. J. Fluid Mech., 38, 689 (1969).

69. Goldin, M., J. Yerushalmi, and R. Shinnar. Trans. Soc. Rehology, 17, 303 (1973).

70. Griffith, R. M. I. E. C. Fund, 3, 245 (1964).

71. Hamana, I., M. Matsui, and S. Katoj. Melliand Textilberichte, 50, 499 (1969).

72. Han, C. D., and L. J. Segal. App. Poly. Sci., 14, 2973 (1970).

73. Han, C. D. and L. J. Segal. App. Poly. Sci., 14, 2999 (1970).

74. Hancock, T. A. "The Solution Fabrication and Wet Spinning of Polyamides," M.S. thesis, University of Tennessee, Knoxville, 1975.

75. Hancock, T. A., J. E. Spruiell, and J. L. White. J. App. Poly. Sci., 21, 1227 (1977).

76. Harmon, J. J. Franklin Inst., 259, 519 (1955).

77. Harwood, D. "Aspects of the Solution Behavior of Aromatic Polyamides Revealed by Dilute Solution Studies," M. S. thesis, University of Tennessee, Knoxville, 1978.

78. Hatta, S. Tech Repts. Tohôku Imp. Univ., 8, 1 (1928).

79. Heikens, D., P. H. Hermans, and S. Smith. J. Poly. Sci., 38, 265 (1959).

80. Hermans, J. J. J. Colloid Sci., 2, 387 (1947).

81. Holland, V. F. J. of Macro. Sci. Chem., A7-1, 173 (1973).

82. Howard, G. J. J. Poly. Sci., 39, 548 (1959).

83. Huggins, M. L. J. Phys. Chem., 46, 151 (1942).

84. Huglin, M. B., and R. W. Richards. Die Angewandte Mak. Chemie, 38, 207 (1974).

85. Ide, Y., and J. L. White. PSE report 39 (1975), also White, J. L. and Y. Ide. App. Poly. Symp., 27, 61 (1975).

86. Ide, Y. and J. L. White. J. App. Poly. Sci., 20, 2511 (1976).

87. Ide, Y. and J. L. White. J. Non-Newt. Fluid Mech., 2, 281 (1977).

88. Iizuka, E. Mol. Crystals and Liq. Crystals, 25, 287 (1974).

89. Jaffe, M. ACS Anaheim Meeting, March, 1978.

90. Kanel, Fred. Personal communication.

91. Kase, S. and T. Matsuo. J. Poly. Sci. PtA, 3, 2541 (1965).

92. Kase, S. and T. Matsuo. J. App. Poly. Sci., 11, 251 (1967).

93. Kay, M. and D. W. McClure. J. Chem. Education, 41, 540 (1970).

94. King, F. W. U.S. Patent 3,079,219, 1963.

95. Kiyotsukuri, T., H. Hasegawa, and R. Imamura. Sen-I Gakkaishi (Japan), 26, 349 (1970).

96. Kiyotsukuri, T., H. Hasegawa, and R. Imamura. Sen-I Gakkaishi (Japan), 26, 356 (1970).

97. Kiyotsukuri, T., H. Hasegawa, and R. Imamura. Sen-I Gakkaishi (Japan), 26, 356 (1970).

98. Kiyotsukuri, T. and I. Hirasi. Sen-I Gakkaishi (Japan), 28, 9 (1972).

99. Kiyotsukuri, T. and I. Hirasi. Sen-I Gakkaishi (Japan), 29, T-45 (1973).

100. Klenin, V. J., L. V. Prozorov, M. Y. Prozorova, and B. I. Zhizdyuk. J. Poly. Sci., Poly. Symp., 44, 93 (1974).

101. Knudsen, J. P. Tex. Res. J., 33, 13 (1963).

102. Kroesser, F. W. and S. Middleman. A. I. Ch. E. J., 15, 383 (1969).

103. Kwolek, S. L. U.S. Patent 3,671,542, 1972.

104. Kwolek, S. L. U.S. Patent 3,819,587, 1974.

105. Laszkiewicz, B. and Z. Lewandowski. Polimery—Tworzywa Wielkoczasteczkowe, 17, 452 (1972).

106. Laun, H. M., and H. Munstedt. Proc. 7th Int. Rheol. Cong., p. 288 (1976).

107. Leslie, F. M. Archive for Rat. Mech. and Analysis, 28 #4, 265 (1968).

108. Leslie, F. M. Mol. Crys. and Liq. Cry., 7, 407 (1969).

109. Leslie, F. M. Rheo. Acta., 10, 91 (1971).

110. Macdonald, D. D., M. E. Estep, M. D. Smith, and J. B. Hyne. J. of Solution Chemistry, 3, 713 (1974).

111. Matovich, M. A. and J. R. A. Pearson. I. E. C. Fund, 8, 513 (1969).

112. Matz, R. Desalination, 10, 1 (1972).

113. Matz, R. Office of Saline Water, Res. Develop. Progr. Rept. No. 542, 1970.

114. McCabe, W. L. Trans. A. I. Ch. E., 31, 129 (1935).

115. Metzner, A. B., W. T. Houghton, R. A. Sailor, and J. L. White. Trans. Soc. Rheo., 5, 133 (1961).

116. Metzner, A. B. and A. P. Metzner. Rheo. Acta., 9, 174 (1970).

117. Middleman, S. and J. Gavis. J. App. Poly. Sci., 3, 367 (1960).

118. Middleman, S. and J. Gavis. Phys. of Fluids, 4, 355 (1961).

119. Miller, P. L. J. Macro. Sci., Chem., A7-1, 183 (1973).

120. Miyosaka, K. and K. Ishikawa. J. Poly. Sci., 2A-6, 1317 (1968).

121. Morawetz, H. Macromolecules in Solution. John Wiley & Sons, Inc., New York, 1975.

122. Morgan, H. S., Jr. U.S. Patent 3,414,645, 1968.

123. Morgan, H. S., Jr. U.S. Patent 3,642,706, 1970.

124. Morehead, F. F., and W. A. Sisson. Tex. Res. J., 15-12, 443 (1945).

125. Morrison, M. E. A. I. Ch. E. J., 16, 57 (1970).

126. Nitschmann, H., and J. Schrade. Helv. Chim. Acta., 31, 297 (1948).

127. Ohzawa Y., Y. Nagano, and T. Matsuo. J. App. Poly. Sci., 13, 257 (1969).

128. Ohzawa, Y., and Y. Nagano. J. App. Poly. Sci., 14, 1879 (1970).

129. Oseen, Trans. Far. Soc., 29, 883 (1933).

130. Papkov, S. P., V. G. Kulichikhin, V. D. Kalmykova, A. Y. Malkin. J. Poly. Sci., 12, 1753 (1974).

131. Parker, James P., personal communication, 1978.

132. Paul, D. R. J. App. Poly. Sci., 12, 383 (1968).

133. Paul, D. R. J. App. Poly. Sci., 12, 3372 (1968).

134. Paul, D. R. J. App. Poly. Sci., 13, 817 (1969).

135. Paul, D. R., and O. M. Ebra-Lima. J. App. Poly. Sci., 14, 2201 (1970).

136. Paul, D. R., V. Mavichak, and D. R. Kemp. J. App. Poly. Sci., 15, 1553 (1971).

137. Paul, D. R. and O. M. Ebra-Lima. J. App. Poly. Sci., 15, 2199 (1971).

138. Paul, D. R. and D. H. Carranza. J. Poly Sci.: Symp., 41, 69 (1973).

139. Paul, D. R. and D. R. Kemp. J. Poly. Sci.: Symp., 41, 79 (1973).

140. Paul, D. R., and A. A. Armstrong. J. App. Poly. Sci., 17, 1269 (1973).

141. Paul, D. R. J. App. Poly. Sci., 18, 473 (1974).

142. Paz, Uri and Hillel Rubin. Ind. Engr. Chem. Fund., 9, 509 (1970).

143. Pearson, J. R. A. J. Fluid Mechanics, 4, 489 (1958).

144. Pelofsky, Arnold H. J. of Chem. and Engr. Data, 11, 394 (1966).

145. Perez, E. Susana DeOrtiz, and H. Sowistowski. Chem. Engr. Sci., 28, 2051 (1973).

146. Preston, J. Poly. Engr. and Sci., 15, 199 (1975).

147. Preston, J., H. S. Morgan and W. B. Black. J. Macro. Sci. Chem., A7-1, 325 (1973).

148. Rayleigh, Lord. Proc. London Math. Soc., 10, 4 (1878).

149. Rayleigh, Lord. Proc. Roy. Soc., 29, 71 (1879).

150. Rayleigh, Lord, Phil. Mag., 34, 145 (1892).

151. Rebenfeld, L., J. Poly. Sci., 9, 91 (1965).

152. Robinson, Conmar. Disc. of Far. Soc., 52, 571 (1956).

153. Robinson, C., J. C. Ward, and R. B. Beevers. Disc. of Far. Soc., 25, 29 (1958).

154. Rohm & Haas Company. "Hollow Fiber Ultrafiltration," Sept., 1976.

155. Roman, J. F. "Die Swell in Molten Polymers," M.S. thesis, University of Tennessee, 1974; also White, James L. and Joseph F. Roman. J. App. Poly. Sci., 20, 1005 (1976).

156. Sakiadis, B. C. A. I. Ch. E. Journal, 7, 26 (1961).

157. Sakiadis, B. C. A. I. Ch. E. Journal, 7, 467 (1961).

158. Sano, Y. and K. Orii. Sen-I Gakkaishi, 24, 212 (1968).

159. Sbrolli, W. et al. Annali di Chimica (Rome), 53, 1199 (1963).

160. Schonhorn, Harold. J. Chem. Engr. Data, 12, 524 (1967).

161. Sbrolli, W. et al. Annali di Chimica (Rome), 53, 1199 (1963).

162. Sherwood, T. K. and J. C. Wei. A. I. Ch. E. Journal, 1, 522 (1955).

163. Sherwood, T. K. and J. M. Ryan. Chem. Engr. Sci., 11, 81 (1959).

164. Sherwood, T. K., R. L. Pigford, and C. R. Wilke. Mass Transfer. McGraw-Hill Book Company, New York, 1975.

165. Singleton, R. W., M. A. Sieminski, and B. S. Sprague. Tex. Res. J., 31, 917 (1961).

166. Smith, S. J. Poly. Sci., 30, 459 (1958).

167. Statton, W. O. J. Poly. Sci., 22, 385 (1956).

168. Statton, W. O. J. Poly Sci., 58, 205 (1962).

169. Sternling, C. V. and L. E. Scriven. A. I. Ch. E. Journal, 5, 514 (1959).

170. Stimson, E. R. and E. E. Schrier. J. Chem. Engr. Data, 19, 354 (1974).

171. Strathmann, H., K. Kock, and P. Amar. Desalination, 16, 179 (1975).

172. Tanford, C. Physical Chemistry of Macromolecules. John Wiley & Sons, Inc., New York, 1961.

173. Tanner, R. I. J. Poly. Sci., A-2, 8, 2067 (1970).

174. Taylor, G. B. J. Amer. Chem. Soc., 69, 635 (1947).

175. Terada, K. Sen-I Gakkaishi, 29, T120 (1973).

176. Terada, K. Sen-I Gakkaishi, 29, T338 (1973).

177. Terada, K. Sen-I Gakkaishi, 29, T345 (1973).

178. Terada, K. Sen-I Gakkaishi, 29 T451 (1973).

179. Terada, K. Sen-I Gakkaishi, 29 T532 (1973).

180. Tomotika, S. Proc. Roy. Soc., A150, 321 (1935).

181. Tomotika, S. Proc. Roy. Soc., A153, 302 (1936).

182. Ucci, P. A. Personal communication.

183. VanVeld, R. D., G. Morris, and H. R. Billica. J. App. Poly. Sci., 12, 2709 (1968).

184. Vasudevan, G. and S. Middleman. A. I. Ch. E. J., 16, 614 (1970).

185. Weast, R. C. Handbook of Chem. and Phys. CRC press, 1973.

186. Weber, C. Z. angew. Math. Mech., 11, 136 (1931).

187. White, J. L. J. App. Poly. Sci., 8, 2339 (1964).

188. Worth, D. L. and J. L. White. Tex. Res. J., 44, 483 (1974).

189. Yerushalmi, J. and R. Shinnar. I. E. C. Proc. Des., 10, 196 (1971).

190. Ying, W. E., and H. Sawistowski. Proc. Int. Solvent Extraction Conference, 1971.

191. Zaukelies, D. A., and B. L. Daniel. J. Macro. Sci. Chem., A7-1, 229 (1973).

192. Ziabicki, A. Kolloid Z., 175, 14 (1961).

193. Ziabicki, A. and K. Kedzierska. Kolloid Z., 171, 51 (1960.

194. Ziabicki, A. Fundamentals of Fibre Formation. John Wiley & Sons, Ltd., New York, 1976.

195. Zwick, M. M. and C. Van Bochave. Tex. Res. J., 34, 417 (1964).

VITA

Tony Alan Hancock was born in Cleveland, Tennessee on October 30, 1952. He attended Charleston Elementary, Mayfield Elementary, and Cleveland High School, graduating from the latter in June 1970. He entered the University of Tennessee at Knoxville in June 1970 and received the Bachelor of Science in Chemical Engineering in June 1974. During this time, he participated in the Co-Operative Engineering Program and was employed by E. K. duPont de Nemours and Company, Inc. in Chattanooga, Tennessee.

Upon receipt of the B.S. degree, he entered the Graduate School at the University of Tennessee and received the Master of Science degree with a major in Chemical Engineering in December 1975. He then continued his research work at the University of Tennessee. In December 1978 he accepted a position with IBM in Lexington, Kentucky. He received the Doctor of Philosophy degree with a major in Chemical Engineering in March 1981.

He is a member of the following organizations: Alpha Chi Sigma; AIChe; Tau Beta Pi; Phi Kappa Phi; Sigma Xi; A.A.T.C.C.; Association of Collegiate Engineers: Board of Directors; Woodmen of the World, and North Cleveland Baptist Church.